CENTER FOR
TRANSPORTATION
STUDIES

UNIVERSITY OF MINNESOTA

DEVELOPMENT OF ADVANCED TRAFFIC FLOW MODELS AND IMPLEMENTATION IN PARALLEL PROCESSING, PHASE 2

Anastasios S. Lyrintzis, Guoqing Liu, and Raja P. Rangiah,
Aerospace Engineering and Mechanics;
Panos G. Michalopoulos,
Civil and Mineral Engineering

Sponsored by:
Center for Transportation Studies

Development of Advanced Traffic Flow Models and Implementation in Parallel Processing

Phase II
(9/15/92 – 9/15/93)

ANASTASIOS S. LYRINTZIS

PANOS G. MICHALOPOULOS

GUOQING LIU

RAJA P. RANGIAH

Feb. 1994

ABSTRACT

In this report, five high-order continuum traffic flow models are compared: Payne's model; Papageorgiou's model; the semi-viscous model and the viscous model as well as a proposed high-order model, and the simple continuum model. The stability of the high-order models is analyzed and the shock structure investigated in all models. In addition, the importance of the proper choice of finite-difference method is addressed. For this reason, three explicit finite-difference methods for numerical implementation, namely, the Lax method, the explicit Euler method and the upwind scheme with flux vector splitting, are discussed. The test with hypothetical data and the comparison of numerical results with field data suggest that high-order models implemented through the upwind method are better than the simple continuum model. The proposed high-order model appears to be more accurate than the other high-order models.

1. INTRODUCTION

Since Lighthill and Whitham first applied a simple continuum model to describe the characteristics of traffic flow in 1955 (Lighthill and Whitham, 1955), much progress has been made in the development and application of macroscopic continuum traffic flow models, especially with the introduction of the high-order continuum models. For example, since 1985, Michalopoulos et al. have developed a microcomputer simulation program, KRONOS, based on the simple continuum model (Michalopoulos et al., 1985, 1991a, 1992). KRONOS has been used by the Minnesota Department of Transportation for simulating freeway traffic. In 1971 Payne developed a high-order continuum model that includes the effects of the drivers' reaction and acceleration (Payne, 1971). Later he applied this high-order model to the computer simulation program, FREFLO (Payne, 1979). Since then, a few new high-order continuum models have been developed by several researchers in traffic flow theory. Some examples are Papageorgiou's improved high-order model (Papageorgiou, 1983; Papageorgiou et al., 1989), the semi-viscous and viscous high-order models (Michalopoulos et al., 1991, 1993) and others (Phillips, 1979; Kühne, 1984; Ross, 1988).

As is well known, high-order continuum models are more sophisticated than the simple continuum model. This is because the simple continuum model is based only on the conservation equation, while high-order models include not only the conservation but also the momentum equation which takes into account the dynamic effects of inertia and acceleration of traffic mass. However, it is unknown whether in practice high-order continuum models produce results that are close to those of the simple continuum model.

Although it is well understood that a finite-difference method can affect the computational accuracy of continuum traffic flow models, the importance of the proper choice of finite-difference method has not been properly addressed in the past and some improper finite-difference methods were applied to the continuum models. Only recently, other finite-difference methods have been applied to the continuum models. For example, some implicit methods for the simple continuum model and the semi-viscous model are discussed by Chronopoulos et al (1992, 1993). Leo and Pretty (1992) used an upwind method for the simple continuum model and the original high-order model. In addition, a survey of the application of upwind methods including TVD (Total Variation Diminishing) method to the simple continuum model was given by Lyrintzis et al. (1992). Although the implicit first-order upwind scheme is strongly recommended for the simple continuum model, it is not clear which finite-difference method should be used with the high-order continuum models to achieve a higher computational accuracy. The purpose of this article is to address these questions.

We have investigated five high-order continuum models and compared them to the simple continuum model. These five high-order models are Payne's original high-order model (Payne, 1971, 1979), Papageorgiou's improved high-order model (Papageorgiou, 1983, 1989), the semi-viscous model and the viscous model (Michalopoulos et al., 1991, 1993) as well as a new high-order model developed here. The stability of the high-order models is analyzed and the shock structure investigated in all models. Three explicit finite-difference methods, the Lax method, the explicit Euler method and the upwind scheme with flux vector splitting, are discussed. Through the mathematical analysis, testing with hypothetical data, and comparison of numerical results with field data, we demonstrate that high-order models implemented through the upwind scheme with flux vector splitting can perform better than the simple continuum

model. Furthermore, the proposed high-order model appears to be more accurate than the other high-order models.

In Section 2 of this report, we review the five existing continuum traffic flow models. In Section 3, we propose a new high-order model that we called the proposed high-order model. In Section 4, we investigate the six continuum models based on a hypothetical pipeline case and three sets of field data. Finally, the conclusions are presented in Section 5. These results were also presented at the 73rd TRB conference (Lyrintzis et al, 1994).

2. CONTINUUM TRAFFIC FLOW MODELS: AN OVERVIEW

2.1 Simple Continuum Model

The simple continuum model proposed by Lighthill and Whitham (1955) consists essentially of a conservation equation

$$\frac{\partial k}{\partial t} + \frac{\partial q}{\partial x} = g(x,t) \tag{1}$$

supplemented by the definition of the flow rate

$$q = ku \tag{2}$$

and a speed-density (u-k) relationship

$$u = u_e(k) \tag{3}$$

where k is the traffic density (veh per mile), q is the flow rate of the traffic stream (veh per hour), u is the space mean speed (mile per hour). t and x represent time and space, respectively. $u_e(k)$ is a equilibrium relationship between the speed and the traffic density. Finally, $g(x,t)$ represents the generation of flow.

Substituting (2) and (3) into (1) and assuming no generation terms, we obtain the equation for density

$$\frac{\partial k}{\partial t} + c(k)\frac{\partial k}{\partial x} = 0 \tag{4}$$

where

$$c(k) = \frac{dq}{dk} = u_e(k) + k\frac{du_e}{dk} \tag{5}$$

Thus, Eq (4) is a nonlinear wave equation because the wave speed c(k) is not a constant.

It is well known that the general solution of Eq (4) can be obtained by the method of characteristics. If the initial condition is

$$k(x,0) = f(x) \tag{6}$$

then the general solution of Eq (4) is

$$k(x,t) = f(x - c(k)t) \tag{7}$$

Differentiating Eq (7) partially with respect to x gives

$$\frac{\partial k}{\partial x} = \frac{f'(x-c(k)t)}{1+tf'(x-c(k)t)c'(k)} \quad , \tag{8}$$

thus $\frac{\partial k}{\partial x}$ becomes infinite whenever

$$1 + tf'(x - c(k)t)c'(k) = 0 \ , \tag{9}$$

where symbol (') denotes differentiation of a function w.r.t. the argument. If traffic flow is considered as a compressible fluid, we have

$$c'(k) = \frac{d^2q}{dk^2} < 0. \tag{10}$$

Hence, it is possible for Eq (9) to hold. Thus, Eq (1) or (4) always leads to discontinuous solutions so that a smooth solution can exist only for a finite time, even when the initial condition is arbitrarily smooth. However, actual traffic flow almost changes smoothly. This means that, from theoretical point of view, the simple continuum model does not accurately describe the traffic dynamics.

It should be noted that the numerical solution of the simple continuum model introduces numerical dissipation that creates smooth solution. For example, we can use the Lax method

(Lax, 1954) because this method introduces a strong numerical dissipation effect to the simple continuum model (Anderson et al, 1984; Hirsch, 1990; Michalopoulos, 1985), thus smoothing the discontinuity. In order to see this, we investigate the modified form of Eq (1). Implementing the Lax method to Eq (1) yields

$$k_j^{n+1} = \frac{1}{2}(k_{j+1}^n + k_{j-1}^n) - \frac{\Delta t}{2\Delta x}(q_{j+1}^n - q_{j-1}^n) \tag{11}$$

where superscripts denote time step and subscripts denote space step. Nodes j+1 and j-1 represent the downstream and upstream of node j, respectively. Let us substitute Taylor-series expansions into Eq (11) for $k_j^{n+1}, k_{j+1}^n, k_{j-1}^n, q_{j+1}^n$ and q_{j-1}^n. The following modified equation is then obtained

$$\frac{\partial k}{\partial t} + \frac{\partial q}{\partial x} = \{\frac{\Delta x^2}{2\Delta t}(1 - (\frac{\Delta t}{\Delta x})^2 c^2) + \frac{\Delta x^2}{2}(3(\frac{\Delta t}{\Delta x})^2 c^2 - 1)\frac{dc}{dk}\frac{\partial k}{\partial x}\}\frac{\partial^2 k}{\partial x^2} + O[\Delta t, \Delta x^2]. \tag{12}$$

Since the first term on the right-hand side of Eq (12) is an even derivative, the resulting truncation error will be predominantly dissipative.

However, when we implemented the discretized form, Eq (11), of the simple continuum model, we found that the results in volume produced by Eq (11) sometimes have small overshoots at the region in which traffic conditions changed from uncongested to congested or from congested to uncongested (Lyrintzis et al., 1992). In other words, the Lax discretized form of the simple continuum model can produce additional errors in volume under those conditions.

Although we might introduce the dissipation effect to the simple continuum model by using the other finite-difference methods, we still face another drawback in the simple continuum model. That is, changes in speed in the simple continuum model occur instantaneously and fluctuations of speed around equilibrium values are not allowed. For this kind of drawback, we cannot use a finite-difference method to overcome it. An additional equation – momentum equation – is needed. Nevertheless, the simple continuum model usually

captures the basic shock wave structure and gives reliable results for various test cases and geometries (Michalopoulos et al., 1992).

2.2 The Original High-Order Model (Payne, 1971, 1979)

Payne (1971) proposed a more attractive high-order continuum traffic flow model in which a momentum equation is included. We call this model the original high-order model. The momentum equation in this model was derived from car-following theory. The state equations of the original high-order model are

$$\frac{\partial k}{\partial t}+\frac{\partial q}{\partial x}=g(x,t) \tag{13a}$$

$$\frac{\partial u}{\partial t}+u\frac{\partial u}{\partial x}=\frac{1}{T}\{u_e(k)-u-\frac{\nu}{k}\frac{\partial k}{\partial x}\} \tag{13b}$$

$$q=uk \tag{13c}$$

where, in addition to the previous notation, T is the constant reaction time and ν is an anticipation coefficient which is the function of the density with the following form

$$\nu=-\frac{1}{2}\frac{du_e}{dk}\ . \tag{14}$$

It should be noted that a constant anticipation coefficient was later suggested by Payne (1979).

Since the momentum equation is included in the original high-order model, some new features emerge. First, an equilibrium state may exist in the original high-order model. To see this, we investigate the original high-order model by using the linearized theory.

Suppose there are small perturbations around an equilibrium state (k_0, $u_0=u_e(k_0)$), i.e.,

$$k=k_0+\hat{k}\ ,\qquad u=u_0+\hat{u}. \tag{15}$$

Substituting (15) into Eq (13), and retaining only first powers of $\hat{k}$ and $\hat{u}$, for the pipeline case we have

$$\frac{\partial \hat{k}}{\partial t} + u_0 \frac{\partial \hat{k}}{\partial x} + k_0 \frac{\partial \hat{u}}{\partial x} = 0 \tag{16a}$$

$$\frac{\partial \hat{u}}{\partial t} + u_0 \frac{\partial \hat{u}}{\partial x} = \frac{1}{T}\{\hat{k}(\frac{du_e}{dk})_{k_0} - \hat{u} - \frac{\nu}{k_0}\frac{\partial \hat{k}}{\partial x}\} . \tag{16b}$$

Since the kinematic wave speed corresponding to k_0 is

$$c_0 = u_0 + k_0(\frac{du_e}{dk})_{k_0} , \tag{17}$$

manipulating the above linear equations, we obtain

$$\frac{\partial \hat{k}}{\partial t} + c_0 \frac{\partial \hat{k}}{\partial x} = \nu \frac{\partial^2 \hat{k}}{\partial x^2} - T(\frac{\partial}{\partial t} + u_0 \frac{\partial}{\partial x})^2 \hat{k} . \tag{18}$$

The same equation holds for $\hat{u}$.

It has been proven that the exponential solutions of the linear equation (18) are stable if and only if the following condition holds (Whitham, 1974):

$$u_0 + \sqrt{\frac{\nu}{T}} > c_0 > u_0 - \sqrt{\frac{\nu}{T}} . \tag{19}$$

Similarly, the exponential solutions for $\hat{u}$ are also stable under the above condition (Eq. (19)). Therefore, the state (k_0, u_0=$u_e(k_0)$) is an equilibrium state.

Another new feature is that there is a smooth shock. To see this, we search the solution of Eq (13)

$$k(x,t) = k(\xi), \qquad u(x,t) = u(\xi) \tag{20}$$

where

$$\xi = x - Ut . \tag{21}$$

If there exists such a real value U, then Eq (20) represents the smooth shock of the system described by Eq (13), and U is the constant speed of the smooth shock.

Suppose there exists a smooth shock so that we can write

$$\frac{\partial k}{\partial t} = -U\frac{dk}{d\xi}, \qquad \frac{\partial u}{\partial t} = -U\frac{du}{d\xi},$$

$$\frac{\partial k}{\partial x} = \frac{dk}{d\xi} , \qquad \frac{\partial u}{\partial x} = \frac{du}{d\xi} ,$$

and substituting the above relationships into Eq (13) (for the pipeline case) to have

$$-U\frac{dk}{d\xi} + u\frac{dk}{d\xi} + k\frac{du}{d\xi} = 0 \tag{22a}$$

$$Tk(u-U)\frac{du}{d\xi}+v\frac{dk}{d\xi}+uk-ku_e(k)=0 \tag{22b}$$

which in turn yields a single equation for the density

$$(v-T(u-U)^2)\frac{dk}{d\xi}=k(u_e(k)-u)\ . \tag{23}$$

It has been proven (Whitham, 1974) that Eq (23) has a unique solution if and only if

$$v>T(u-U)^2, \qquad \text{i.e.,} \qquad u-\sqrt{\frac{v}{T}}<U<u+\sqrt{\frac{v}{T}}\ . \tag{24}$$

If the pair values of the density and speed before and after the shock are (k_1, u_1) and (k_2, u_2), then we have the speed of the smooth shock

$$U=\frac{k_1u_1-k_2u_2}{k_1-k_2}. \tag{25}$$

Consequently, there exists a smooth shock for the original high-order model if the condition (Eq (24)) holds. Moreover, the coefficient (v-$T(u$-$U)^2$) determines the shock thickness that represents the space containing the shock. The larger the value of the coefficient, the thicker the shock, and vice versa. It should be pointed out that, if the condition (Eq (24)) does not hold, the smooth shock does not exist but a discontinuity occurs.

From the above discussion, we can see that the original high-order model is superior to the simple continuum model conceptually. Unfortunately, because the explicit Euler-like finite-difference method was applied to the original high-order model (Payne, 1971), application of this model does not show the superiority. Indeed, applying the explicit Euler-like method to the original high-order model (Eq (13)) (for the pipeline case) yields

$$k_j^{n+1}=k_j^n+\frac{\Delta t}{\Delta x}[q_j^{n+1}-q_{j+1}^{n+1}] \tag{26a}$$

$$u_j^{n+1}=u_j^n-\frac{\Delta t}{\Delta x}u_j^n[u_j^n-u_{j-1}^n]+\frac{\Delta t}{T}\{u_e(k_j^n)-u_j^n-\frac{v}{k_j^n\Delta x}[k_{j+1}^n-k_j^n]\} \tag{26b}$$

$$q_j^{n+1}=\frac{1}{4}[k_{j-1}^n+k_j^n][u_{j-1}^n+u_j^n] \tag{26c}$$

where the notation is the same as before. From this discretized form, it is evident that the original high-order model cannot work at the smaller values of the density because of the term $\frac{v}{k_j^n\Delta x}\left[k_{j+1}^n-k_j^n\right]$. Since this discretized form does not come from the conservation form of the

system, it cannot produce the correct shock intensities (Hirsch, 1988). Moreover, this discretized form is unstable from the computational point of view. To see this, we investigate the truncation error associated with Eq (26a). Here only those terms that involve a second space derivative of the density k are needed, since they are the only ones that contribute to a diffusion. The effective diffusion coefficient for Eq (26a), through terms of order Δt^2 and Δx^2, is

$$-\frac{\Delta t}{2}u^2(1-\frac{\Delta t}{T})-\frac{\Delta t}{2}\frac{v}{T}(1-\frac{\Delta t}{3T})+\{\frac{\Delta t^2}{6}(9u^2+\frac{7v}{T})-\frac{\Delta x^2}{4}\}\frac{\partial u}{\partial x}-\frac{\Delta t^2}{6}\frac{u}{T}(5k\frac{du_e}{dk}+3u_e). \qquad (27)$$

It has been proven that instabilities can occur wherever a diffusion coefficient is negative (Hirt, 1968). From Eq (27), it is easy to see that the first two terms are always negative; the third term will be negative when traffic becomes congested. Thus, under congested flow, the computed solutions provided by this discretized form of the original high-order model become unstable. Therefore, in order to effectively implement the original high-order model, a new finite-difference method is needed.

Although we can apply another finite-difference method to the original high-order model to improve its performance, there is still a problem in the model -- the reaction time problem. As car-following theory suggests, the reaction time is the time measured from the time at which the lead driver initiates his stop, until the second driver initiates his own stopping maneuver. After such a time, the velocities of the two vehicles are assumed equal (Gerlouph and Huber, 1975). This would mean that the second vehicle has a jump in speed, but this not the case. In fact, after the reaction time, there is still a process of adjusting speed for the second vehicle, which we call the relaxation process. Such a relaxation process is not included in the original high-order model because only the reaction time is taken into account. For this reason, we propose the new high-order continuum model presented in Section 3.

2.3 The Improved High-Order Model (Papageorgiou, 1983, 1989)

Based on the original high-order model, Papageorgiou (1983, 1989) proposed an improved high-order continuum model. The equations for this high-order model are

$$\frac{\partial k}{\partial t} + \frac{\partial q}{\partial x} = g(x,t) \tag{28a}$$

$$\frac{\partial u}{\partial t} + u\zeta\frac{\partial u}{\partial x} = \frac{1}{T}\{[u_e(k) - u] - \frac{\nu}{K+\kappa}\frac{\partial k}{\partial x}\} \tag{28b}$$

$$q = uk \tag{28c}$$

where, in addition to the previous notation, κ and ζ are constants. The improved high-order model was developed based on the Euler-like discretized form of the original high-order model. So to improve the computational effect of the original high-order model, κ was added in order to keep the third term on the right-hand side of Eq (26b) limited when the density k becomes small; ζ was added only for the numerical computation of the model.

In order to see the difference between the improved high-order model and the original high-order model, we linearize the improved high-order model for small perturbations around the state (k_0, $u_0=u_e(k_0)$). Thus, using the same method as in section 2.2, for the pipeline case we have

$$\frac{\partial \hat{k}}{\partial t} + u_0\frac{\partial \hat{k}}{\partial x} + k_0\frac{\partial \hat{u}}{\partial x} = 0 \tag{29a}$$

$$\frac{\partial \hat{u}}{\partial t} + u_0\zeta\frac{\partial \hat{u}}{\partial x} = \frac{1}{T}\{\hat{k}(\frac{du_e}{dk})_{k_0} - \hat{u} - \frac{\nu}{k_0+\kappa}\frac{\partial \hat{k}}{\partial x}\} \tag{29b}$$

Manipulating the above linear equations and using

$$c_0 = u_0 + k_0(\frac{du_e}{dk})_{k_0}\ , \tag{30}$$

we have

$$\frac{\partial \hat{k}}{\partial t} + c_0\frac{\partial \hat{k}}{\partial x} = \frac{k_0\nu}{k_0+\kappa}\frac{\partial^2 \hat{k}}{\partial x^2} - T_0[\frac{\partial^2 \hat{k}}{\partial t^2} + u_0(1+\zeta)\frac{\partial^2 \hat{k}}{\partial x \partial t} + u_0^2\zeta\frac{\partial^2 \hat{k}}{\partial x^2}]\ . \tag{31}$$

It can be proven that the exponential solutions of the linear equation (31) are stable if and only if the following condition holds:

$$u_0 + \sqrt{\frac{k_0 v}{(k_0+\kappa)T} + \frac{1}{4}u_0^2(1-\zeta)^2} - \frac{1}{2}u_0(1-\zeta) > c_0 > u_0 - \sqrt{\frac{k_0 v}{(k_0+\kappa)T} + \frac{1}{4}u_0^2(1-\zeta)^2} - \frac{1}{2}u_0(1-\zeta), \quad (32)$$

where the notation is the same as before. Comparing with the stable condition (Eq (19)) of the original high-order model, we can see that, when $\zeta = 1$ and $\kappa \neq 0$, the range of stability of Eq (32) is less than that of Eq (19); when $\zeta > 1$ or $\zeta < 1$, the range of stability of Eq (32) shifts right or left relatively to the range of stability of Eq (19).

Now let us investigate the shock structure of the improved high-order model. Using the same method as in the original high-order model, we have

$$[\frac{kv}{k+\kappa} - T(u\zeta - U)(u-U)]\frac{du}{d\xi} = k[u_e(k) - u] \quad (33)$$

Thus, the smooth shock exists if and only if

$$\frac{kv}{k+\kappa} > T(u\zeta - U)(u-U) . \quad (34)$$

Moreover, Comparing Eq (33) with Eq (23), we can see that the shock thickness of the improved high-order model is less than or equal to that of the original high-order model because the coefficient of the left-hand side term of Eq (33) is less than or equal to that of the left-hand side term of Eq (23).

From the above discussion, we can see that the improved high-order model might have more accurate computational results than the original high-order model. However, this conclusion depends on the choice of the parameters κ and ζ. Since the improved high-order model was developed based on the Euler-like discretized form of the original high-order model, the discretized form of the improved high-order model still suffers the same instability problem. Moreover, we cannot use the upwind scheme with flux vector splitting (see next section) to overcome the instability problem of this model because the Jacobian is not homogenous.

2.4 The Semi-Viscous Model (Michalopoulos, 1991, 1993)

Michalopoulos et al. (1991) proposed two high-order continuum models. The first is the semi-viscous model. The second is the viscous model which is presented in the next subsection. The equations for the semi-viscous model are

$$\frac{\partial k}{\partial t} + \frac{\partial q}{\partial x} = g(x,t) \tag{35a}$$

$$\frac{\partial u}{\partial t} + u\frac{\partial u}{\partial x} = \frac{1}{T(k)}[u_f(x) - u] - G\frac{\partial u}{\partial t} - \alpha k^{\beta}\frac{\partial k}{\partial x} \tag{35b}$$

$$q = uk \tag{35c}$$

where, in addition to the previous notation, $u_f(x)$ is a free flow speed, α is the positive constant and $\sqrt{\alpha}$ has the dimension of velocity. β is a parameter and usually chosen as -1. Note that the first term on the right side of Eq (35b) represents relaxation, which is the process whereby drivers adjust their speed to the free flow speed. Thus T(k) is the relaxation time, which is a function of density, and is given as

$$T(k) = T_0[1 + \frac{\gamma k}{k_{jam} - \gamma k}] \tag{36}$$

in which $T_0 > 0$ and $0 < \gamma < 1$ are constants and K_{jam} is the jam density. It should be noted that this relaxation term can contribute to Eq (35b) only when $u_f(x)$ is changed from one section of the roadway to another. The second term on the right side of Eq (35b) addresses the traffic friction at freeway ramp junctions due to ramp flows. G is the friction parameter. It is a function of both roadway conditions and the ramp volume entering or leaving the freeway and is derived experimentally as

$$G = \mu k^{\varepsilon} g \tag{37}$$

where μ is a geometry parameter depending on the type of road geometry, ε is a dimensionless constant, and g is the generation term.

In comparison to the previous models, we can see that the main feature of the semi-viscous model is that the model does not require an explicit equilibrium speed-density relationship. The semi-viscous model seems to be more appealing for field applications, but, because of the simplification, new problems occur. Let us first consider a pipeline case with a fixed free flow speed where the relaxation term has disappeared. The semi-viscous model is reduced to the perfect gas dynamic model:

$$\frac{\partial k}{\partial t} + \frac{\partial (uk)}{\partial x} = 0 \tag{38a}$$

$$\frac{\partial u}{\partial t} + u\frac{\partial u}{\partial x} = -\frac{\alpha}{k}\frac{\partial k}{\partial x} \tag{38b}$$

where the value of β is chosen as -1. It has been shown that, for an originally continuous compression wave, the system described by Eq (38) always yields a discontinuity (Becker, 1968). In fact, Eq (38b) is Greenberg's one-dimensional fluid state equation (Greenberg, 1959). Thus, when the free flow speed is fixed for the pipeline, the semi-viscous model produces the same results as the simple continuum model.

Next, let us consider a pipeline with two different free flow speeds. In this case, we need to use the full form of the semi-viscous model to describe traffic flow. If the free flow speeds are decreasingly distributed on the pipeline, then the contribution of the first term on the right-hand side of Eq (35b) to the upstream always represents acceleration. Clearly, this is not the case. This means that the relaxation process in which the free flow speed serves as the desired state for the adjustment of speed is incorrect. Hence, some modifications to the semi-viscous model are needed.

Nevertheless, when combined with the upwind scheme with flux vector splitting (Steger and Warming, 1981; Hirsch, 1990), the semi-viscous model appears to be working more effectively

than the simple continuum model, the original high-order model and the improved high-order model. This is because the upwind scheme with flux vector splitting introduces physical propagation properties in the discretization process of the semi-viscous model. That is, a forward difference is used for an upstream moving wave and a backward difference for a downstream moving wave. Indeed, applying the upwind scheme with flux vector splitting (which is going to be referred as the "upwind method" from here on) to Eq (35) (for the pipeline case) leads to

For $u_j^n > \sqrt{\alpha}$,

$$k_j^{n+1} = k_j^{n+1} - \frac{\Delta t}{\Delta x}[q_j^n - q_{j-1}^n] \tag{39a}$$

$$q_j^{n+1} = q_j^n - \frac{\Delta t}{\Delta x}\{k_j^n[(u_j^n)^2 + \alpha] - k_{j-1}^n[(u_{j-1}^n)^2 + \alpha]\} + \frac{\Delta t k_j^n}{T(k_j^n)}[u_{f,j} - u_j^n] \tag{39b}$$

$$u_j^{n+1} = q_j^{n+1}/k_j^{n+1} \tag{39c}$$

For $u_j^n < \sqrt{\alpha}$,

$$k_j^{n+1} = k_j^n - \frac{\Delta t}{2\Delta x}[k_j^n(u_j^n + \sqrt{\alpha}) - k_{j-1}^n(u_{j-1}^n + \sqrt{\alpha}) - k_{j+1}^n(u_{j+1}^n - \sqrt{\alpha}) + k_j^n(u_j^n - \sqrt{\alpha})] \tag{40a}$$

$$q_j^{n+1} = q_j^n - \frac{\Delta t}{2\Delta x}[k_j^n(u_j^n + \sqrt{\alpha})^2 - k_{j-1}^n(u_{j-1}^n + \sqrt{\alpha})^2 - k_{j+1}^n(u_{j+1}^n - \sqrt{\alpha})^2 + k_j^n(u_j^n - \sqrt{\alpha})^2] + \frac{\Delta t k_j^n}{T(k_j^n)}[u_{f,j} - u_j^n] \tag{40b}$$

$$u_j^{n+1} = q_j^{n+1}/k_j^{n+1} \tag{40c}$$

Thus, $u_j^n > \sqrt{\alpha}$ represents the uncongested flow, whereas $u_j^n < \sqrt{\alpha}$ represents the congested flow. Finally, the upwind method still introduces a numerical viscosity into the discretized form so that shocks can be smeared out. It should be pointed out that the semi-viscous model should be modified when the free flow speed is not constant.

2.5 The Viscous Model (Michalopoulos et al., 1991)

The viscous model discussed here was proposed by Michalopoulos et al. (1991). The equations for the viscous model are

$$\frac{\partial k}{\partial t} + \frac{\partial q}{\partial x} = g(x,t) \tag{41a}$$

$$\frac{\partial u}{\partial t} + u\frac{\partial u}{\partial x} = -\alpha k^{\beta}\frac{\partial k}{\partial x} + \eta k^{\rho}\frac{\partial^2 u}{\partial x^2} \tag{41b}$$

$$q = uk \tag{41c}$$

where, in addition to the previous notation, η is the viscous parameter and ρ is a dimensionless constant. The first term on the right-hand side of Eq (41b) represents anticipation. The second term on the right-hand side of Eq (41b) is the viscosity term which is used to address traffic friction. It should be noted that the viscous term always exists in the model regardless of the geometry of the freeway. In addition, the viscous model does not use the equilibrium speed-density relationship.

Comparing the semi-viscous model with the viscous model, we can see that the viscous model can be derived from the semi-viscous model if the relaxation term is replaced by the viscous term for the pipeline case. Indeed, both relaxation and viscosity have the same effect -- smearing out of the shock. However, from gas dynamics we know that only when the relaxation time is small, the effect of the relaxation can be replaced by a corresponding bulk viscosity (Talbot and Scala, 1961). As we will see in the next section, the relaxation time in the congested traffic flow is small, whereas the relaxation time in the uncongested traffic flow is large. Therefore, the relaxation process cannot be totally replaced by viscosity. Hence, the viscous model could lead to inaccuracies.

Finally, since the Euler method was used with the viscous model, the discretized form of the viscous model is unstable because this discretized form lacks a positive mass diffusion, even though there is a viscous term in the momentum equation.

3. THE PROPOSED HIGH-ORDER MODEL

As mentioned in section 2.2, the original high-order model considers only the reaction time and ignores the relaxation time. A question that may arise is whether the relaxation property does in fact exist in a macroscopic sense. Clearly, from the microscopic point of view, there is a process of adjusting speed for the second vehicle after the reaction time. Moreover, it has been suggested that drivers have different behavior at different density levels. For example, at low density level, interaction between drivers becomes negligible, but at high density level, the interaction becomes strong. Hence, from the macroscopic point of view, the process of adjusting speed can be considered as the process of relaxation of drivers' speed to the equilibrium speed and the relaxation time at high density level should be shorter than that at low density level in order to avoid a collision. Therefore, we propose the following high-order continuum model:

$$\frac{\partial k}{\partial t} + \frac{\partial q}{\partial x} = g(x,t) \tag{42a}$$

$$\frac{\partial u}{\partial t} + u\frac{\partial u}{\partial x} = \frac{1}{T(k)}[u_e(k) - u] - \frac{\sigma}{k}\frac{\partial k}{\partial x} \tag{42b}$$

$$q = uk \tag{42c}$$

where, in addition to the previous notation, σ is an anticipation constant and $\sqrt{\sigma}$ has the dimension of velocity. $T(k)$ is the relaxation time which should be a function of density k. Since the relaxation time at high density level is shorter than that at low density level, the following general function for $T(k)$ is suggested:

$$T(k) = T_0[1 + \frac{1}{\left(\frac{k}{k_m}\right)^{\theta}}] \tag{43}$$

where k_m , T_0 and θ are parameters. In fact, k_m is the critical density, T_0 is the constant reaction time and $\theta > 0$. Thus, when $k \to 0$, $T(k) \to \infty$; when $k > k_m$, $T(k) \to T_0$. This means that, at high density levels, the relaxation time is equal to the driver's reaction time. This formula of *T(k)* is physically acceptable. Moreover, for simplicity, the following equilibrium speed $u_e(k)$ can be used

$$u_e(k) = u_f[1 - \left(\frac{k}{k_{jam}}\right)^{\varphi}] \tag{44}$$

where φ is a positive parameter. Other forms of u-k relationship can also be used with this model, i.e., the model is independent of the choice of u-k relationship. The above form of Eq (44) was only selected for easy parameter calibration.

In comparison to the original high-order model, we can see that the proposed high-order model takes the relaxation process into account and the relaxation time is treated as a function of the density. In addition, the relaxation time in the new model appears only at the first term of Eq (42b), making the new model more reasonable from the physical point of view and easier to be treated by finite-difference methods.

Comparing the proposed high-order model with the semi-viscous model, we can see that the difference between these two models is that a different relaxation process is adopted by each model. It can be seen that when traffic becomes congested, the relaxation process adopted by the proposed high-order model does not produce the incorrect speed change that occurs in the semi-viscous model.

In order to see a detailed difference between the proposed high-order model and the original high-order model, we linearize the proposed high-order model for small perturbations around the state (k_0, u_0=$u_e(k_0)$). Thus, using the same method as in section 2.2, for the pipeline case we have

$$\frac{\partial \hat{k}}{\partial t} + u_0 \frac{\partial \hat{k}}{\partial x} + k_0 \frac{\partial \hat{u}}{\partial x} = 0 \tag{45a}$$

$$\frac{\partial \hat{u}}{\partial t} + u_0 \frac{\partial \hat{u}}{\partial x} = \frac{1}{T(k_0)}[\hat{k}(\frac{du_e}{dk})_{k_0} - \hat{u}] - \frac{\sigma}{k_0}\frac{\partial \hat{k}}{\partial x} \tag{45b}$$

Manipulating the above linear equations and using

$$c_0 = u_0 + k_0(\frac{du_e}{dk})_{k_0}\ , \tag{46}$$

we have

$$\frac{\partial \hat{k}}{\partial t} + c_0\frac{\partial \hat{k}}{\partial x} = T(k_0)[\sigma\frac{\partial^2 \hat{k}}{\partial x^2} - (\frac{\partial}{\partial t} + u_0\frac{\partial}{\partial x})^2\hat{k}]. \tag{47}$$

It can be shown that the exponential solutions of the linear equation (47) are stable if and only if the following condition holds:

$$u_0 + \sqrt{\sigma} > c_0 > u_0 - \sqrt{\sigma}\ , \tag{48}$$

where the notation is the same as before. Comparing with the stable condition (Eq (19)) of the original high-order model, we can see that, if σ=v/T, then Eq (48) is equal to Eq (19); if σ>v/T, then the range of stability given by Eq (48) is larger than that given by Eq (19); if σ<v/T, then the range of stability given by Eq (48) is smaller than that given by Eq (19). For the cases tested in Section 4, we have σ>v/T so that the range of stability for the proposed high-order model is larger than that of the original high-order model.

Now let us investigate the shock structure of the proposed high-order model for the pipeline case. Using the same method as in section 2.2, we have

$$T(k)[\sigma - (u-U)^2]\frac{dk}{d\xi} = k[u_e(k) - u]. \tag{49}$$

Thus, the smooth shock exists when the following condition holds:

$$\sigma > (u-U)^2\ , \tag{50}$$

where the notation is the same as before. In addition, Comparing Eq (49) with Eq (23), we can see that, when traffic is uncongested, the shock thickness of the proposed high-order model is larger than that of the original high-order model when the value of $T(k)$ is large; when traffic is congested, the shock thickness of the proposed high-order model may be equal to that of the original high-order model because the value of $T(k)$ will approach the constant reaction time.

In order to implement the proposed high-order model, we apply the powerful upwind method to the proposed high-order model for the pipeline case. Thus we have the following discretized form of the proposed high-order model:

For $u_j^n > \sqrt{\sigma}$,

$$k_j^{n+1} = k_j^{n+1} - \frac{\Delta t}{\Delta x}[q_j^n - q_{j-1}^n] \tag{51a}$$

$$q_j^{n+1} = q_j^n - \frac{\Delta t}{\Delta x}\{k_j^n[(u_j^n)^2 + \sigma] - k_{j-1}^n[(u_{j-1}^n)^2 + \sigma]\} + \frac{k_j^n \Delta t}{T(k_j^n)}[u_e(k_j^n) - u_j^n] \tag{51b}$$

$$u_j^{n+1} = q_j^{n+1}/k_j^{n+1} \tag{51c}$$

For $u_j^n < \sqrt{\sigma}$,

$$k_j^{n+1} = k_j^n - \frac{\Delta t}{2\Delta x}[k_j^n(u_j^n + \sqrt{\sigma}) - k_{j-1}^n(u_{j-1}^n + \sqrt{\sigma}) - k_{j+1}^n(u_{j+1}^n - \sqrt{\sigma}) + k_j^n(u_j^n - \sqrt{\sigma})] \tag{52a}$$

$$q_j^{n+1} = q_j^n - \frac{\Delta t}{2\Delta x}[k_j^n(u_j^n + \sqrt{\sigma})^2 - k_{j-1}^n(u_{j-1}^n + \sqrt{\sigma})^2 - k_{j+1}^n(u_{j+1}^n - \sqrt{\sigma})^2 + k_j^n(u_j^n - \sqrt{\sigma})^2] + \frac{k_j^n \Delta t}{T(k_j^n)}[u_e(k_j^n) - u_j^n] \tag{52b}$$

$$u_j^{n+1} = q_j^{n+1}/k_j^{n+1} \,. \tag{52c}$$

It should be noted that preliminary results show that a high-order TVD method is computationally very expensive and less accurate than the first-order upwind method used, because the former results in shock waves sharper than they are in reality. However, implicit methods have some merits (Chronopoulos et al, 1993) and should be investigated further.

4. TEST RESULTS

4.1 Preliminary Testing

In this subsection we investigate the continuum models discussed above based on hypothetical cases in order to find the model that can produce a reasonable description of traffic when an incident occurs downstream. For this reason, we assume four hypothetical cases described next. The freeway geometry for these four cases is a three-lane pipeline section with 18000 feet long which is shown in Figure 1. The arrival and departure traffic patterns (flow and speed) for the four cases are shown in Figures 2, 3, 4 and 5, respectively. The analysis period for the first three cases is 15 minutes. For case 4 the analysis period is 35 minutes. For cases 1, 2 and 3, traffic flow during the first 5 minutes is assumed to be uncongested. After the first 5 minutes congestion occurs at the downstream end and continues for 5 minutes. Then the incident is removed from the downstream end. The differences among these three cases are that they have the different intensities of congestion. The intensity of congestion for case 1 is light, for case 2 medium, and for case 3 strong. Case 4 is a combination of cases 1, 2 and 3. In order to compare the results produced by the proposed high-order model, the simple continuum model and the original high-order model as well as the improved high-order model, the equilibrium speed-density relationship of KRONOS (Michalopoulos et al., 1992) was used for implementing these models. This relationship is

$$u_e(mile/hr) = \begin{cases} 65 & for\ k \le 15 (veh/mile) \\ -\frac{1125}{1849}k + \frac{130500}{1849} + \frac{98400}{1849k} & for\ 15 \le k \le 58 \\ -\frac{525}{4096}k + \frac{15225}{1024} + \frac{1708875}{1024k} & for\ 58 \le k \le 186 \end{cases}$$

In this subsection, first a theoretical analysis of shock waves is done. Then the simulation results are given.

4.1.1 Theoretical Analysis of Shock waves

In case 1, we assume that the volume at the downstream boundary decreases from 5000 (veh/hr/3-lanes) to 4000 (veh/hr/3-lanes) and the corresponding speed also decreases from 53.226 (mile/hr) to 9.851 (mile/hr). Thus, the speed, u_s, of the shock wave is calculated by

$$u_s = \frac{4000-5000}{\frac{4000}{9.851}-\frac{5000}{53.226}} = \frac{-1000}{312.11} = -3.2(mile/hr) = -4.7(feet/\sec).$$

Hence, after 5 minutes, the shock wave will propagate backwards 1410(= 4.7×300) feet.

For case 2, we assume that the volume at the downstream boundary decreases from 5000 (veh/hr/3-lanes) to 2000 (veh/hr/3-lanes) and the corresponding speed also decreases from 53.226 (mile/hr) to 4.072 (mile/hr). Therefore, the speed, u_s, of the shock wave can be given by

$$u_s = \frac{2000-5000}{\frac{2000}{4.072}-\frac{5000}{53.226}} = \frac{-3000}{397.22} = -7.55(mile/hr) = -11.08(feet/\sec).$$

Thus, after 5 minutes, the shock wave will go backwards 3323(= 11.08×300) feet.

In case 3, we assume that the volume at the downstream boundary decreases from 5000 (veh/hr/3-lanes) to 1000 (veh/hr/3-lanes) and the corresponding speed also decreases from 53.226 (mile/hr) to 1.90 (mile/hr). Therefore, the speed, u_s, of the shock wave is calculated by

$$u_s = \frac{1000-5000}{\frac{1000}{1.9}-\frac{5000}{53.226}} = \frac{-4000}{432.377} = -9.25(mile/hr) = -13.57(feet/\sec).$$

Thus, the shock wave will spillback 4071(= 13.57×300) feet after 5 minutes.

Case 4 is the combination of cases 1, 2 and 3. First, after reducing from 5000 (mile/hr/3-lanes) to 4000 (veh/hr/3-lanes), the volume at the downstream boundary continues to decrease to 2000 (veh/hr/3-lanes) and the corresponding speed also decreases to 4.072 (mile/hr). Thus, the speed, u_s, of the shock wave is calculated by

$$u_s = \frac{2000 - 4000}{\frac{2000}{4.851} - \frac{4000}{9.851}} = \frac{-2000}{85.11} = -23.5(mile/hr) = -34.47(feet/\sec).$$

Therefore, the shock wave will go backwards 10,341(= 34.47×300) feet.

Next, the volume decreases from 2000 (veh/hr/3-lanes) to 1000 (veh/hr/3-lanes) and the relative speed decreases from 4.072 (mile/hr) to 1.90 (mile/hr). Thus, the speed of the shock wave is

$$u_s = \frac{1000 - 2000}{\frac{1000}{1.90} - \frac{2000}{4.072}} = \frac{-1000}{35.16} = -28.44(mile/hr) = -41.72(feet/\sec).$$

Hence, after 5 minutes, the shock wave will propagate backwards 12515(= 41.72×300) feet.

4.1.2 Simulation Results

In this subsection, we will show all the simulation results of the hypothetical cases. The simulation results for the simple continuum model come from KRONOS (version 7.2L). For the high-order models we have created a versatile code that allows the model and the numerical method to be chosen by the user. We have also implemented CORFLO (FHWA, 1992) which is based on the original high-order model with the discretization of the Euler method. Since there were some difficulties with the implementation of CORFLO for the boundary conditions needed in the tested cases, results from our own implementation of the Euler discretized form of the original high-order model will be also shown for cases 1 and 2.

In case 1, the simulation results of 5-minute average volume produced by KRONOS, CORFLO, the improved high-order model, the semi-viscous model and the viscous model as well as the proposed high-order model are shown in Figure 6. The results of 5-minute average speed are shown in Figure 7. Figure 8 shows the results of 5-minute average density produced by KRONOS, the improved high-order model, the semi-viscous model and the viscous model as

well as the proposed high-order model. From Figures 6.2 and 7.2, it is clear that CORFLO cannot capture the shock wave. However, from Figures 6.3, 7.3 and 8.2, we can see that the results from the our own implementation of the Euler discretized form of the original high-order model match the shock wave. We think that the reason for this difference is that CORFLO has some limitation on the boundary condition.

KRONOS can capture the basic shock wave propagation (see Figures 6.1, 7.1 and 8.1). However, it is observed that an overshoot of the shock wave is produced by KRONOS. Looking at the results produced by the improved high-order model (see Figures 6.4, 7.4 and 8.3), we can see that the improved high-order model can basically capture the shock wave in this case.

Comparing the results produced by the proposed high-order model and the semi-viscous model (see Figures 6.5, 6.8, 7.5, 7.8, 8.4 and 8.7), we can see that there are some differences although the differences are small. The first difference is that the proposed high-order model is more accurate in capturing the shock wave than the semi-viscous model. The shock wave in the proposed high-order model can propagate backwards between 1400 and 1600 feet which is the same as the theoretic value. But the shock wave in the semi-viscous model can only go backwards 1200 feet. The second difference is that the proposed high-order model discharges the queue more quickly than the semi-viscous model does.

It is surprising that the viscous model cannot capture the shock wave (see Figures 6.6, 6.7, 7.6, 7.7, 8.5 and 8.6). In principle, the viscous model should produce a smooth shock. Unfortunately, the computational results of the viscous model do not match the theoretical results. The reason for this is that, we think, the explicit Euler method is applied to the viscous model. This implies that a finite-difference method seriously affects the computational effects of

a traffic flow model. Since the Euler discretized form of the viscous model cannot capture the shock wave in this case, we will no longer investigate the viscous model in the following cases.

In case 2, the simulation results of 5-minute average volume produced by KRONOS, CORFLO, the improved high-order model and the semi-viscous model as well as the proposed high-order model are shown in Figure 9. The results of 5-minute average speed are shown in Figure 10. Figure 11 shows the results of 5-minute average density produced by KRONOS, the improved high-order model and the semi-viscous model as well as the proposed high-order model. From Figures 9.2 and 10.2, it is clear that, like case 1, CORFLO cannot capture the shock wave for this heavy congestion case. Our own implementation of the Euler discretized form of the original high-order model did not capture the shock wave, either (see Figures 9.3, 9.4, 10.3, 10.4, 11.2 and 11.3). We believe this is because of the Euler method. In order to demonstrate this assertion, we applied the upwind scheme with flux vector splitting to the original high-order model. The results shown in Figures 9.5, 10.5 and 11.4 indicate that the upwind discretized form of the original high-order model can capture the shock wave in this case.

From the results produced by KRONOS in this case (see Figures 9.1, 10.1 and 11.1), we can still draw the same conclusions as those in case 1. From the results produced by the improved high-order model in this case (see Figures 9.6, 9.7, 10.6, 10.7, 11.5 and 11.6), we can see that, unlike case 1, the improved high-order model cannot correctly capture the shock wave for this heavy congestion case. This is also because of the Euler method.

Comparing the results produced by the proposed high-order model and the semi-viscous model (see Figures 9.8, 9.9, 10.8, 10.9, 11.7 and 11.8), we can still see that there are those differences like case 1. It should be pointed out that, in order to match the setting values at the

downstream boundary for congested traffic in case 2, we adjusted the value of α of the semi-viscous model.

In case 3, the simulation results of 5-minute average volume produced by KRONOS, CORFLO, the improved high-order model and the semi-viscous model as well as the proposed high-order model are shown in Figure 12. The results of 5-minute average speed are shown in Figure 13. Figure 14 shows the results of 5-minute average density produced by KRONOS, the improved high-order model and the semi-viscous model as well as the proposed high-order model. From these figures, we can still get the same conclusions for each model as those in case 2. It is worth noting that, although the parameters ν and τ were adjusted, the improved high-order model cannot capture the shock wave. This means that the ability of the improved high-order model to capture a correct shock wave is limited. The reason for this is that, we still think, the explicit Euler method is applied to the improved high-order model.

In case 4, the simulation results of 5-minute average volume produced by KRONOS, CORFLO, the improved high-order model and the semi-viscous model as well as the proposed high-order model are shown in Figure 15. The results of 5-minute average speed are shown in Figure 16. Figure 17 shows the results of 5-minute average density produced by KRONOS, the improved high-order model and the semi-viscous model as well as the proposed high-order model. From Figures 15.2 and 16.2, it is clear that, like cases 1, 2 and 3, CORFLO cannot capture the shock wave.

From Figures 15.1 and 16.1, it is interesting to see that the speed of KRONOS seems to be distributed discontinuously on the freeway and that the overshoot in this case is smaller than those in the previous cases. From Figures 15.3, 16.3 and 17.2, we can see that the improved

high-order model cannot correctly capture the shock wave except for the situation in which the volume decreases from 5000 (veh/hr/3-lanes) to 4000 (veh/hr/3-lanes).

Comparing the results produced by the proposed high-order model and the semi-viscous model (see Figures 15.4, 15.5, 16.4, 16.5, 17.3 and 17.4), we can still see that there are those differences like case 1. Moreover, it can be observed that the setting values at the downstream boundary for congested traffic were not matched by the simulation results produced by the semi-viscous model. This shows that we need the different value of the anticipation parameter α for the different case.

Through the hypothetical cases, we can get the following conclusions:

1). CORFLO cannot correctly capture shock waves.

2). The improved high-order model can only capture a weak shock wave.

3). KRONOS produces an overshoot in volume when traffic becomes congestion. In addition, the speed produced by KRONOS becomes discontinuous when traffic congestion becomes heavier.

4). Comparing simulation results with the theoretic results, it can be said that the proposed high-order model is more accurate than the semi-viscous model in capturing the shock wave. Moreover, the proposed high-order model can discharge the queue more quickly than the semi-viscous model does.

5). The anticipation parameter α in the semi-viscous model needs to be adjusted case by case in order to match the setting condition at the downstream boundary for congested traffic.

6). The Euler discretized form of the viscous model does not make the model work well.

7). Comparing the Euler method with the upwind scheme with flux vector splitting regardless of the models, it can be said that the Euler method is not a good finite-difference method for the numerical simulation of traffic flow models. The upwind scheme with flux vector splitting should be strongly recommended for accuracy.

4.2 Parameter Calibration

We have shown that all the high-order continuum models include parameters. So, before using these models with field data, we need to calibrate these parameters. In the past, the calibration of parameters was done by a trial-and-error. This kind of calibration process is very time-consuming and requires a lot of effort. In order to minimize the effort, we have developed a procedure for parameter calibration which has been incorporated in our simulation program without user interface beyond the supply of field data.

This parameter calibration is considered as an optimization problem in which the objective function is defined as follows:

$$\min \ f(x_1, x_2, \ldots x_p) = \sum_{i=1}^{n} \{MSE_i(V) + MSE_i(S)\} \tag{53}$$

where x_j (j=1, 2, ... p) are parameters to be calibrated. n is the number of check points. and

$$MSE(y) = \frac{1}{N} \sum_{i=1}^{N} [y_i^o - y_i^c]^2 \tag{54}$$

in which y stands for volume or speed, y^o is the observed data and y^c is the computed result. N is the number of observations. The optimization procedure is based on the Fletcher-Reeves conjugate method (Luenberger, 1973). The gradients in this method are evaluated by a finite-difference approximation in the procedure. Thus, by using this optimization procedure in

parameter calibration, the minimization of the objective function, Eq (53), at least local minimization, yields an optimized set of parameters. Other more sophisticated optimization strategies (e.g., Monte Carlo methods) will be explored in the future.

4.3 Testing with Field Data

In this subsection, three test cases (5, 6 and 7) with field data are presented. Case 5 is based on a two-lane freeway of the Minneapolis I-35W between the 76th and 70th streets. Traffic data used by case 5 were the northbound traffic, which went into the metro area during the morning peak period from 6:30am to 8:30am on Nov. 7, 1989. The roadway geometry and arrival and departure traffic patterns for case 5 are shown in Figure 18. Case 6 is based on a four-lane freeway from the I-35W close to downtown Minneapolis, starting from 26th street and ending at 31st street. Traffic data used by case 6 were the southbound traffic, which came out of Minneapolis during the afternoon peak period from 4:00pm to 6:30pm on Nov. 14, 1989. Congestion started at 4:05pm at the downstream boundary and lasted two hours and 15 minutes. The geometry and arrival and departure patterns for case 6 are shown in Figure 19. Case 7 uses the same geometry as in case 6 but the different traffic data from 3:00pm to 7:00pm on Nov. 20, 1989. Congestion starts at 4:40pm at the downstream boundary and lasts one hour. Figure 20 shows the arrival and departure patterns for case 7.

In order to evaluate each model quantitatively, the following statistics are calculated to get the error indices based on the deviations of simulation results from the field observations:

$$Mean\ Absolute\ Error\ (MAE) = \frac{1}{N}\sum_{1}^{N} |Observed - Computed|$$

$$Mean\ Percentage\ Error\ (MPE) = \frac{1}{N}\sum_{1}^{N}\frac{|Observed - Computed|}{Observed}$$

$$Mean\ Square\ Error\ (MSE) = \frac{1}{N}\sum_{1}^{N}(Observed - Computed)^2$$

$$Std.\ Deviation = \sqrt{\frac{1}{N-1}\sum_{1}^{N}(Observed - Computed)^2}$$

where N is the number of observations (i.e., the number of time intervals).

In these three cases, we also investigate six models, namely, the simple continuum model, the original high-order model (the CORFLO program), the improved high-order model, the semi-viscous model, the viscous model and the proposed high-order model. Δx=200 ft and Δt=1 sec are adopted for each model except the simple continuum model and CORFLO in which Δx=100 ft and Δt=1 sec are adopted. In fact, the step size in space and time (Δx=100 ft and Δt=1 sec) are determined internally in CORFLO. The u_e-k curve wherever it applies was obtained from data collected from I-35W. CORFLO has built in three types of u_e-k curves to choose from, all the three types have been tried and the best results are presented. Except for the simple continuum model and CORFLO, the parameters in the other four models were calibrated by using the optimization procedure mentioned in subsection 4.2.

Results for the three test cases are shown in tables 1, 2 and 3. It can be seen that

a) when there is no downstream congestion (as in case 5), all models including the simple continuum model performed at about the same error level except CORFLO.

b) when downstream congestion begins, different model produces different results. The simple continuum model gave very good results that were better than CORFLO. Comparing the results produced by CORFLO and the improved high-order model, which are solved with the same numerical method, we can see that the improved high-order model was more accurate than the original high-order model. It is clear that

the proposed high-order model was the overall best in terms of accuracy with a MSE of 290 for case 6 and a MSE of 216 for case 7. The viscous model produces a larger error in MSE than the other high-order models (except CORFLO).

c) All the high-order models except the proposed high-order model use the different values of parameters for cases 5, 6 and 7, respectively, in order to get good results. This means that the proposed high-order model is the easiest one to calibrate.

d). From Tables 2.1, 2.2, 3.1 and 3.2, it can be seen that the results from the simple continuum model seem to be relatively sensitive to the choice of the speed-density relationship. The proposed high-order model is less dependent of the choice of the speed-density relationship.

e). Comparing the results produced by the original high-order model with the Euler method and the upwind method, it can be seen that the upwind method gives better results.

5. CONCLUSIONS

Five existing continuum models plus a proposed high-order model have been reviewed. Merits and limitations of the various formulations were identified. Preliminary comparative testing of the models was also undertaken. From the hypothetical cases which were constructed with the assumption of a downstream incident, we can see that the simple continuum model, the semi-viscous model and the proposed high-order model properly capture the shock wave structure. The ability of CORFLO (the original high-order model), the improved high-order model and the viscous model to capture accurately shock waves is limited.

In our preliminary testing with field data, we can see that all models including the simple continuum model give reliable results. For uncongested cases tested, no apparent merit of high-order modeling versus simple continuum modeling was found. For congested cases tested most high-order models show some error reductions. For all the cases we tested, the proposed high-order model seems to produce a smaller error than the other models. Moreover, the proposed high-order model has the strong robust property of parameters for various cases, that is, the parameters are independent of cases. This property is very important for implementing the proposed high-order model in practice because one can use only a set of precalibrated parameters.

For finite-difference methods, the Euler method is not a good method for the numerical implementation of traffic flow models. The upwind scheme with flux vector splitting is recommended for computational accuracy and efficiency.

Finally, the simple continuum model is more sensitive to the choice of the speed-density relationship, whereas the proposed high-order model is less sensitive.

REFERENCES

Anderson, D.A., Tannehill, J.C. and Pletcher, R.H. (1984) *Computational Fluid Mechanics and Heat Transfer.* Hemisphere Publishing. Cambridge.

Becker, E. (1968) *Gas Dynamics.* Academic Press. New York.

Chronopoulos, A., Michalopoulos, P.G. and Donohoe, J. (1992) "Efficient Traffic Flow Simulation Computations." *Mathl. Comput. Modelling.* Vol. 16, No. 5, pp107-120.

Chronopoulos, A., Lyrintzis, A.S., Michalopoulos, P.G., Rhee, C. and Yi, P. (1993) "Traffic Flow Simulation Through High-Order Traffic Modelling" *Mathl. Comput. Modelling.* Vol. 17, No. 8, pp11-22.

Federal Highway Administration (FHWA) (1992) *TRAF User Reference Guide.*

Gerlough, D.L. and Huber, M.J. (1975) *Traffic Flow Theory.* Special Report 165. TRB. Natl. Res. Council., Washington, D.C.

Greenberg, H. (1959) "An Analysis of Traffic Flow." *Oper. Res.*, 7(1). pp79-85.

Hirsch, C. (1988) *Numerical Computation of Internal and External Flows. Vol 1: Fundamentals of Numerical Discretization.* John Wiley & Sons. Chichester.

Hirsch, C. (1990) *Numerical Computation of Internal and External Flows. Vol 2: Computational Methods for Inviscid and Viscous Flows.* John Wiley & Sons. Chichester.

Hirt, C.W. (1968) "Heuristic Stability Theory for Finite-Difference Equations." *Jour. Comp. Phys.* 2. pp339-355.

Kühne, R. (1984) " Macroscopic Freeway Model for Dense Traffic - Stop-Start Waves and Incident Detection". *9th Int. Symp. on Transportation and Traffic Theory,* VNU Science Press. pp21-42.

Lax, P.D. (1954) "Weak Solution of Non-linear Hyperbolic Equations and Their Numerical Computations." *Communs. Pure Appl. Math.* 7. pp159-173.

Leo, C.J. and Pretty, R.L. (1992) "Numerical Simulation of Macroscopic Continuum Traffic Models." *Transpn. Res.* 26B. pp207-220.

Lighthill, M.H. and Whitham, G.B. (1955) "On Kinematic Waves II: A Theory of Traffic Flow on Long Crowded Roads." *Proc. R. Soc. London Ser.* A. 229. pp317-345.

Luenberger, D.G. (1973) *Introduction to Linear and Nonlinear Programming.* Addison-Wesley. New York.

Lyrintzis, A.S., Michalopoulos, P.G., Chronopoulos, A., Yi, P., Liu, G. and Rhee, C. (1992) "Development of Advanced Traffic Flow Models and Implementation in Parallel Processing [phase I]." Final Report. Center for Transportation Studies, University of Minnesota. Minneapolis, Minnesota.

Lyrintzis, A.S., Liu, G. and Michalopoulos, P.G (1994) "Development and Comparitive Evaluation of High-Order Traffic Flow Models." Presented at the 73rd Annual Conference of Transportation Research Board, Washington, D.C., Jan. 9-13, 1994 (To be appeared on Transportation Research Record).

Michalopoulos, P.G. and Lin, J. (1985) "A Freeway Simulation Program for Microcomputers." *Proc. of the 1st National Conf. on Microcomputers in Urban Transp.,* ASCE, California. pp330-341.

Michalopoulos, P.G., Yi, P. Beskos, D.E. and Lyrintzis, A.S. (1991) "Continuum Modeling of Traffic Dynamics." *Proc. of the 2nd Int. Conf. on Appl. of Advanced Tech. in Transportation Eng.*, August 18-21. Minneapolis, Minnesota. pp36-40.

Michalopoulos, P.G., Kwon, E., Lee, C.-F., Mahadevan, G., and Kang, J.-G. (1992) " Development of an Integrated Simulation Package for Freeway Design, Operations and Adaptive Traffic Management [phase 1: Enhancement of the KRONOS Simulation Program]." Final Report. Center for Transportation Studies, University of Minnesota. Minneapolis, Minnesota.

Michalopoulos, P.G, Yi, P. and Lyrintzis, A.S. (1993) "Development of an Improved High Order Continuum Traffic Flow Model." *Transpn. Res. Rec.* 1365. pp125-132.

Papageorgiou, M. (1983) "A Hierarchical Control System for Freeway Traffic." *Transpn. Res.* 17B. pp251-261.

Papageorgiou, M., Blosseville, J.M. and Hadj-Salem, H. (1989) "Macroscopic Modelling of Traffic Flow on the Boulevard Peripherique in Peris." *Transpn. Res.* 23B. pp 29-47.

Payne, H.J. (1971) "Models of Freeway Traffic and Control." *Mathematical Models of Public Systems* (G.A. Bekey ed). Simulation Counc. Proc. Ser., 1. pp51-61.

Payne, H.J. (1979) "FREFLO: A Macroscopic Simulation Model of Freeway Traffic." *Transpn. Res. Rec.* 722. pp68-77.

Pihillips, W. F. (1979) "A New Continuum model for Traffic Flow". Utah State Univ., Logan, Utah. Report DOT-RC-82018, 1979.

Ross, P. (1988) "Traffic Dynamics", *Transp. Res.* 22B. pp421-435.

Steger, J.L. and Warming, R.F. (1981) "Flux Vector Splitting of the inviscid gas-dynamic equations with applications to finite difference methods." *Jour. Comp. Phys.* 40. pp263-293.

Talbot, L. and Scala, S.M. (1961) "Shock Wave Structure in a Relaxing Diatomic Gas." *Advan. Appl. Mech.* (H.L. Dryden and T. Von Karman, eds.), Supplement 1. Academic, New York. pp603-622.

Whitham, G.B. (1974) *Linear and Nonlinear Waves.* John Wiley & Sons. New York.

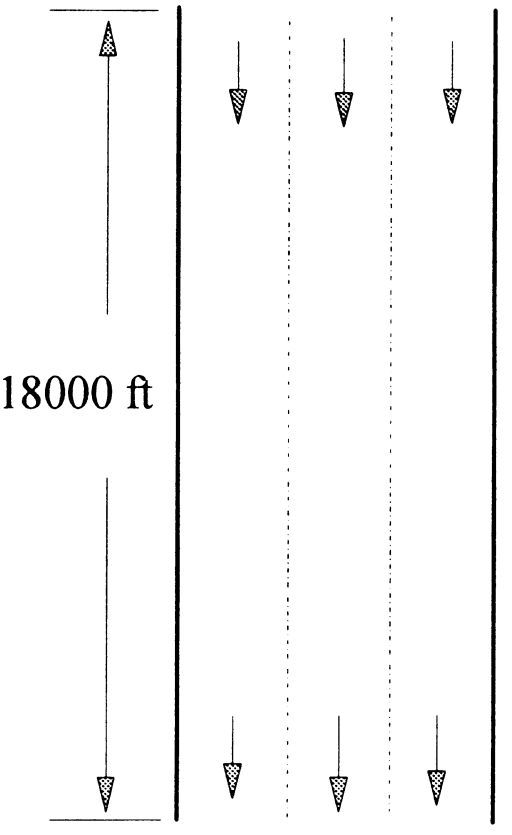

Figure 1. Geometry for hypothetical cases

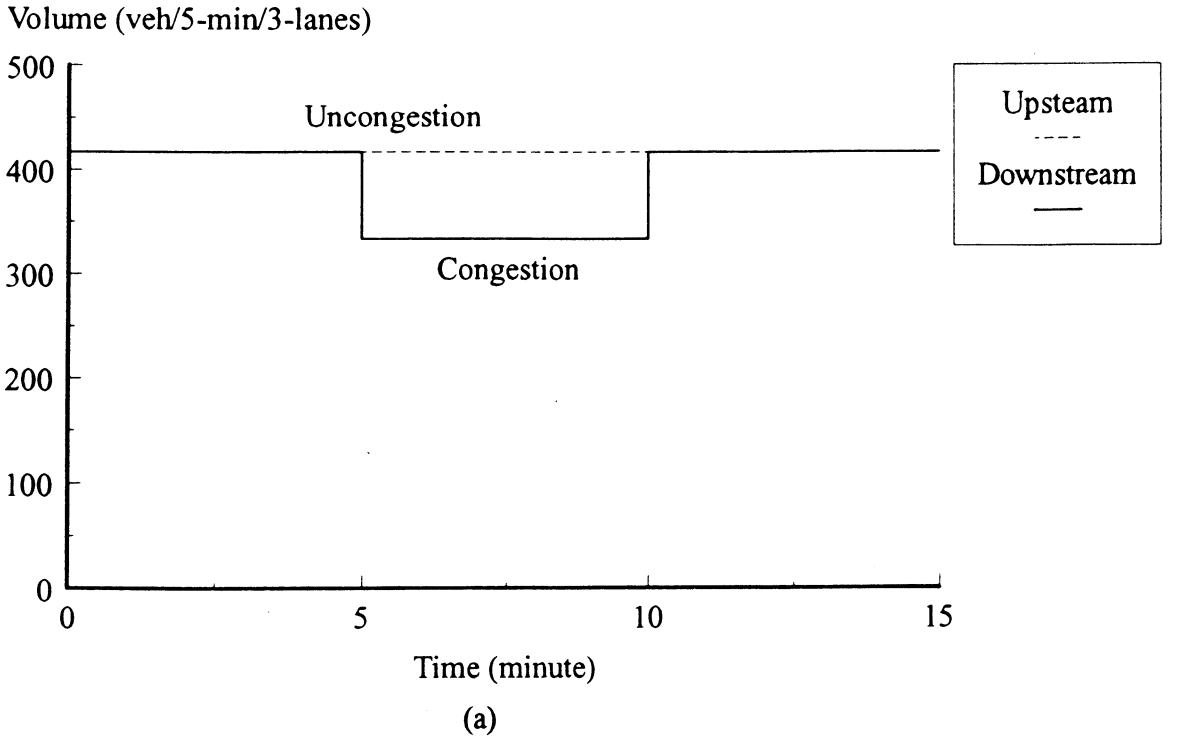

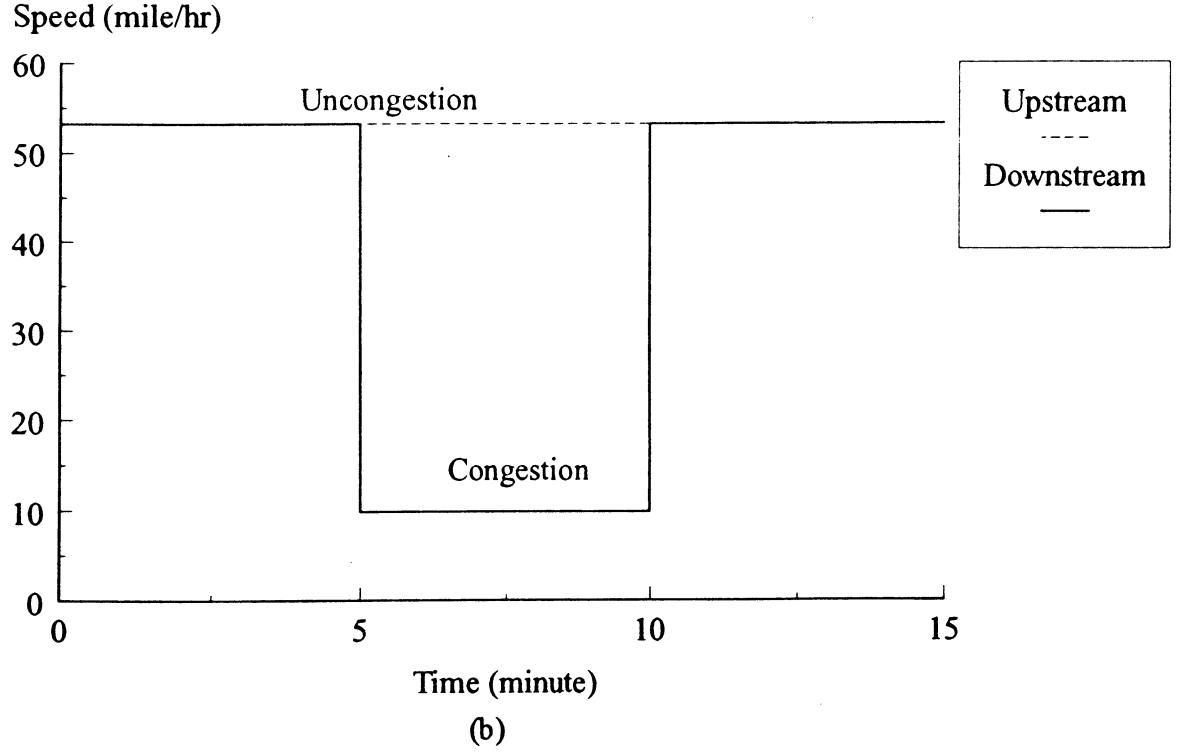

Figure 2. (a) Volume and (b) Speed at Upstream and Downstream boundaries for case 1.

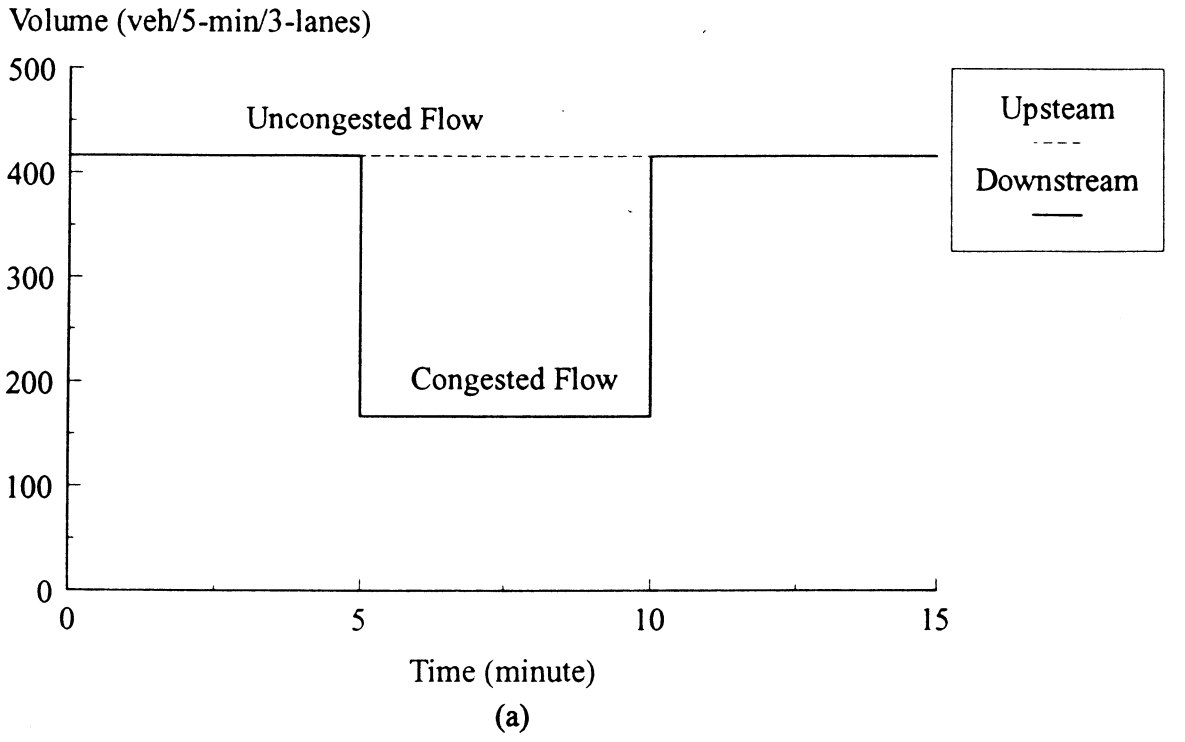

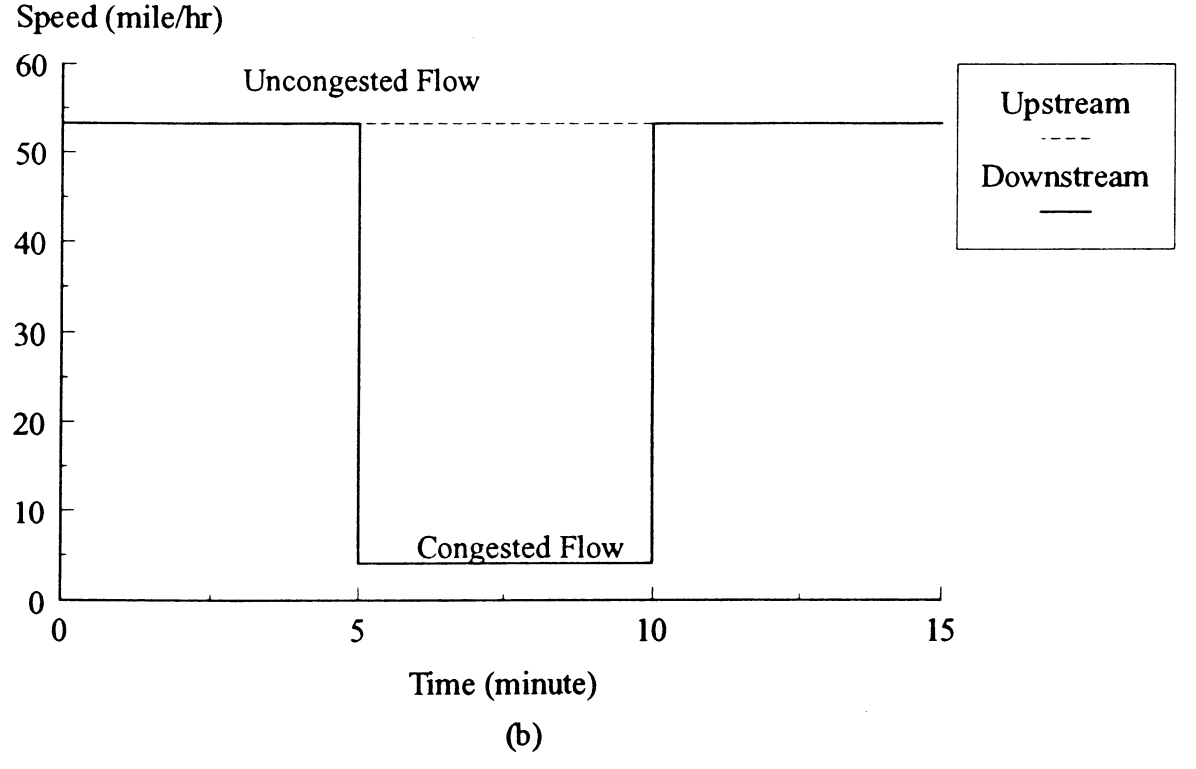

Figure 3. (a) Volume and (b) Speed at the upstream and downstream boundaries for case 2.

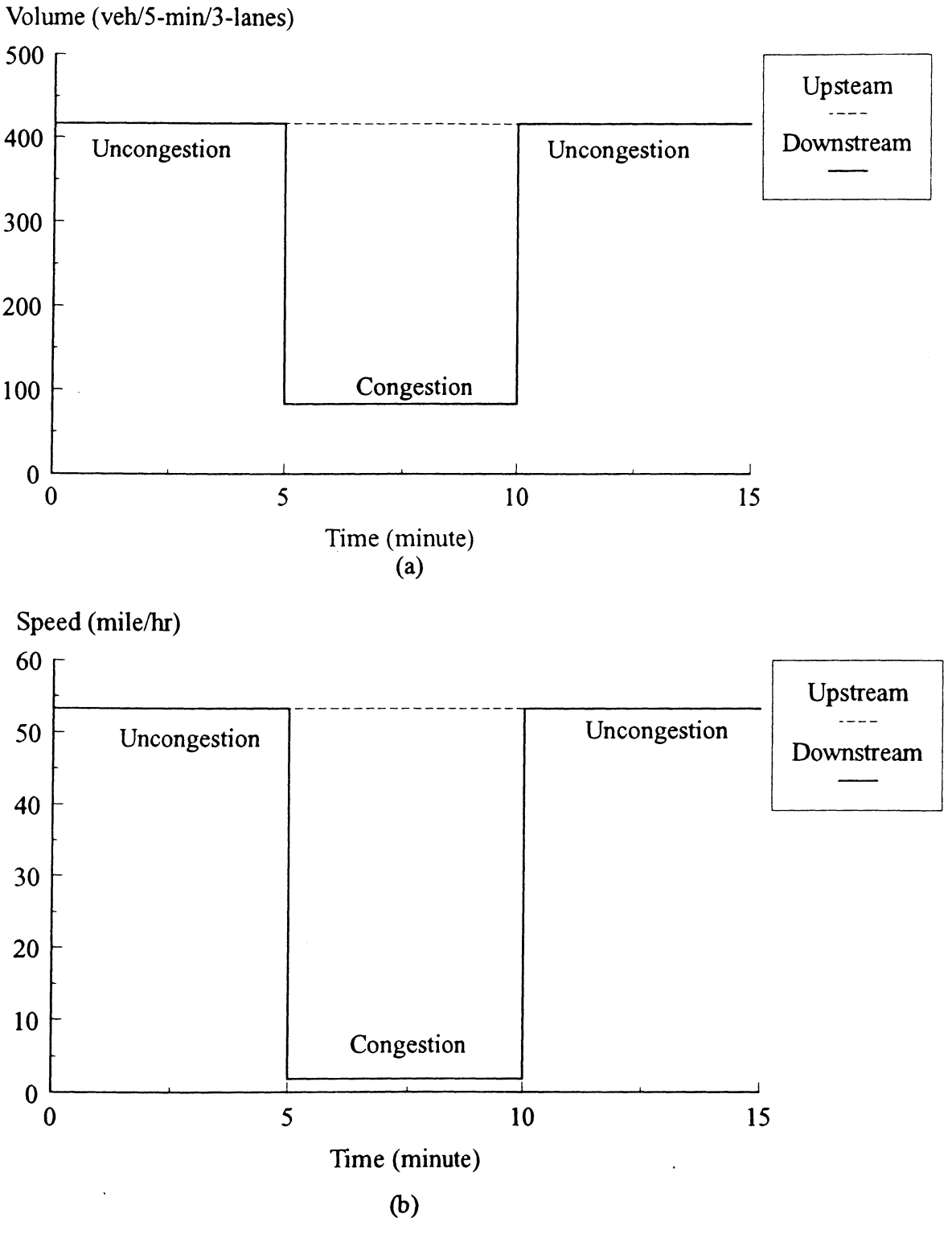

Figure 4. (a) Volume and (b) Speed at Upstream and Downstream boundaries for case 3.

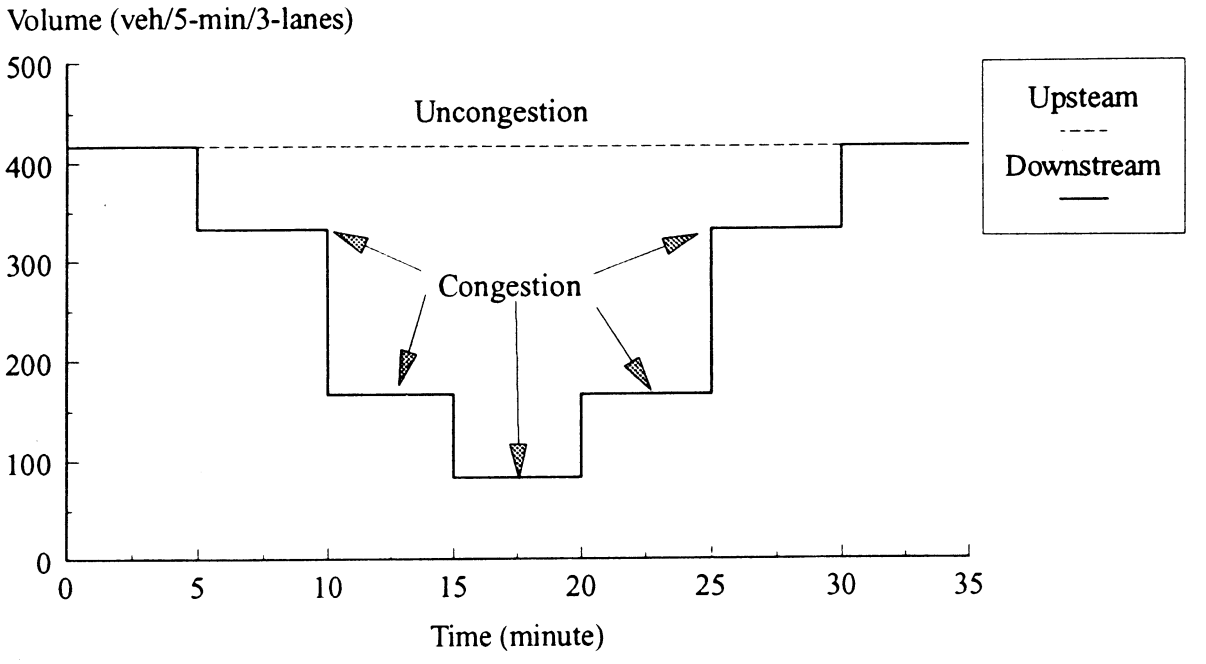

(a)

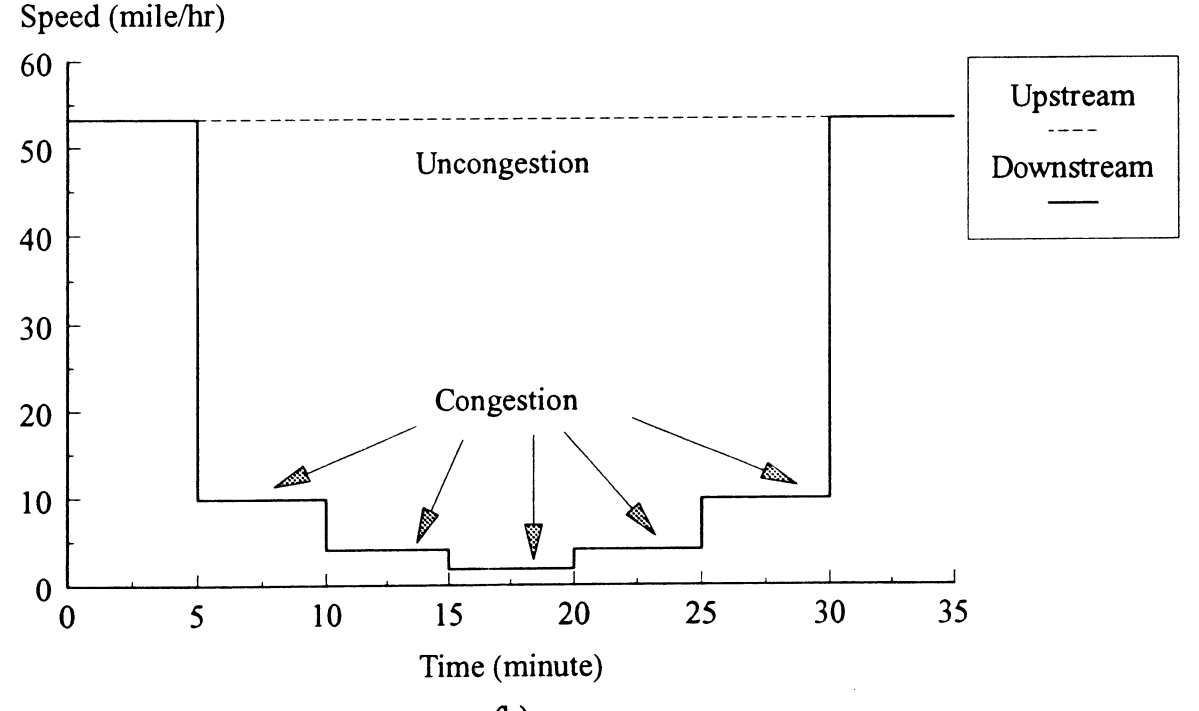

(b)

Figure 5. (a) Volume and (b) Speed at Upstream and Downstream boundaries for case 4.

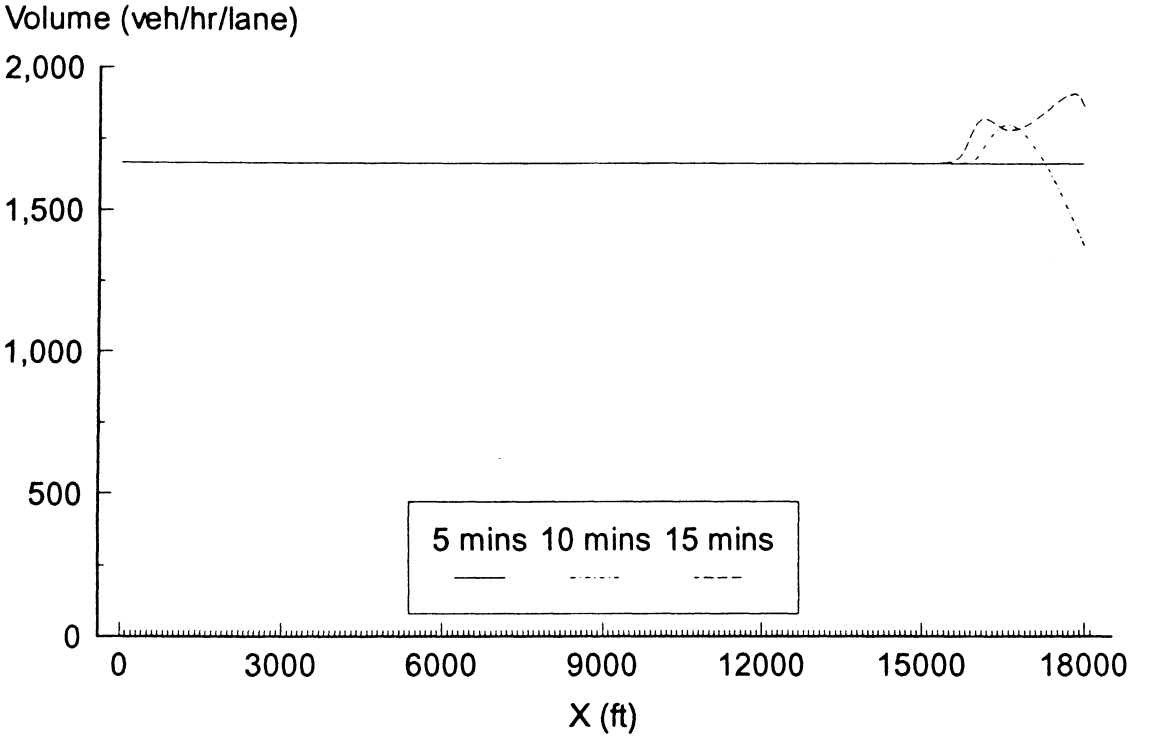

Figure 6.1 5-minute average volume produced by KRONOS for case 1.

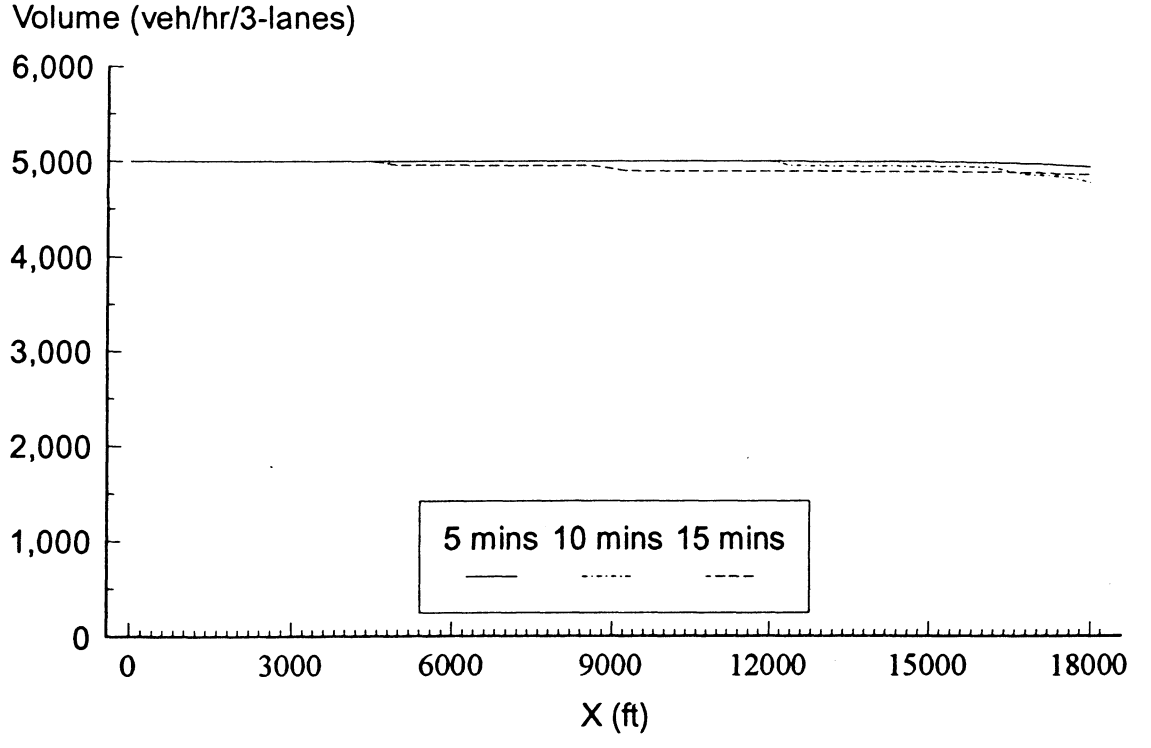

Figure 6.2 5-minute average volume produced by CORFLO for case 1.

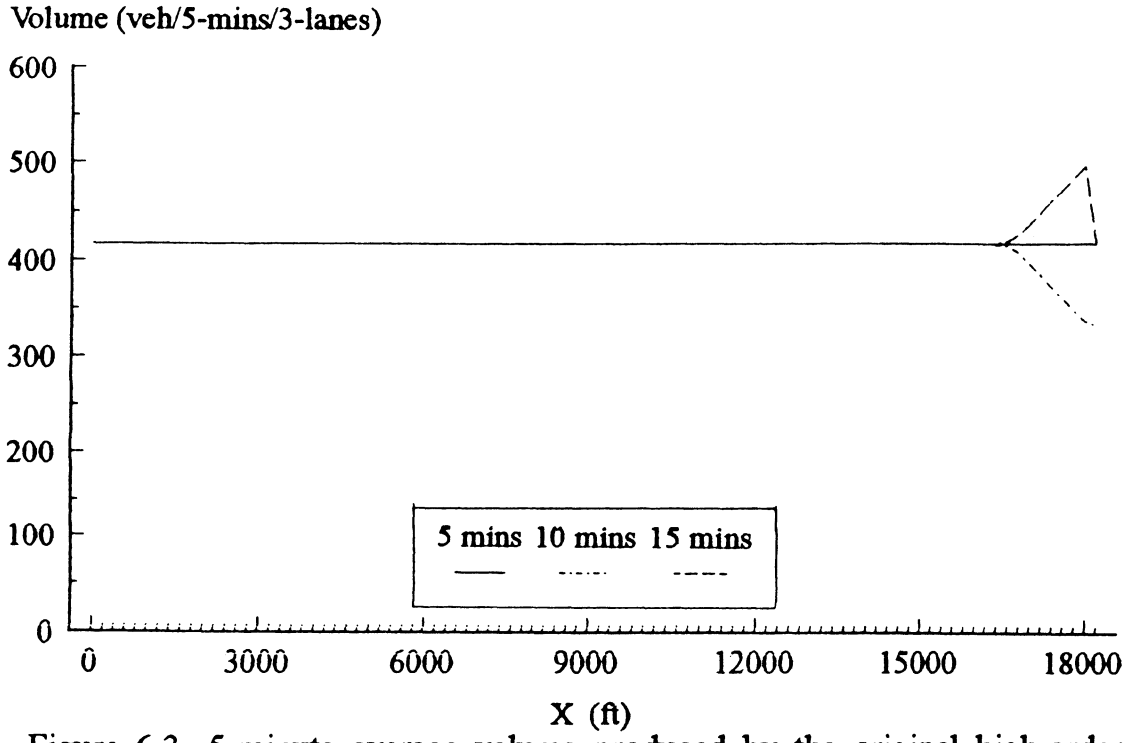

Figure 6.3 5-minute average volume produced by the original high-order model (Euler method) for case 1 when ν = 6250.0 (feet^2/sec) and τ = 2.0 (sec).

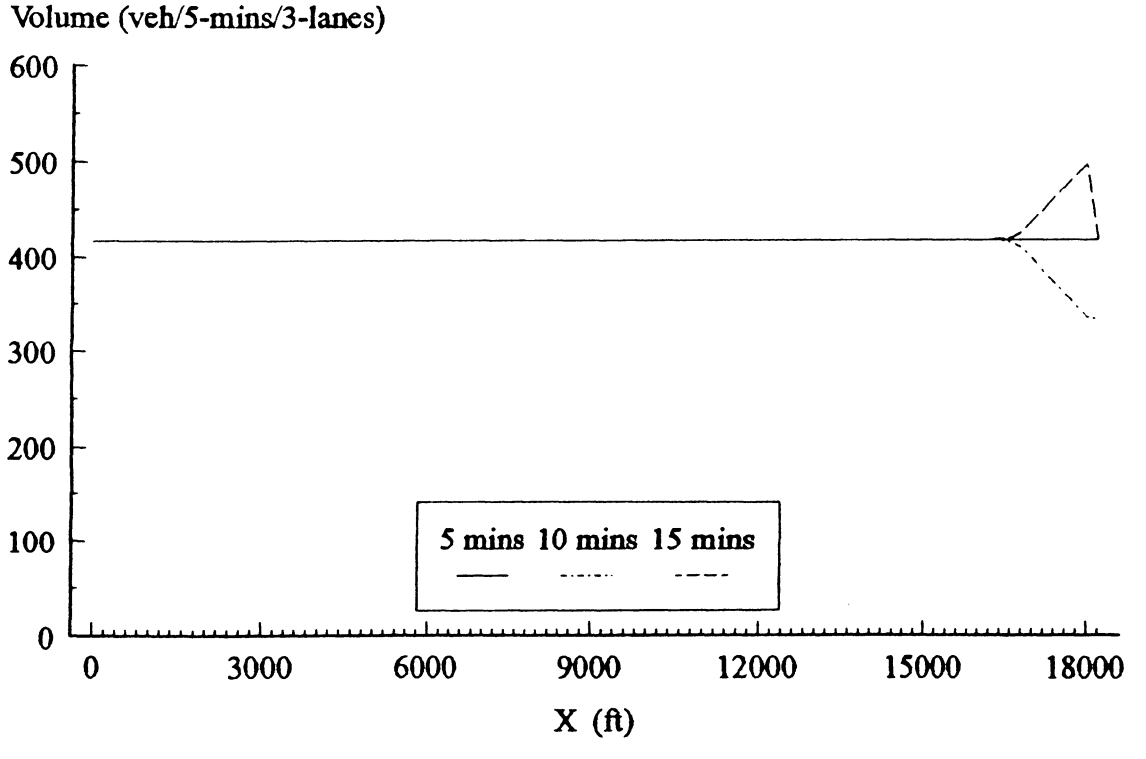

Figure 6.4 5-minute average volume produced by the improved high-order model (Euler method) for case 1 when ν = 68070.0 (feet^2/sec) and τ = 36 (sec).

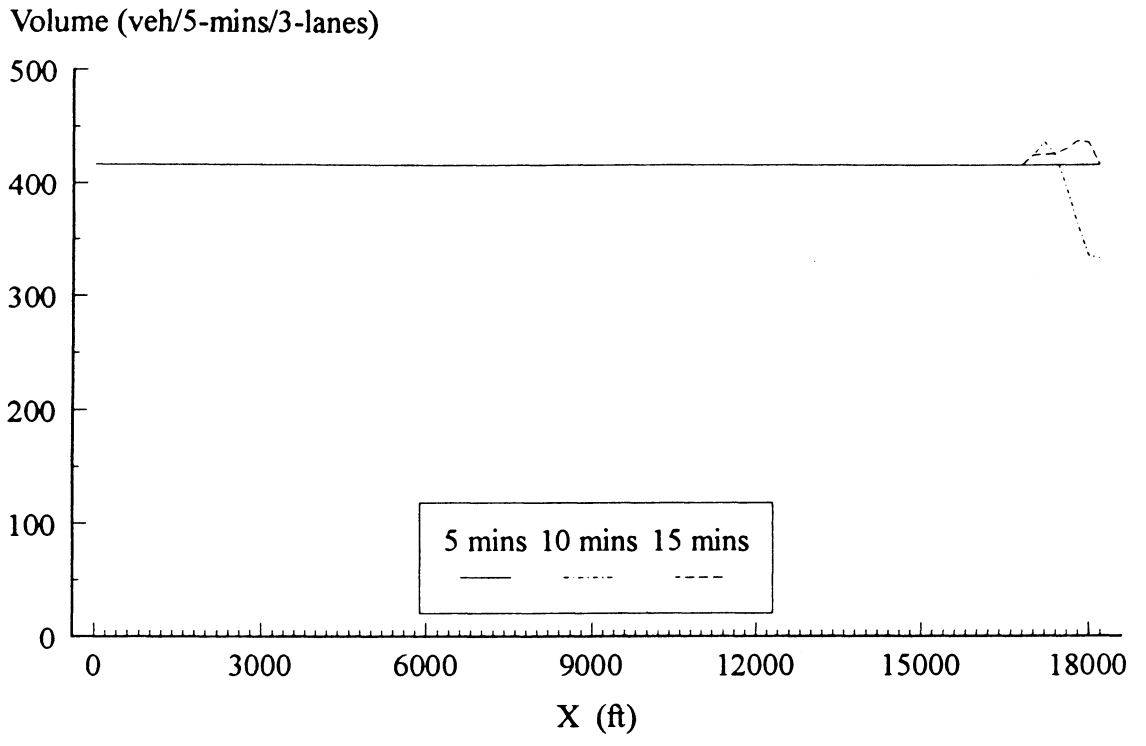

Figure 6.5 5-minute average volume produced by the semi-viscous model for case 1.

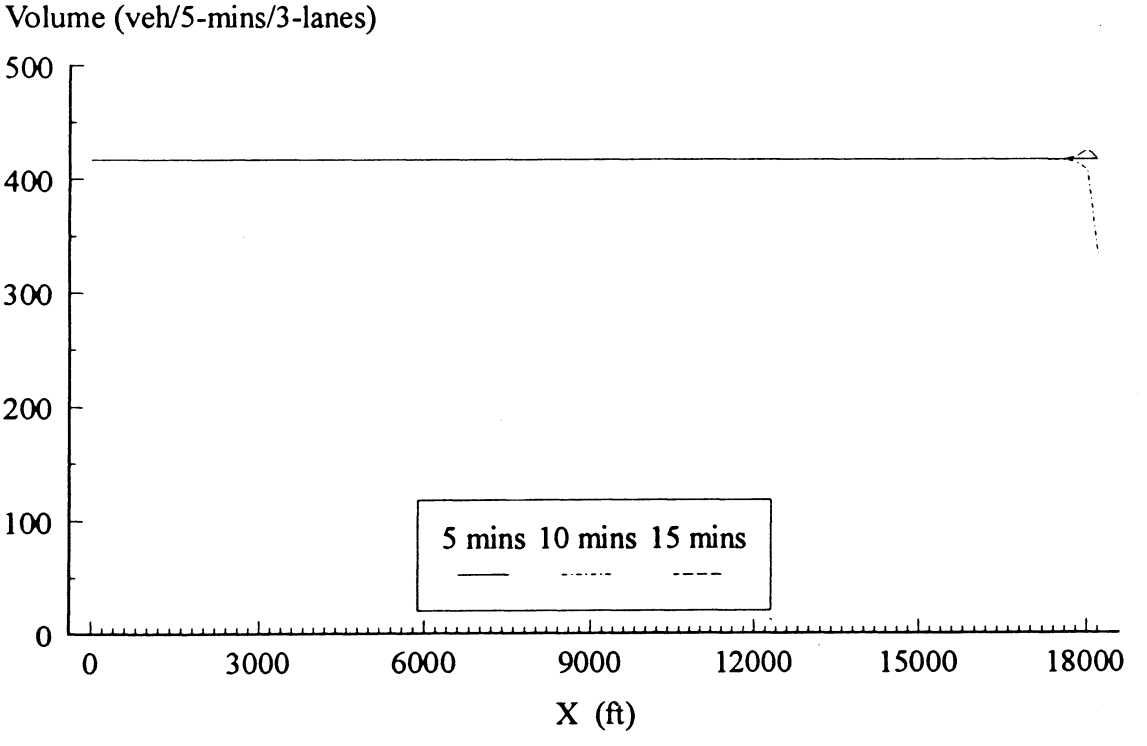

Figure 6.6 5-minute average volume produced by the viscous model (Euler method) when α = 1181.0 (feet/sec)^2. for case 1.

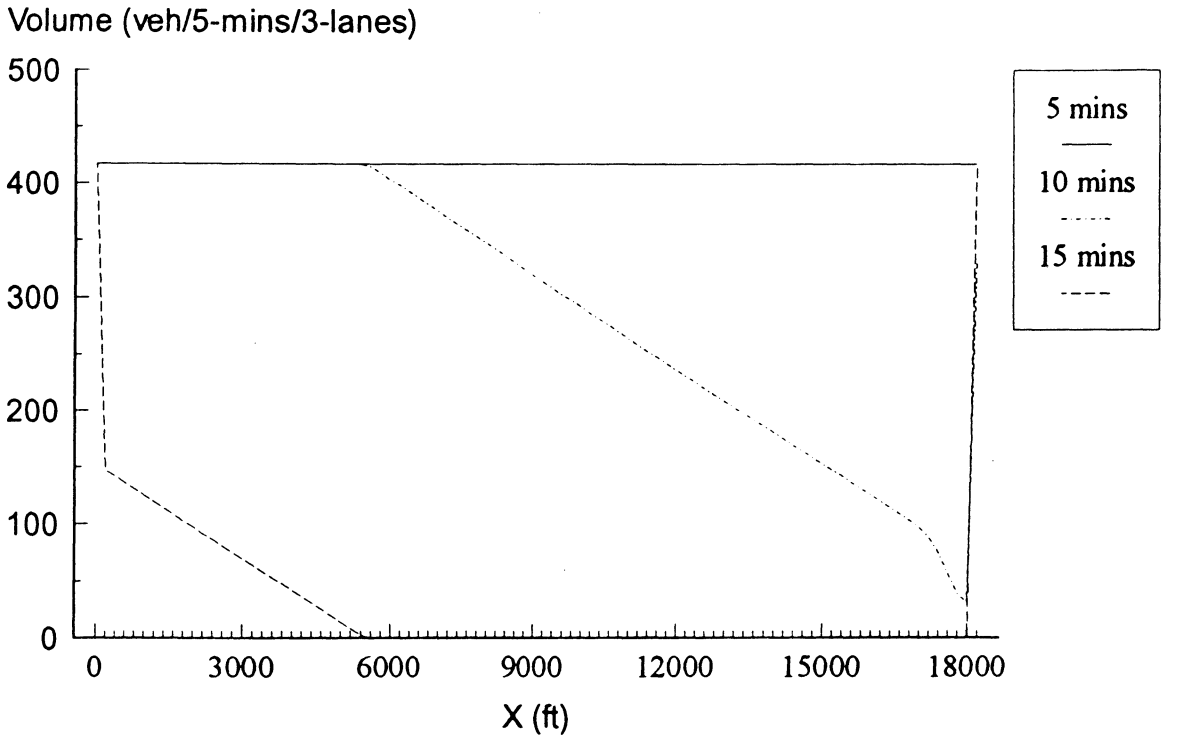

Figure 6.7 5-minute average volume produced by the viscous model (Euler method) when $\alpha = 1182.0$ (feet/sec)^2.

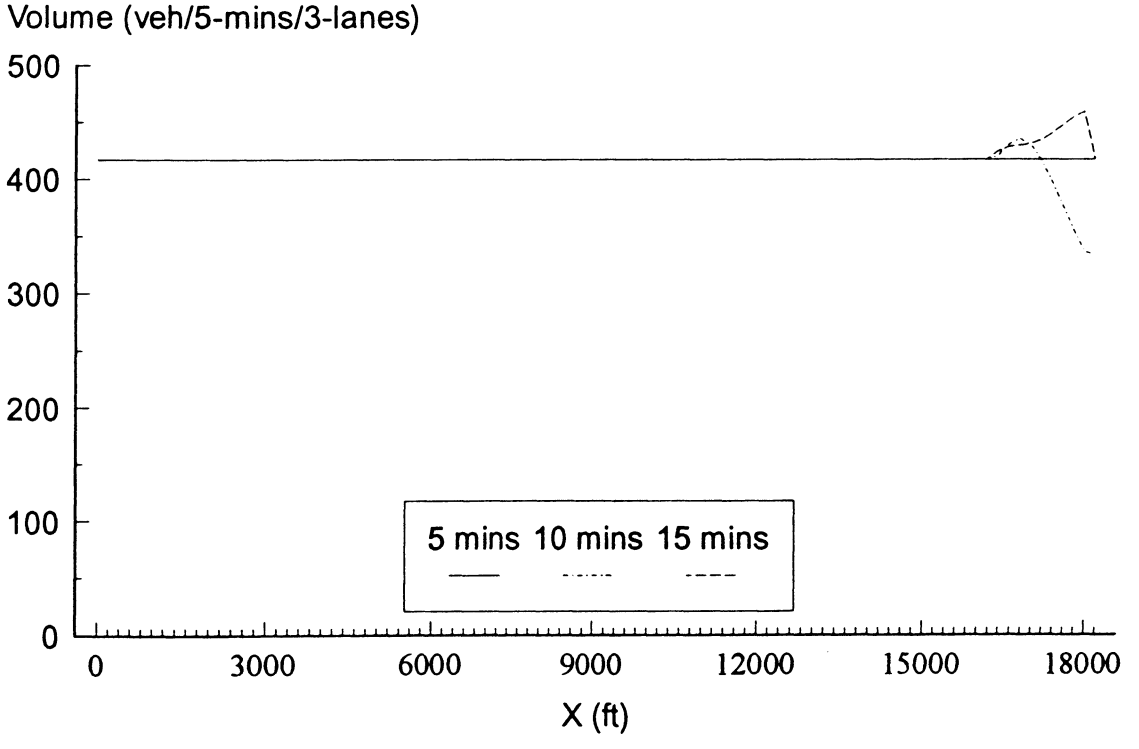

Figure 6.8 5-minute average volume produced by the proposed high-order model (Upwind method) for case 1.

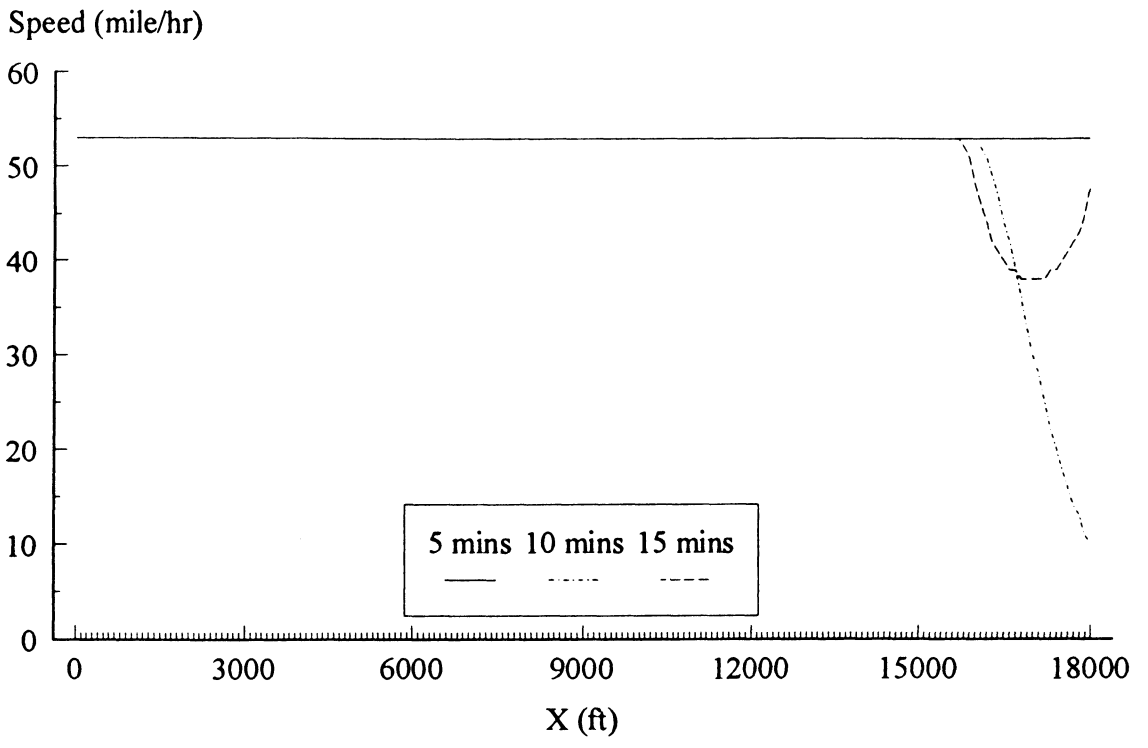

Figure 7.1 5-minute average speed produced by KRONOS for case 1.

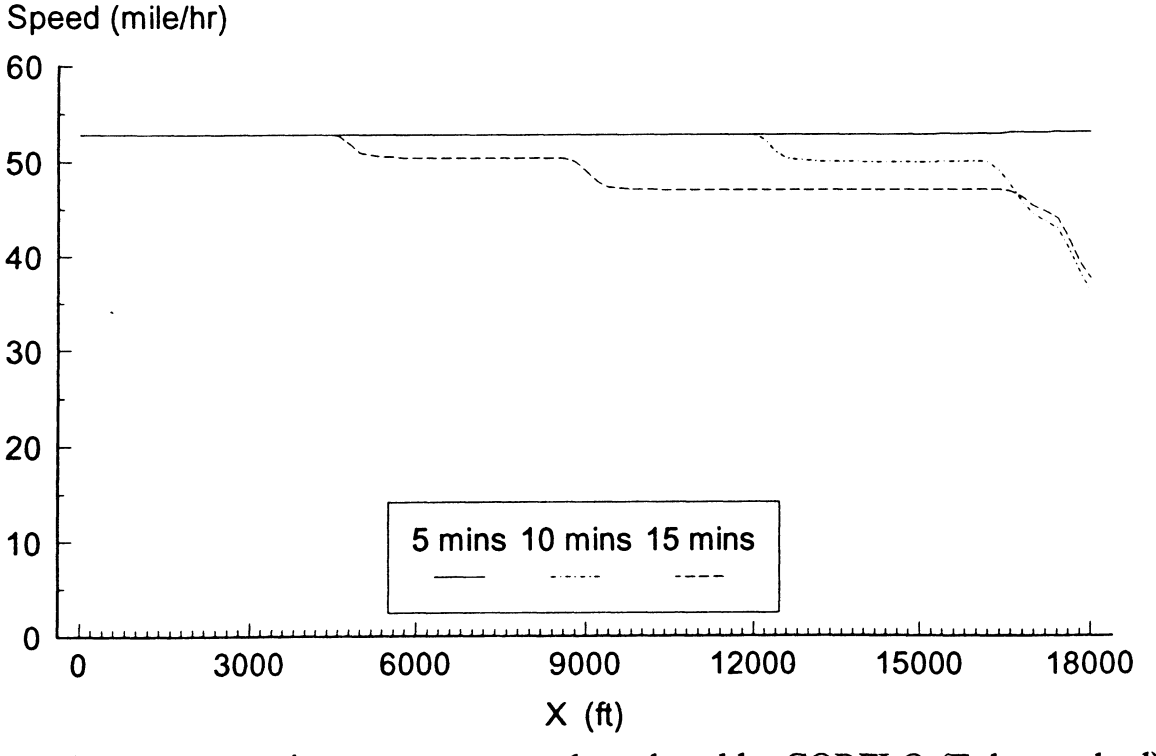

Figure 7.2 5-minute average speed produced by CORFLO (Euler method) for case 1.

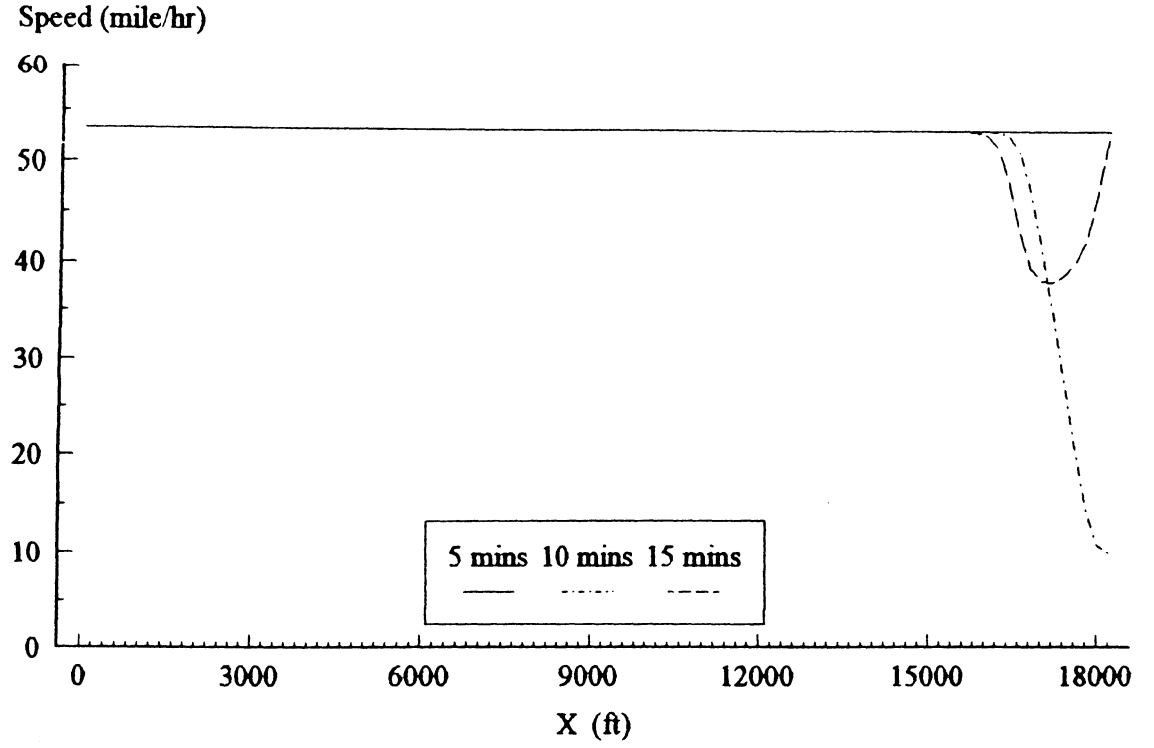

Figure 7.3 5-minute average speed produced by the original high-order model (Euler method) for case 1 when $\nu = 6250.0$ (feet^2/sec) and $\tau = 2.0$ (sec).

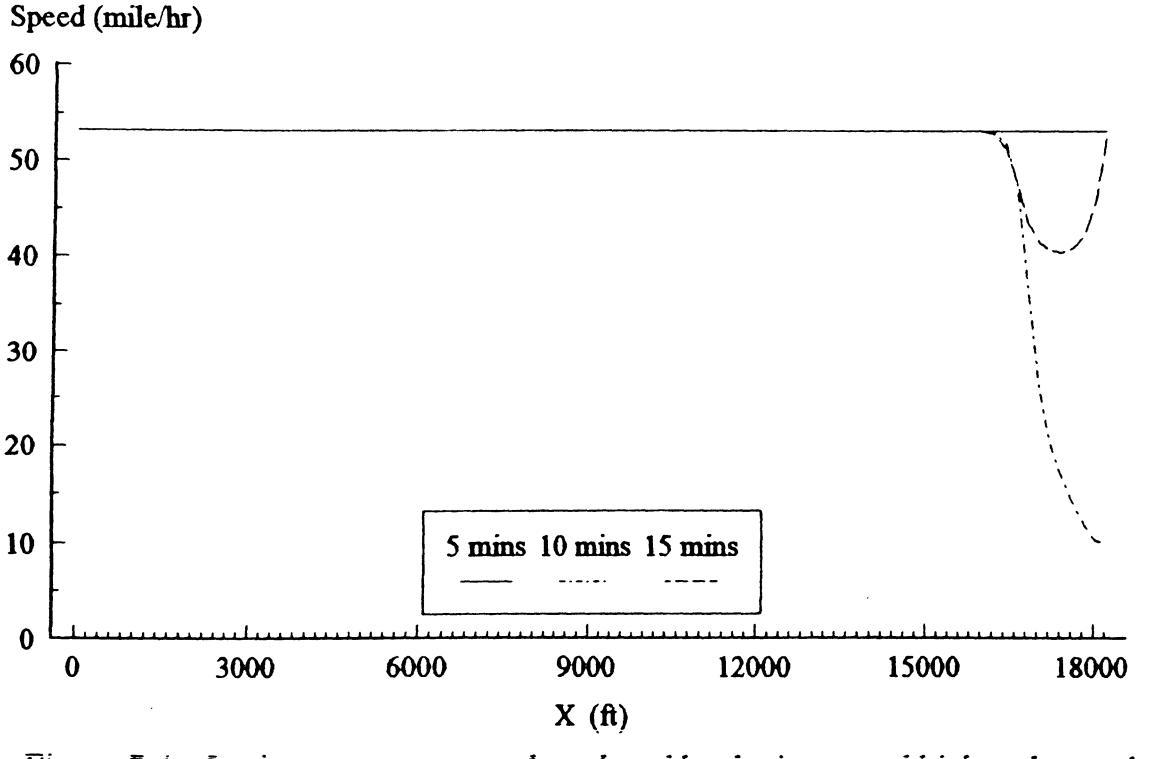

Figure 7.4 5-minute average speed produced by the improved high-order model (Euler method) for case 1 when $\nu = 68070.0$ (feet^2/sec) and $\tau = 36$ (sec).

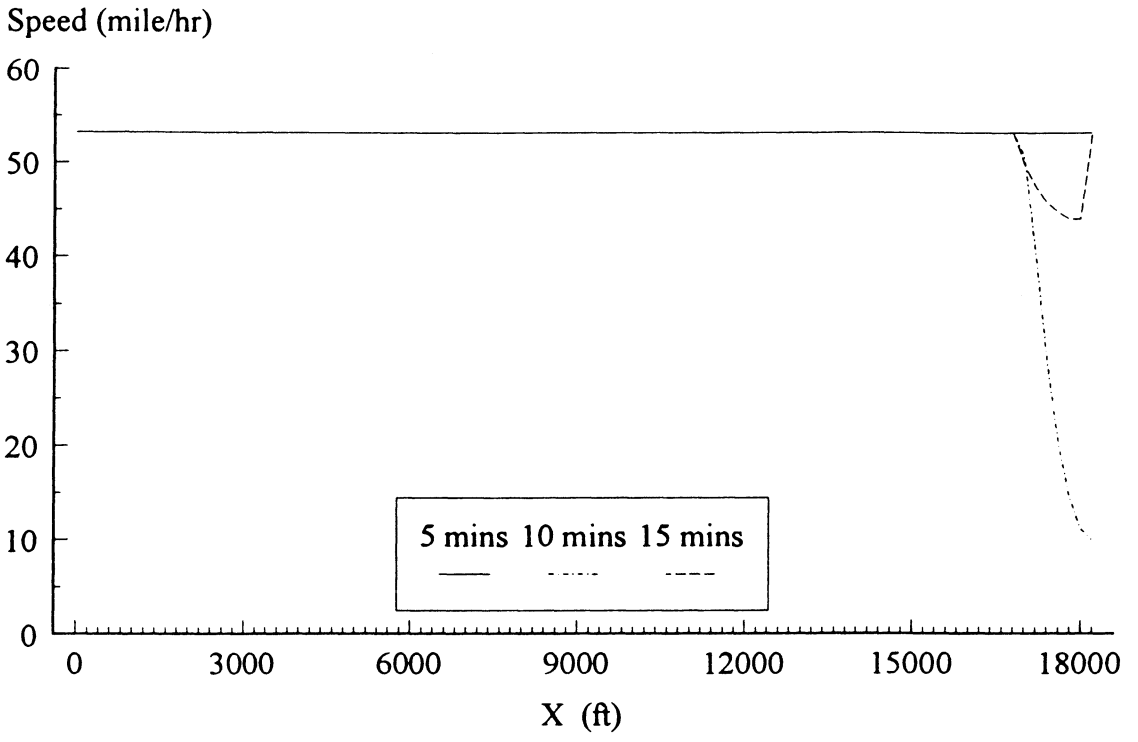

Figure 7.5 5-minute average speed produced by the semi-viscous model (Upwind Method) for case 1.

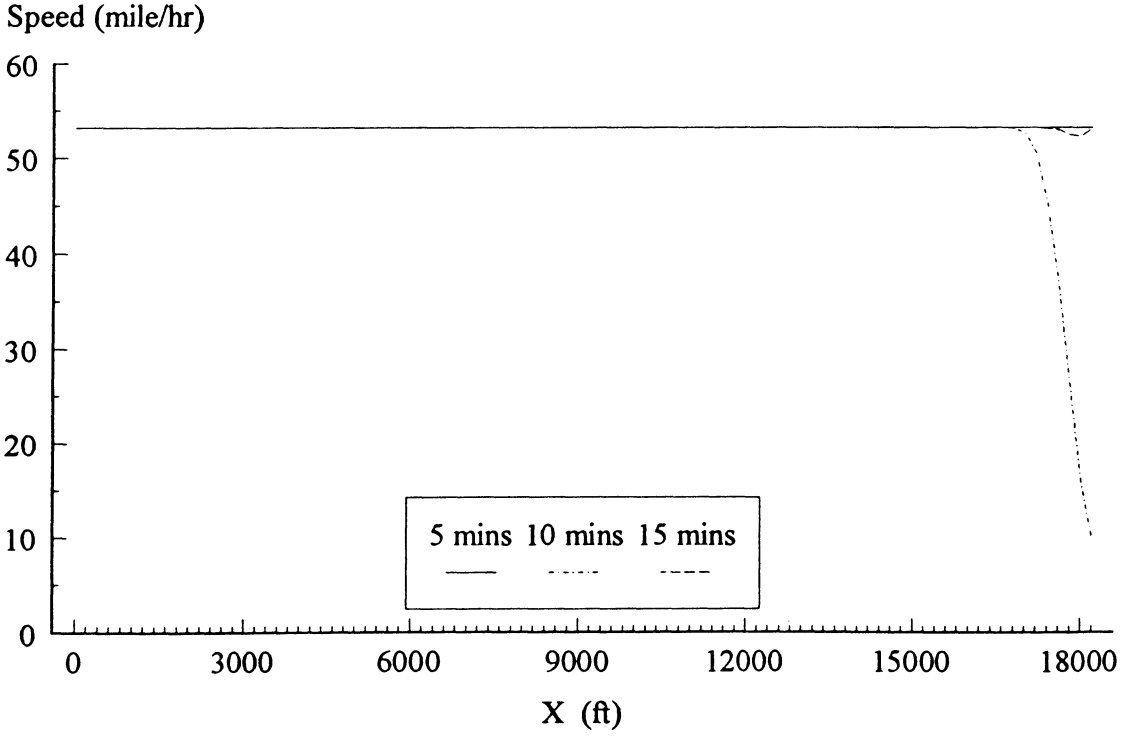

Figure 7.6 5-minute average speed produced by the viscous model (Euler method) for case 1 when $\alpha = 1181.0$ (feet /sec)^2.

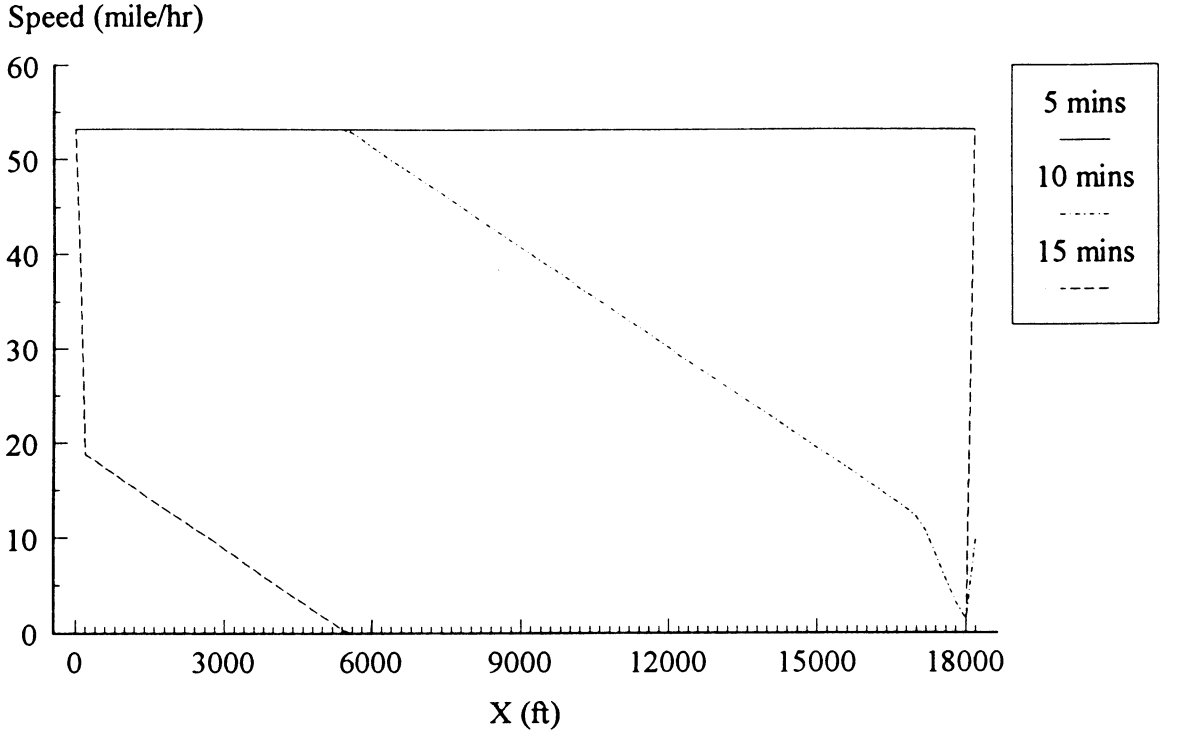

Figure 7.7 5-minute average speed produced by the viscous model (Euler method) for case 1 when $\alpha = 1182.0$ (feet /sec)^2.

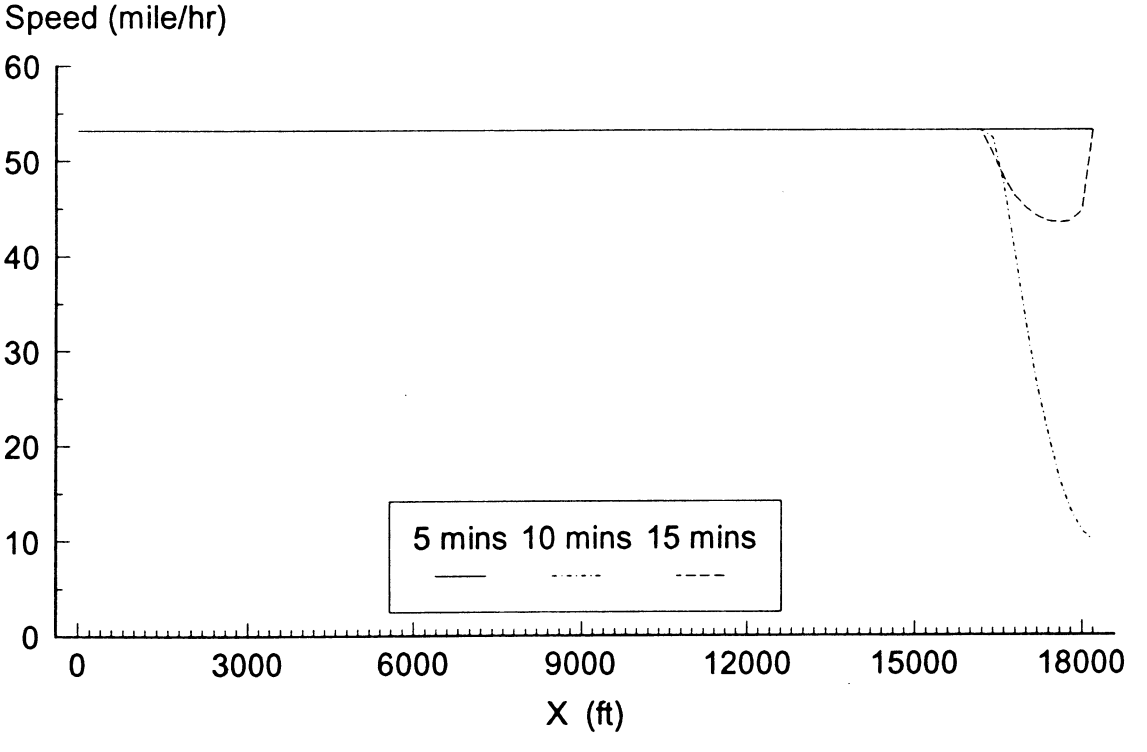

Figure 7.8 5-minute average speed produced by the proposed high-order model (Upwind method) for case 1.

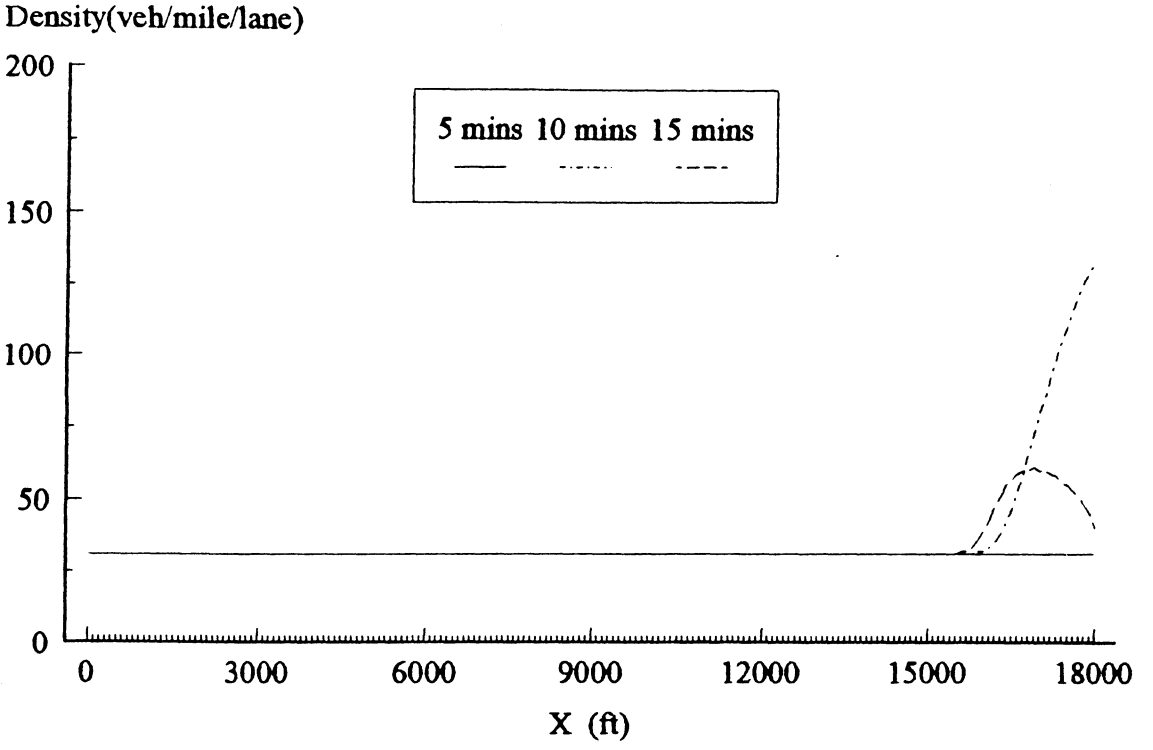

Figure 8.1 5-minute average density produced by KRONOS for case 1.

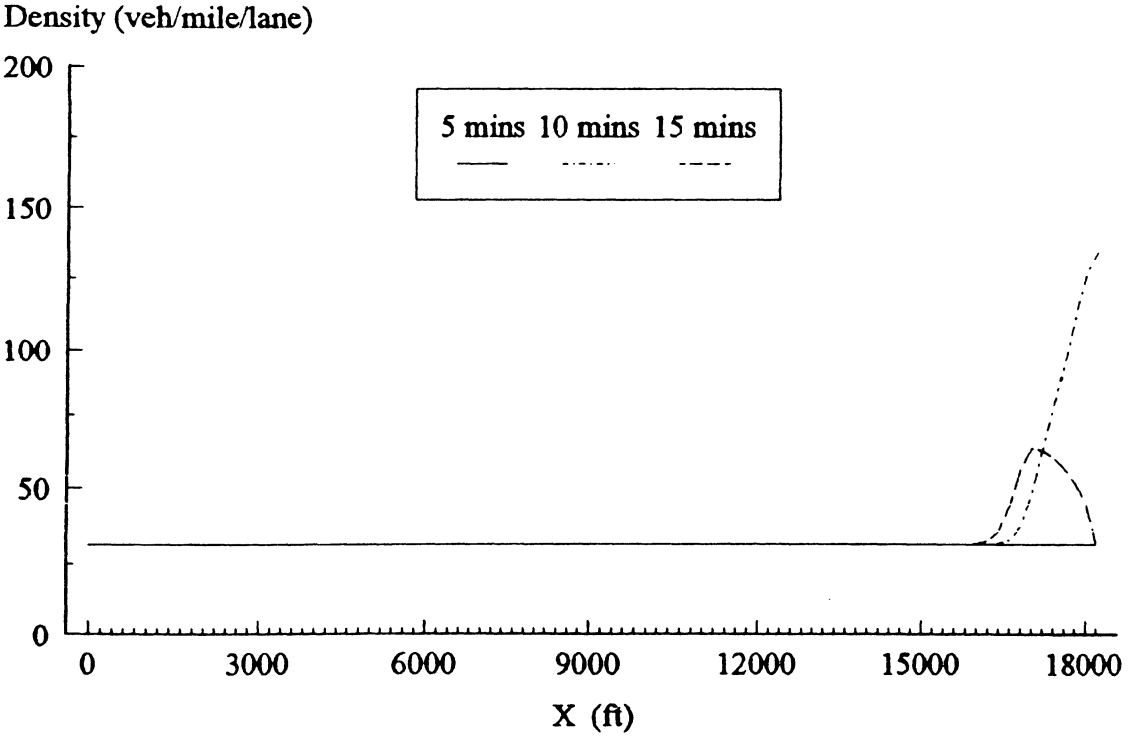

Figure 8.2 5-minute average density produced by the original high-order model (Euler method) for case 1 when $\nu = 6250.0$ (feet^2/sec) and $\tau = 2.0$ (sec).

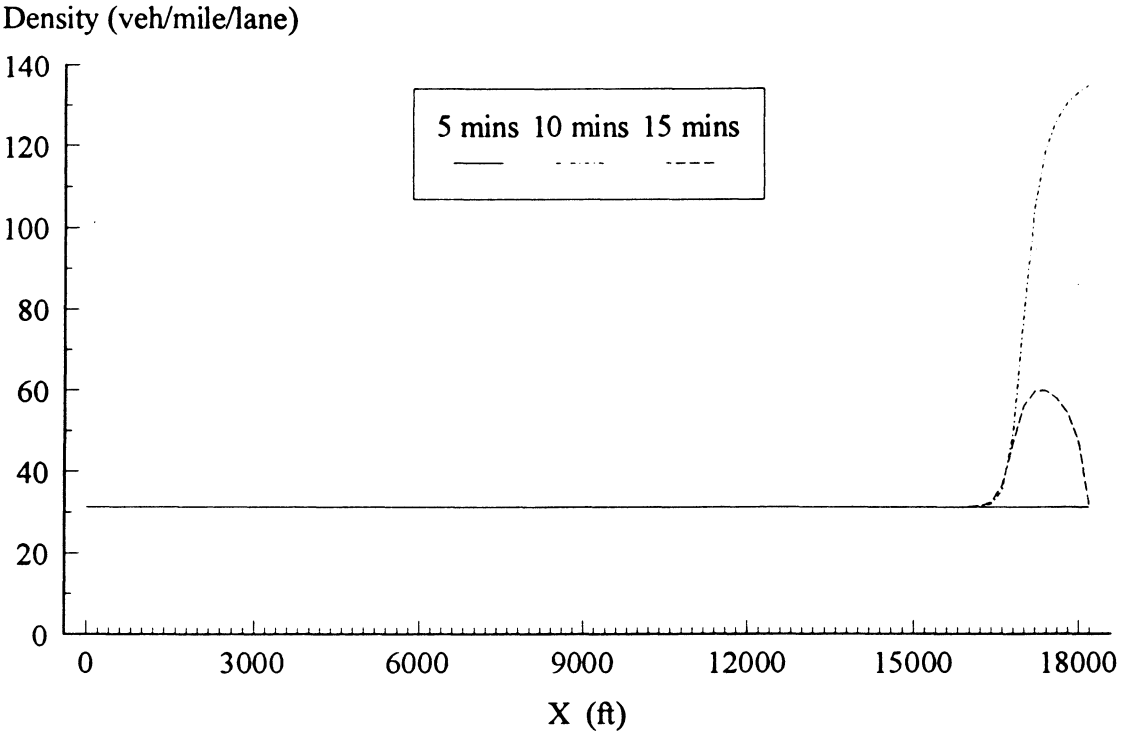

Figure 8.3 5-minute average density produced by the improved high-order model (Euler method) for case 1 when $\nu = 68070.0$ (feet^2/sec) and $\tau = 36$ (sec).

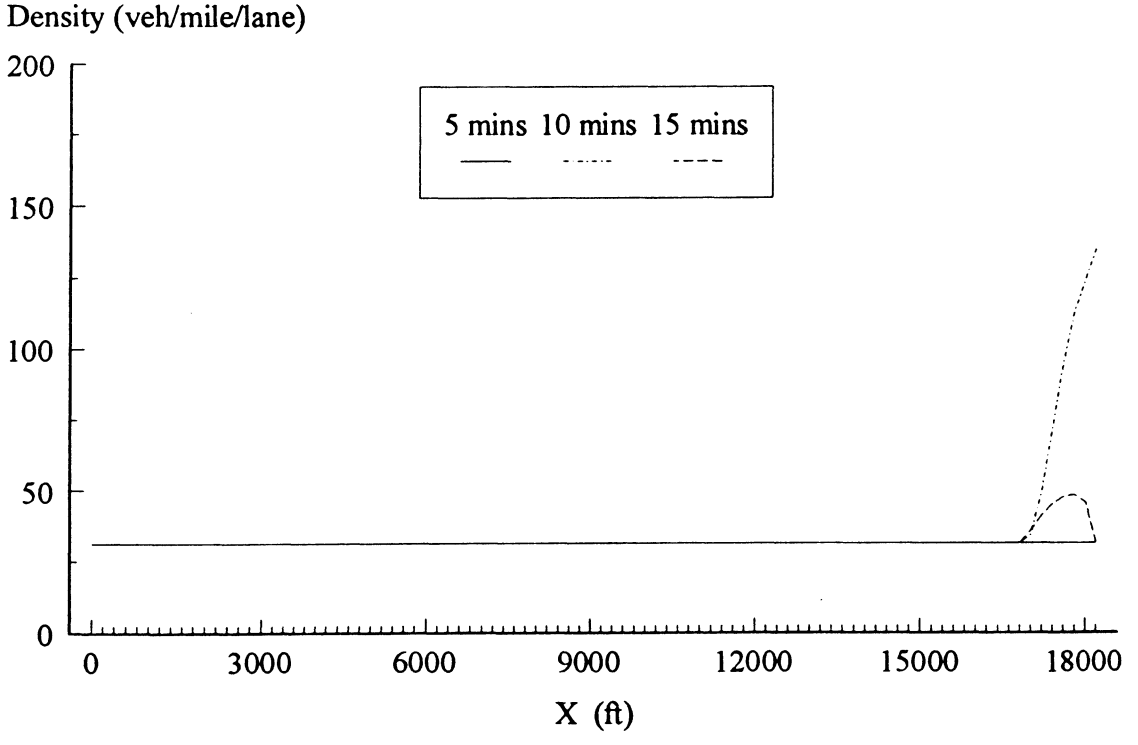

Figure 8.4 5-minute average density produced by the semi-viscous model (Upwind method) for case 1.

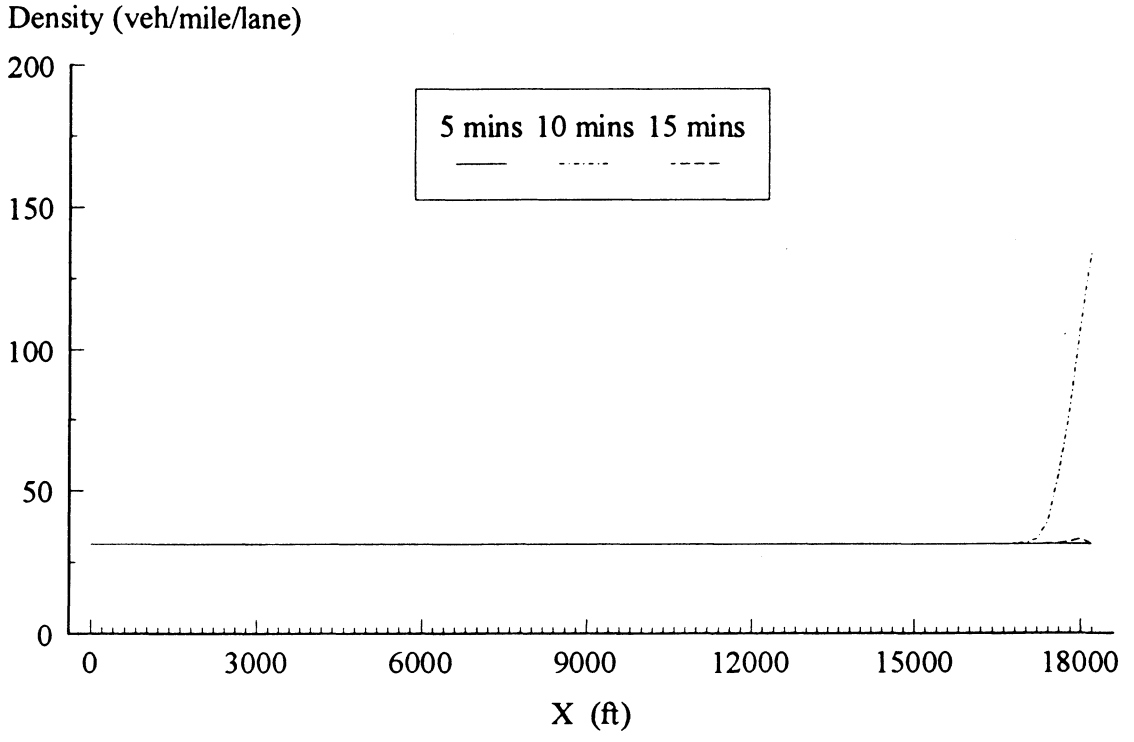

Figure 8.5 5-minute average density produced by the viscous model (Euler method) for case 1 when $\alpha = 1181.0$ (feet/sec)^2.

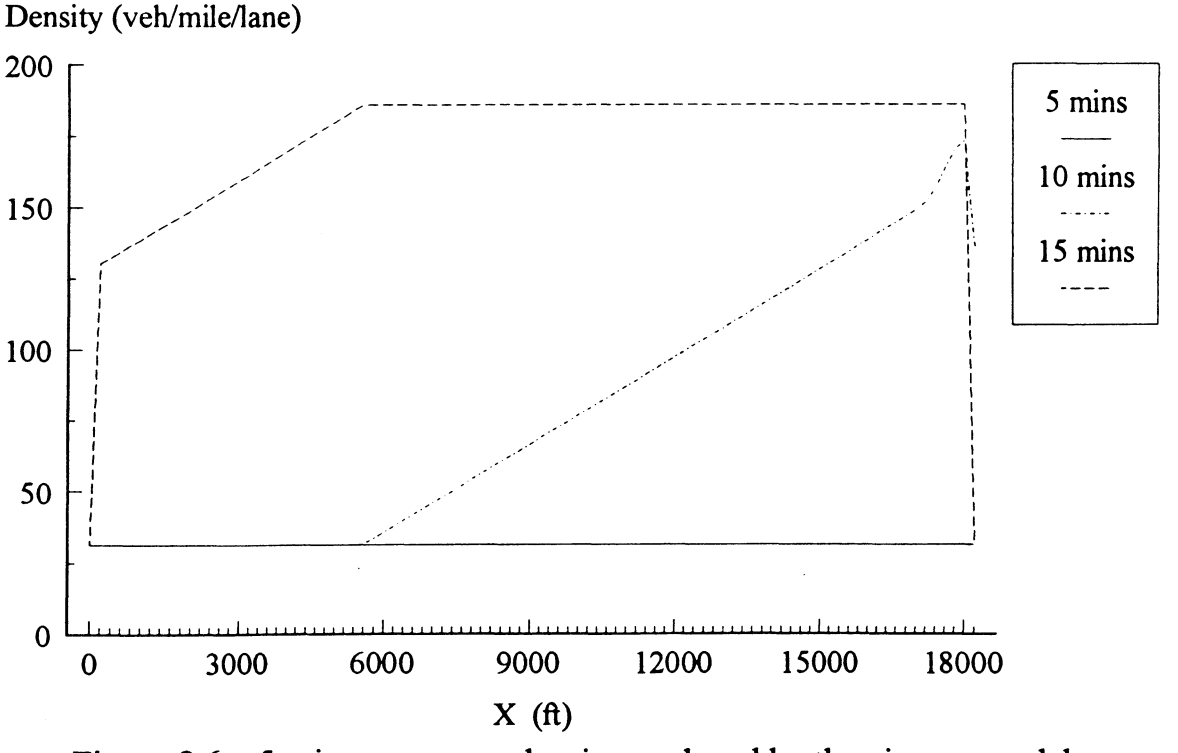

Figure 8.6 5-minute average density produced by the viscous model (Euler method) for case 1 when $\alpha = 1182.0$ (feet/sec)^2.

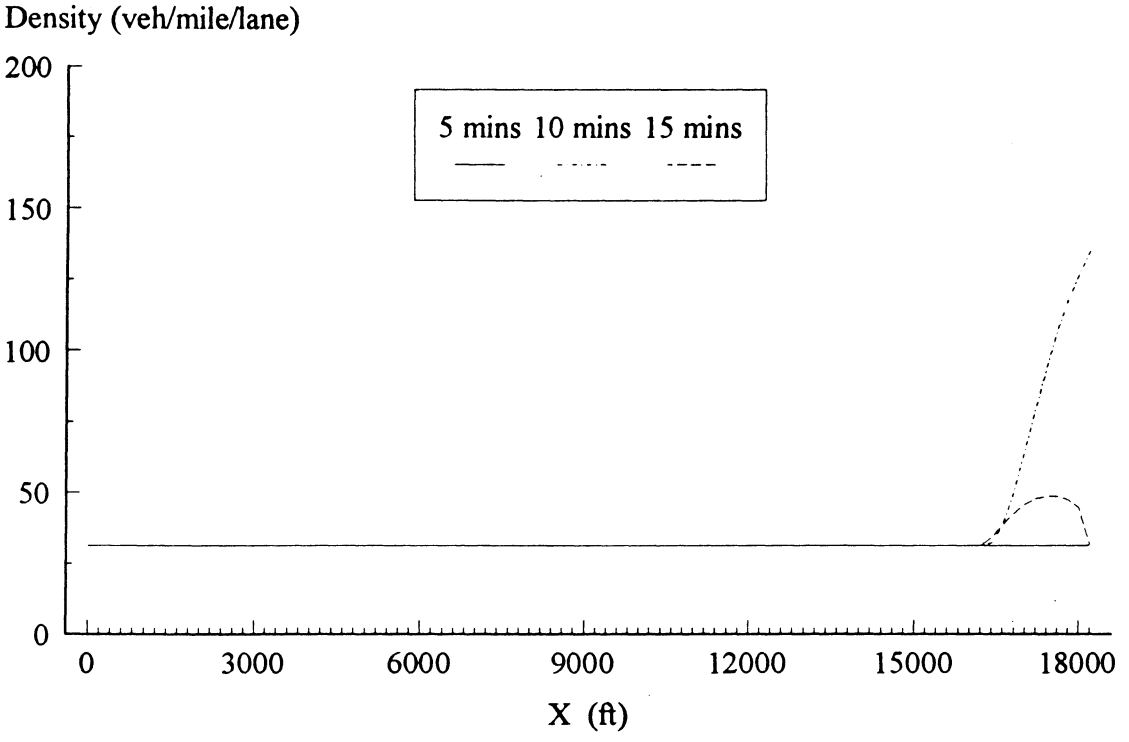

Figure 8.7 5-minute average density produced by the proposed high-order model (Upwind method) for case 1.

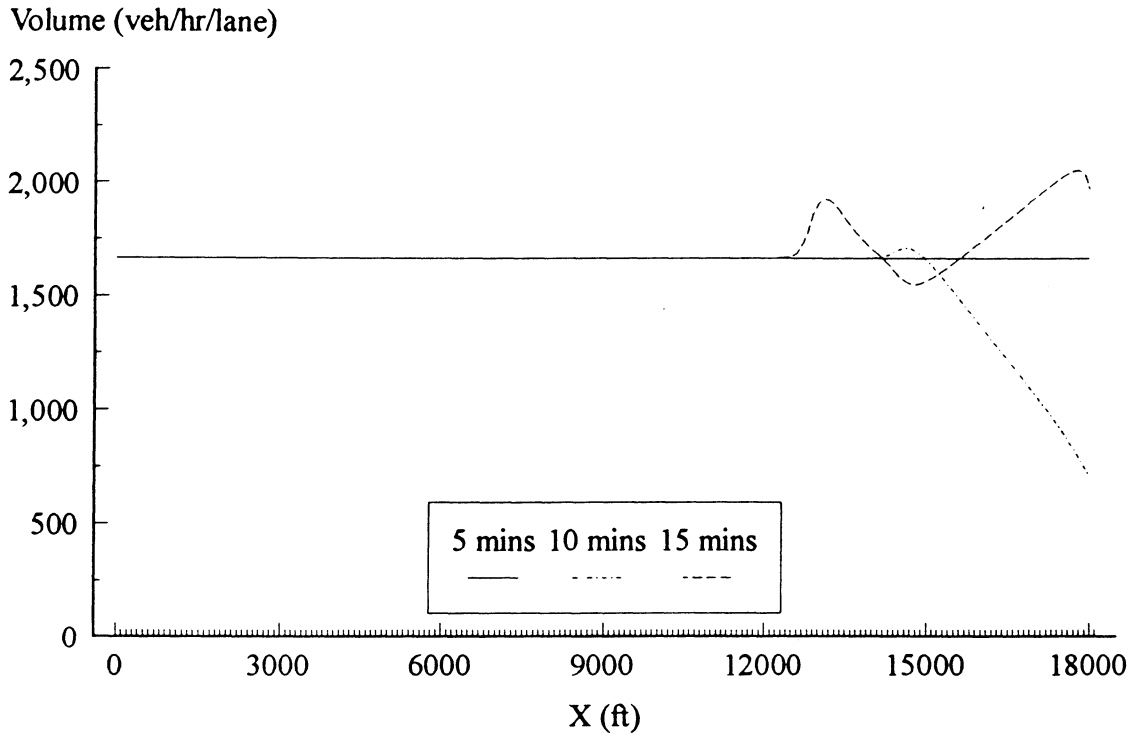

Figure 9.1 5-minute average volume produced by KRONOS for case 2.

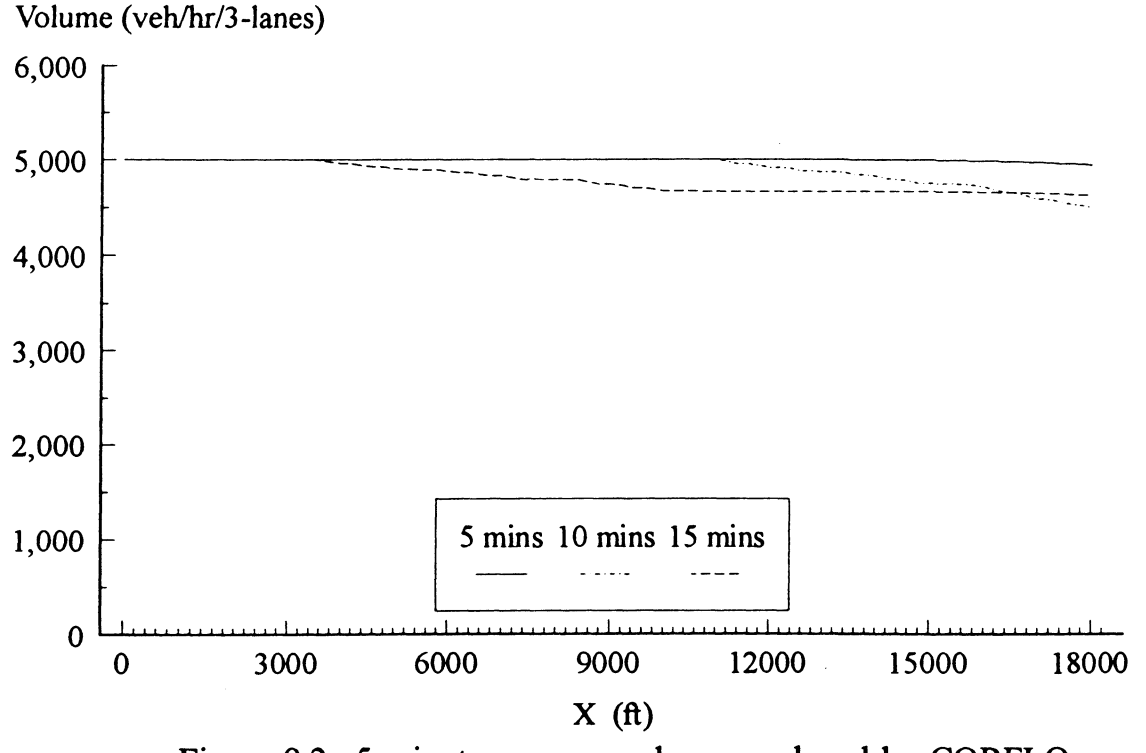

Figure 9.2 5-minute average volume produced by CORFLO (Euler method) for case 2.

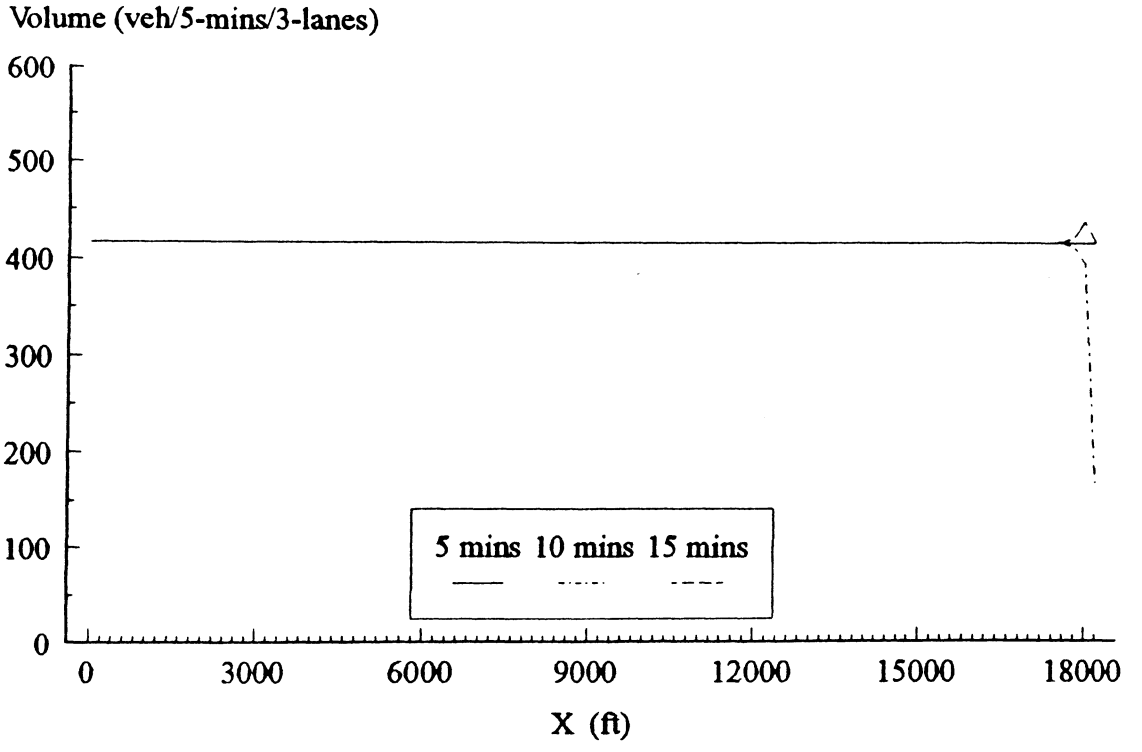

Figure 9.3 5-minute average volume produced by the original high-order model (Euler method) for case 2 when ν= 3382 (feet^2/sec) and τ = 2.0 (sec).

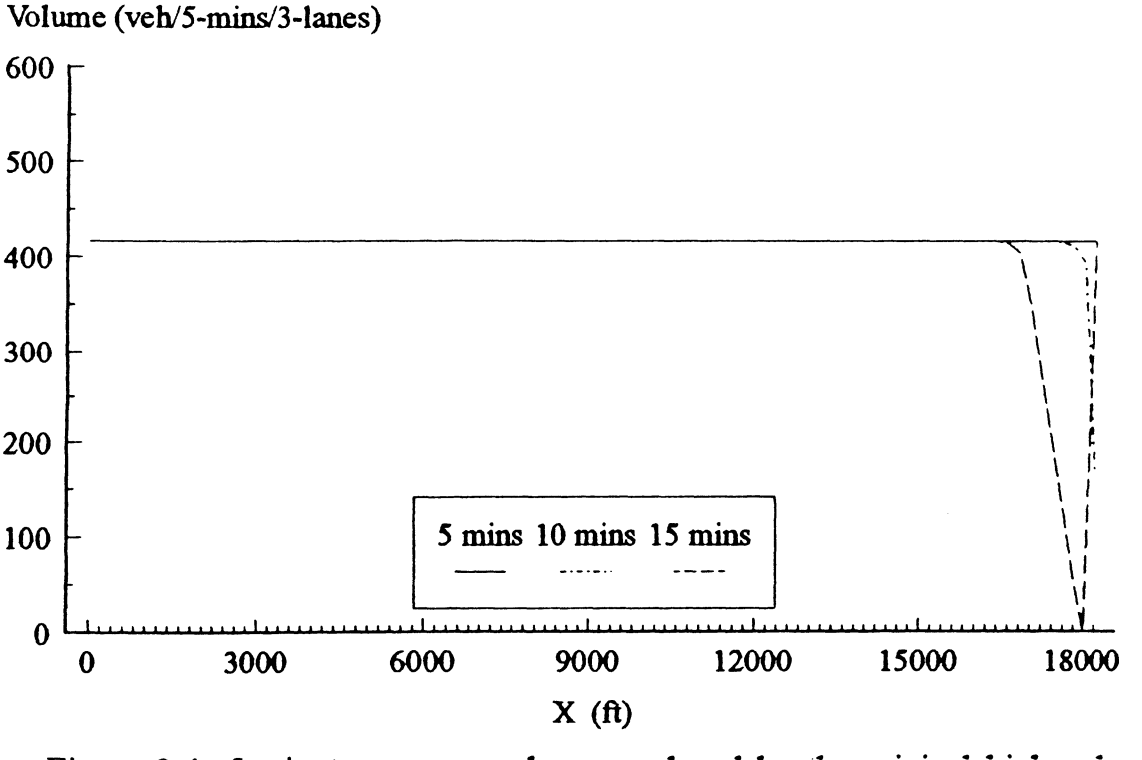

Figure 9.4 5-minute average volume produced by the original high-order model (Euler method) for case 2 when ν= 3383 (feet^2/sec) and τ = 2.0 (sec).

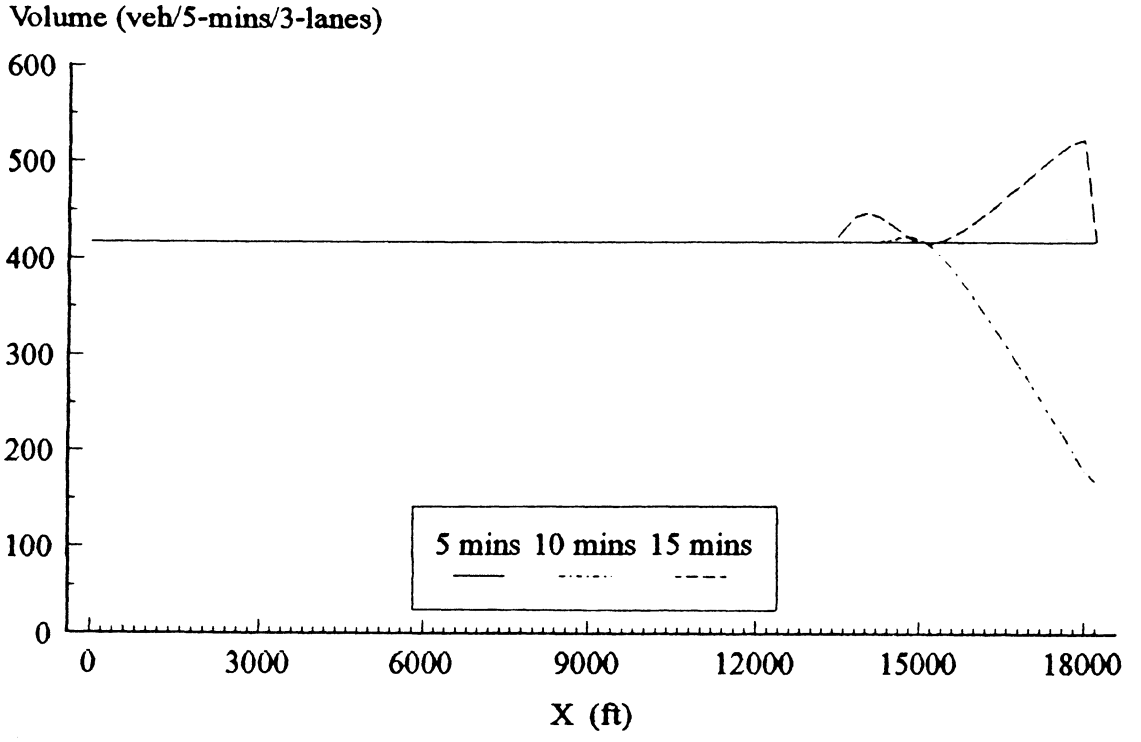

Figure 9.5 5-minute average volume produced by the original high-order model (Upwind method) for case 2.

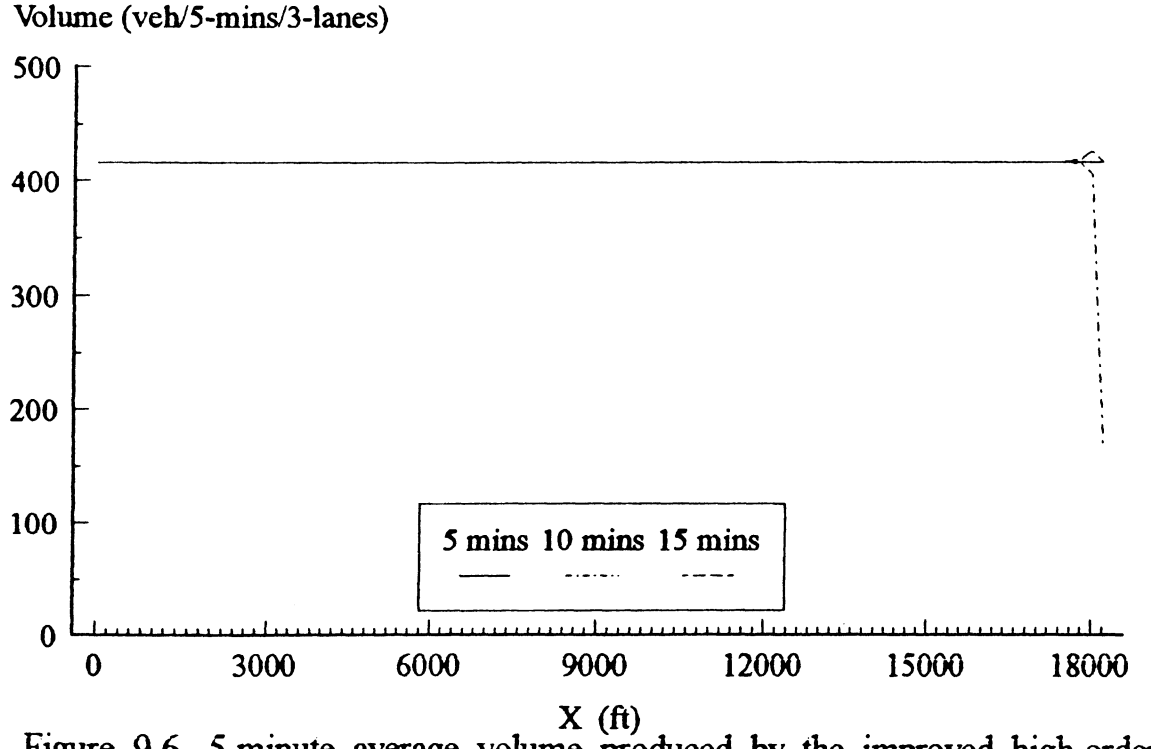

Figure 9.6 5-minute average volume produced by the improved high-order model (Euler method) for case 2 when ν = 50229.0 (feet^2/sec) and τ = 36 (sec).

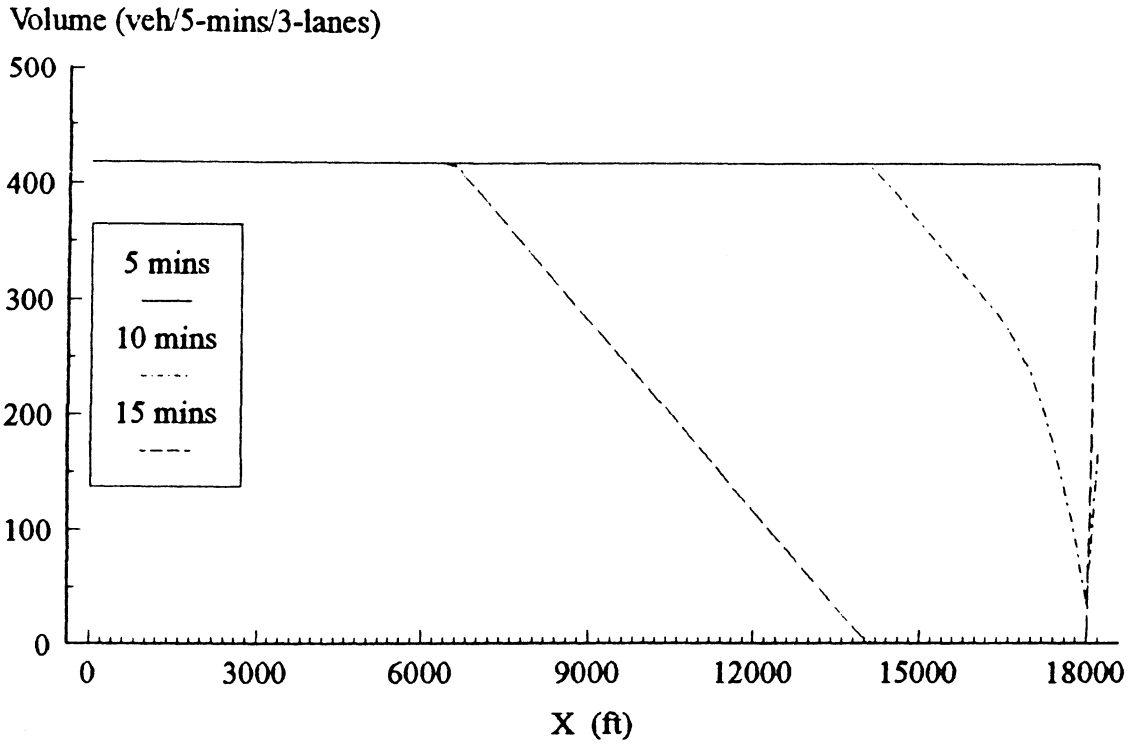

Figure 9.7 5-minute average volume produced by the improved high-order model (Euler method) for case 2 when $\nu = 50230.0$ (feet^2/sec) and $\tau = 36$ (sec).

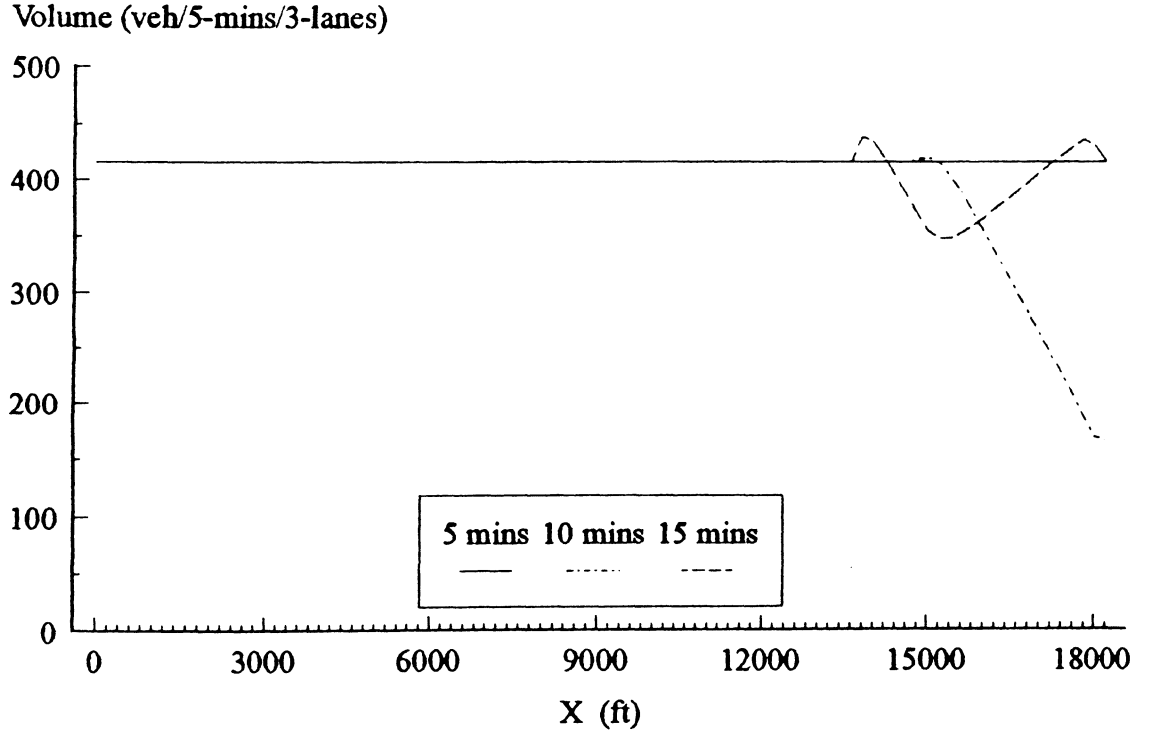

Figure 9.8 5-minute average volume produced by the semi-viscous model (Upwind method) for case 2.

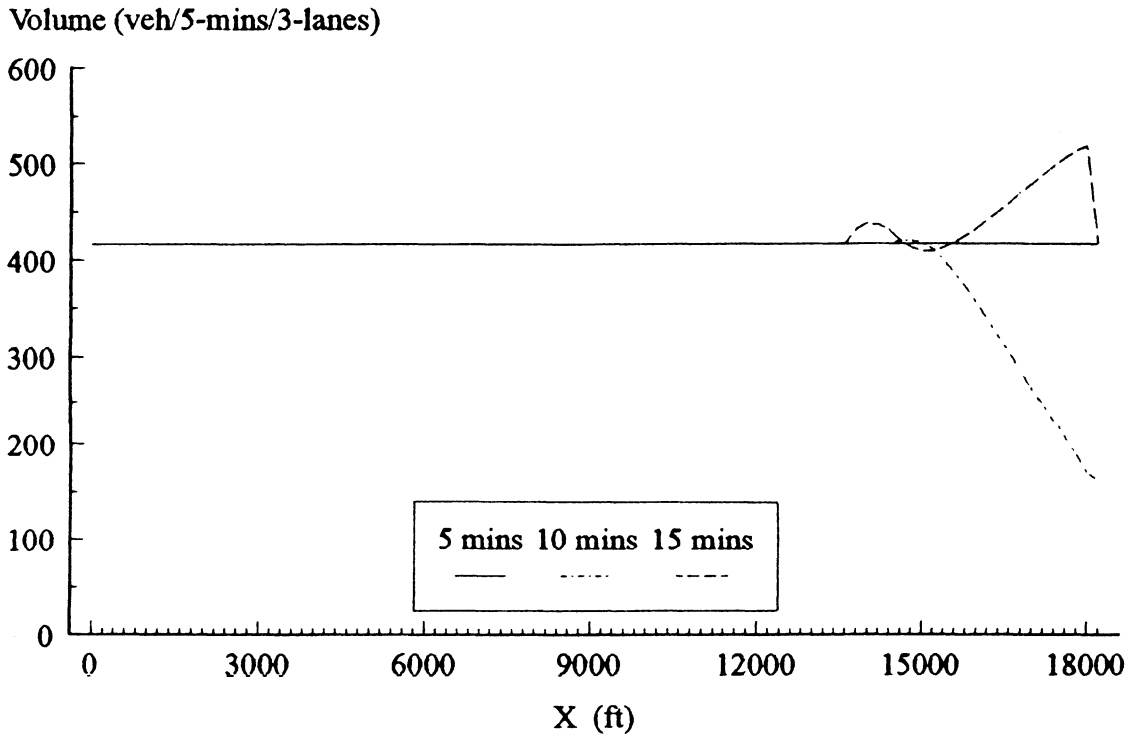

Figure 9.9 5-minute average volume produced by the proposed high-order model (Upwind method) for case 2.

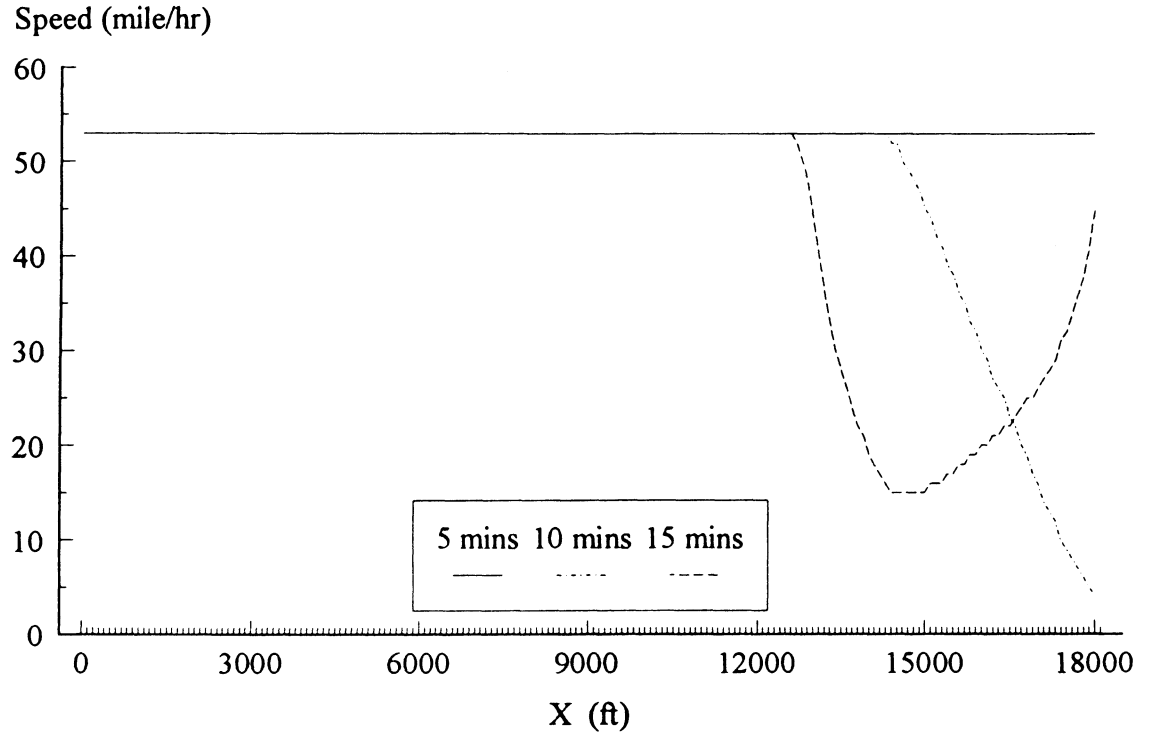

Figure 10.1 5-minute average speed produced by KRONOS for case 2.

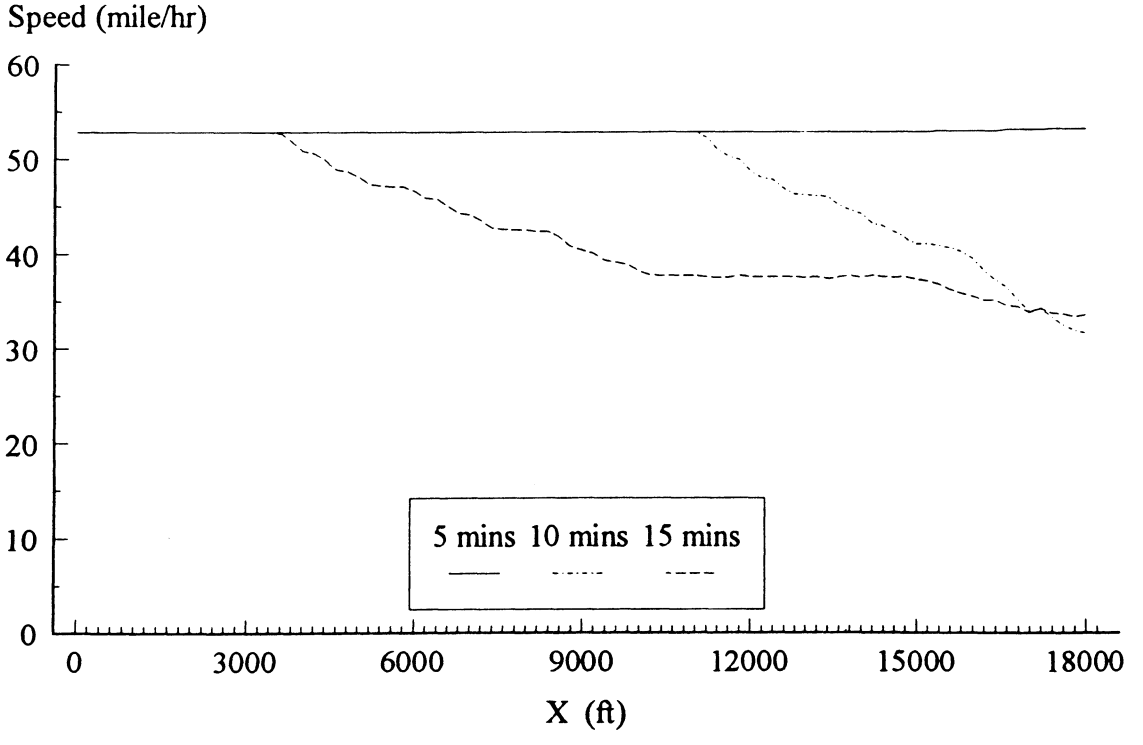

Figure 10.2 5-minute average speed produced by CORFLO (Euler method) for case 2.

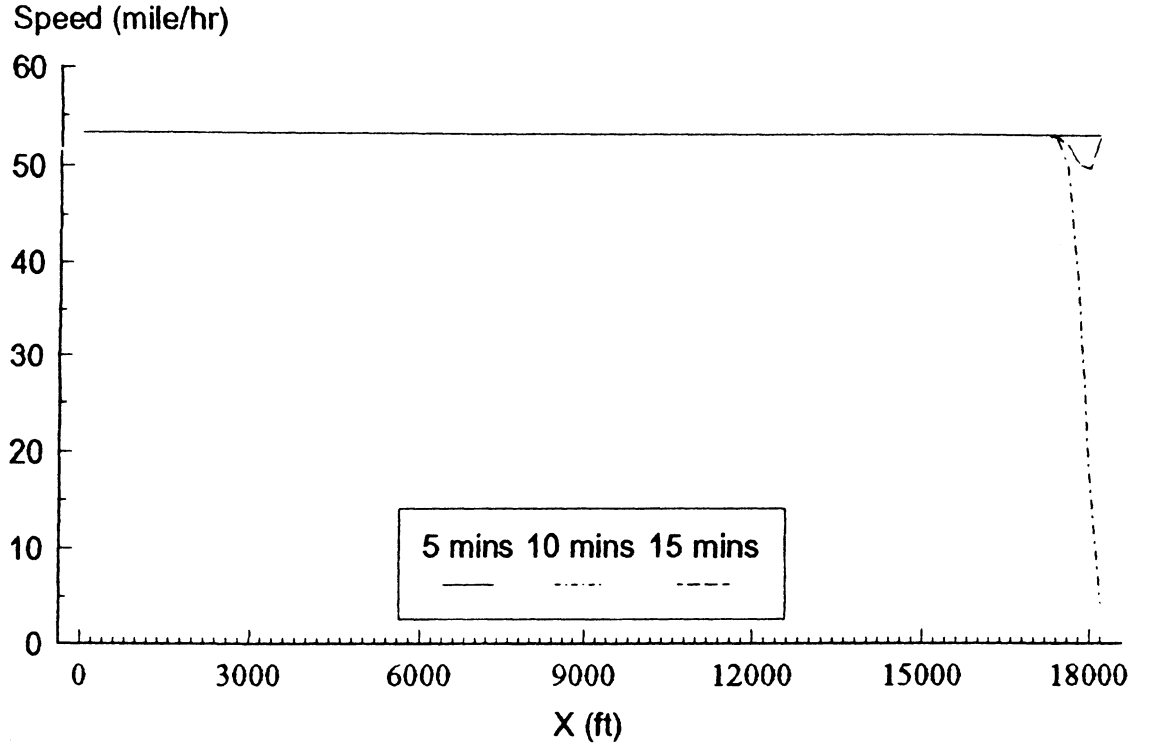

Figure 10.3 5-minute average speed produced by the original high-order model (Euler method) for case 2 when ν = 3382.0 (feet^2/sec) and τ = 2.0 (sec).

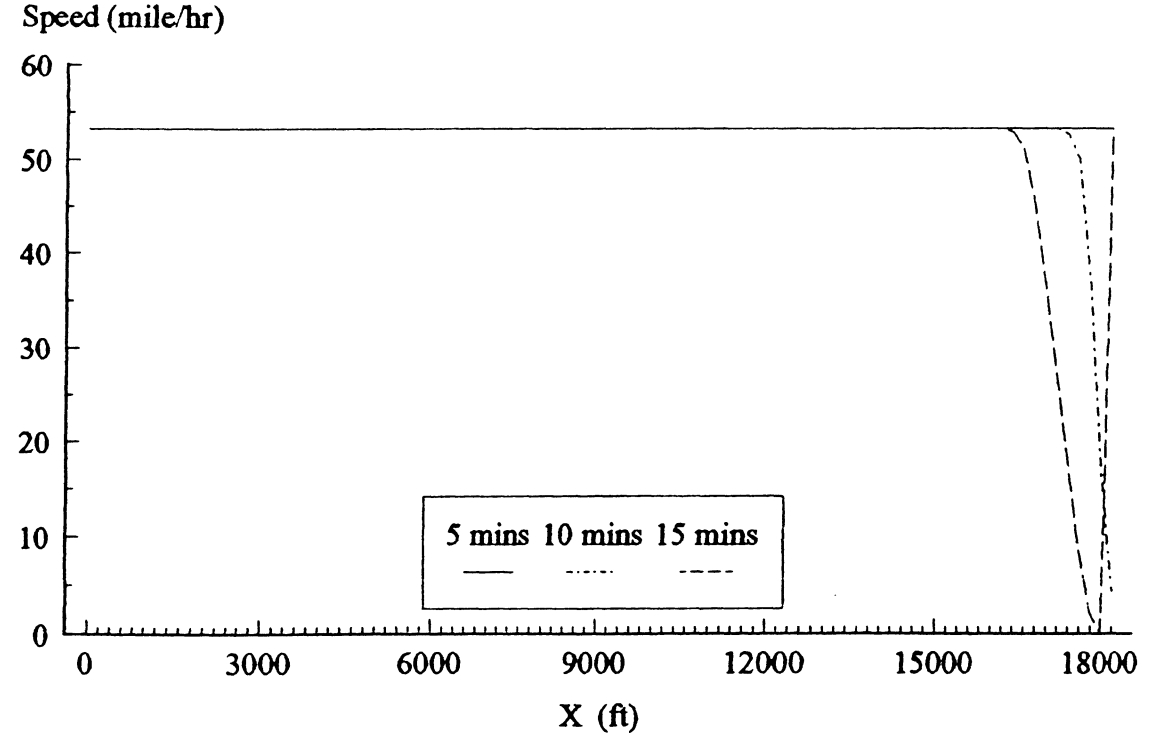

Figure 10.4 5-minute average speed produced by the original high-order model (Euler method) for case 2 when ν = 3383.0 (feet^2/sec) and τ = 2.0 (sec).

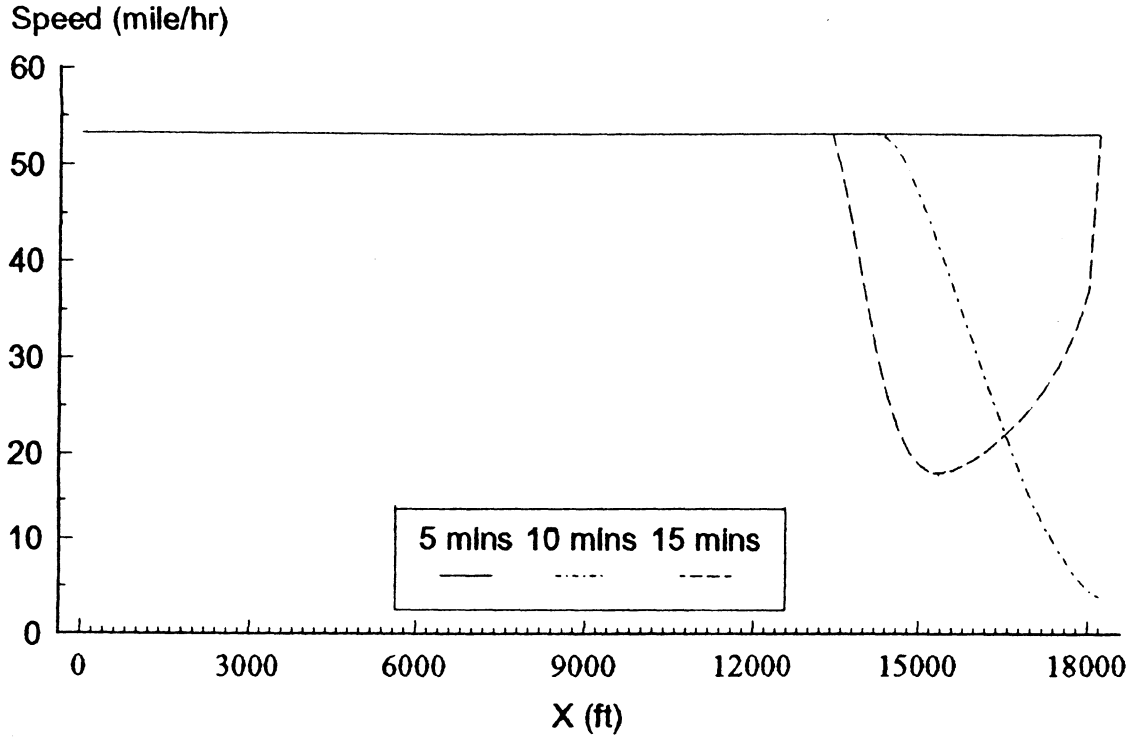

Figure 10.5 5-minute average speed produced by the original high-order model (Upwind method) for case 2.

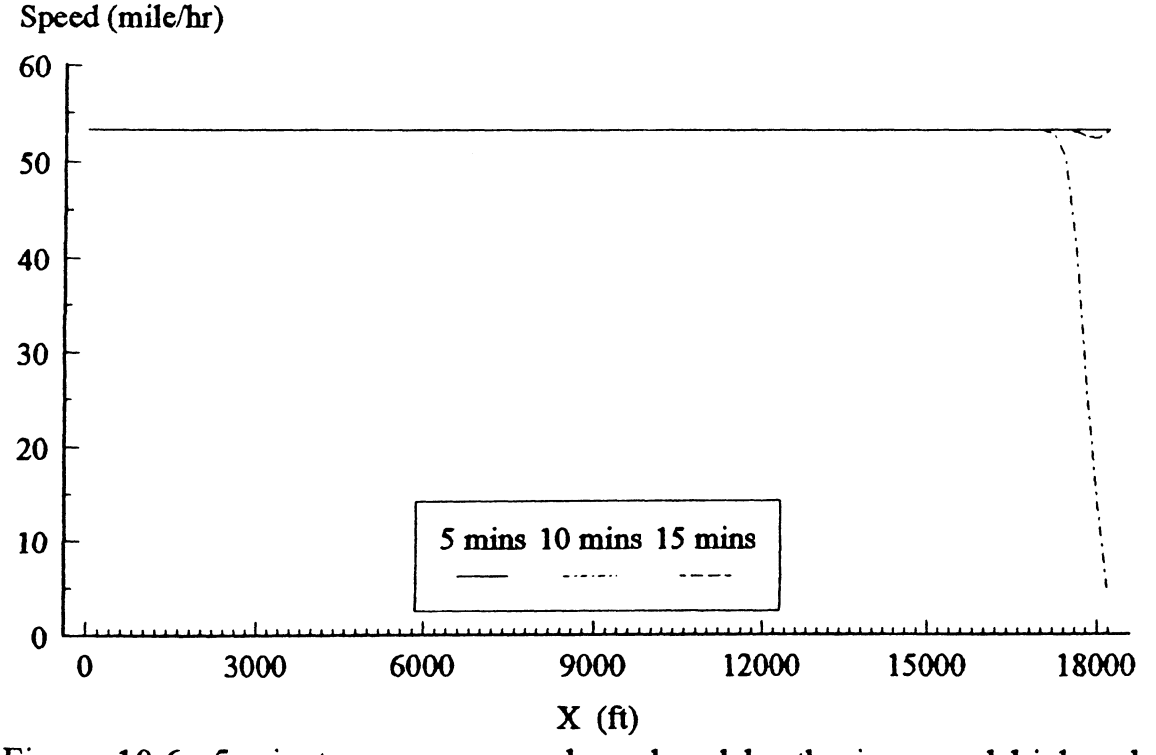

Figure 10.6 5-minute average speed produced by the improved high-order model (Euler method) for case 2 when ν = 50229.0 (feet^2/sec) and τ = 36 (sec).

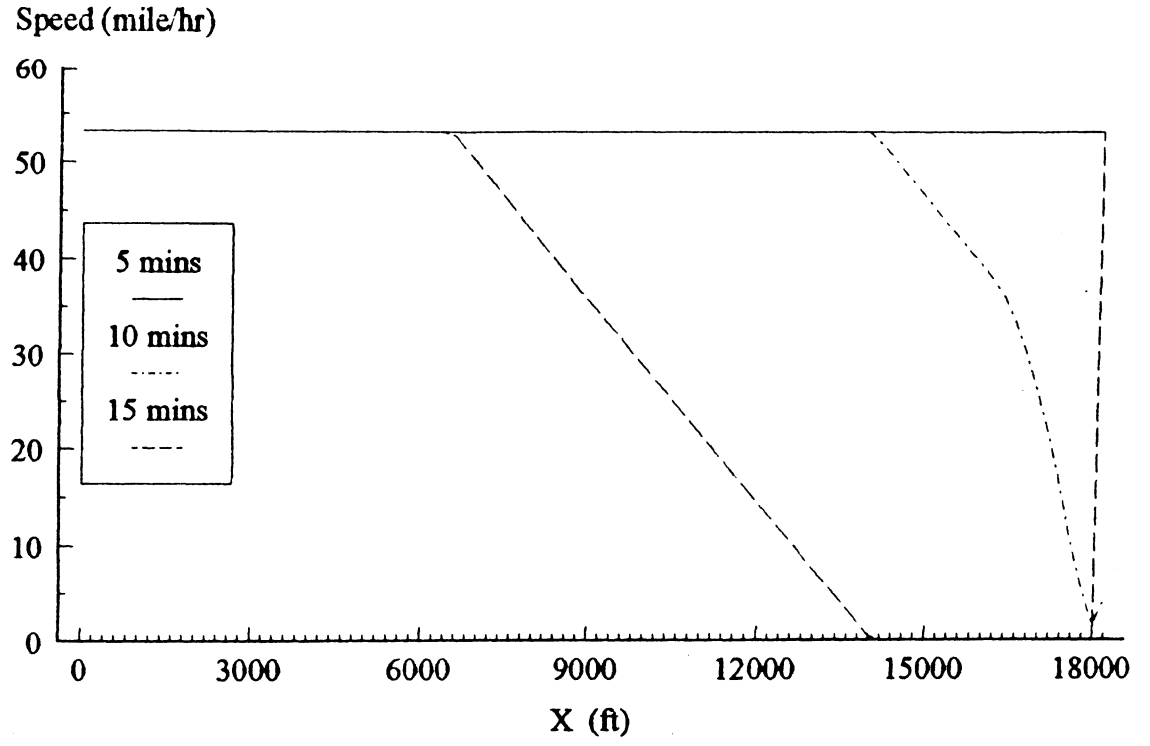

Figure 10.7 5-minute average speed produced by the improved high-order model (Euler method) for case 2 when ν = 50230.0 (feet^2/sec) and τ = 36 (sec).

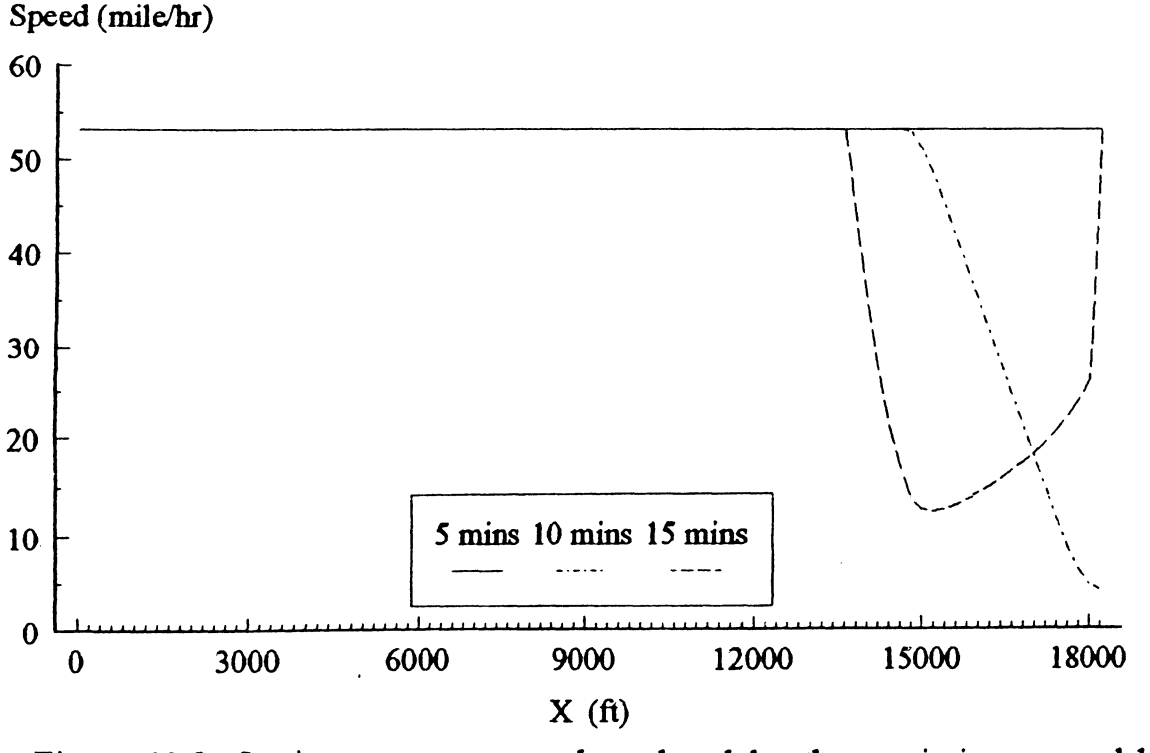

Figure 10.8 5-minute average speed produced by the semi-viscous model (Upwind method) for case 2.

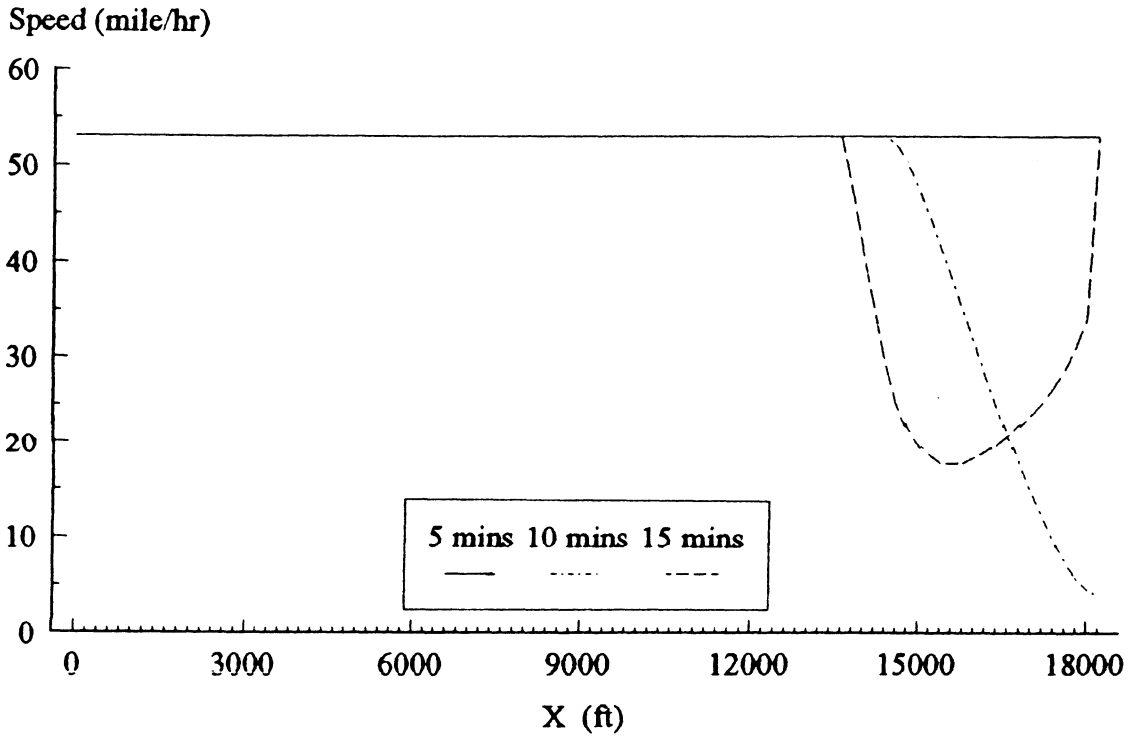

Figure 10.9 5-minute average speed produced by the proposed high-order model (Upwind method) for case 2.

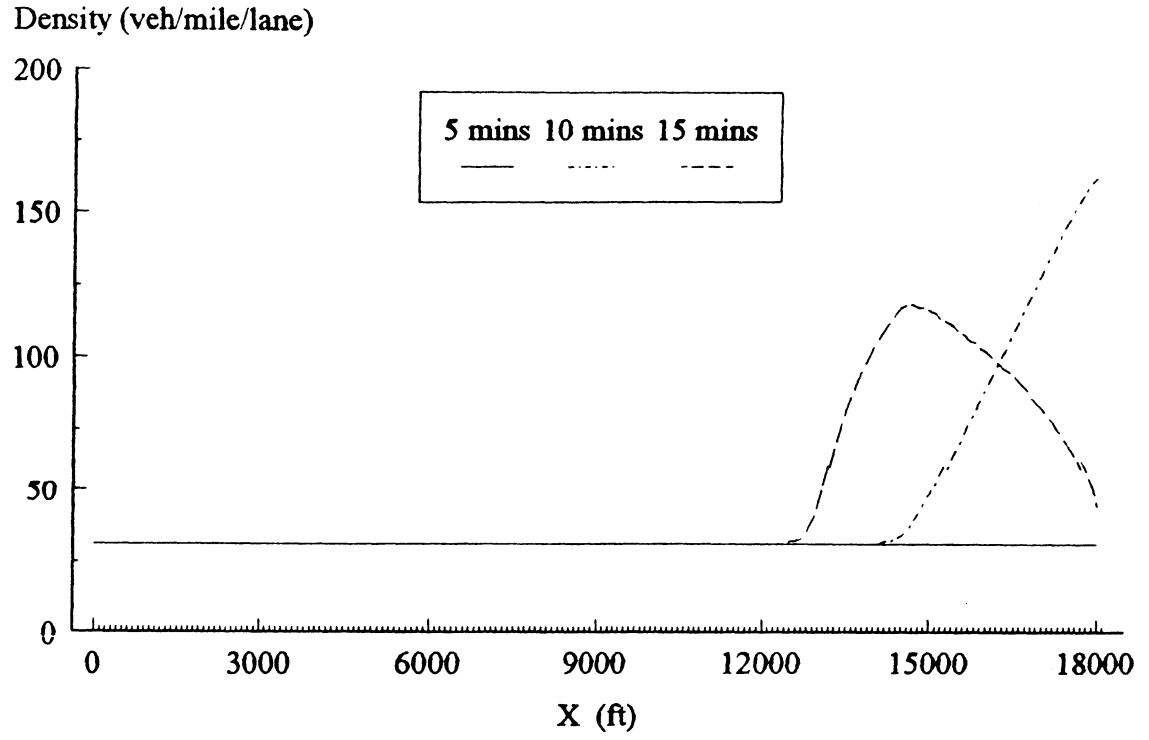

Figure 11.1 5-minute average density produced by KRONOS for case 2.

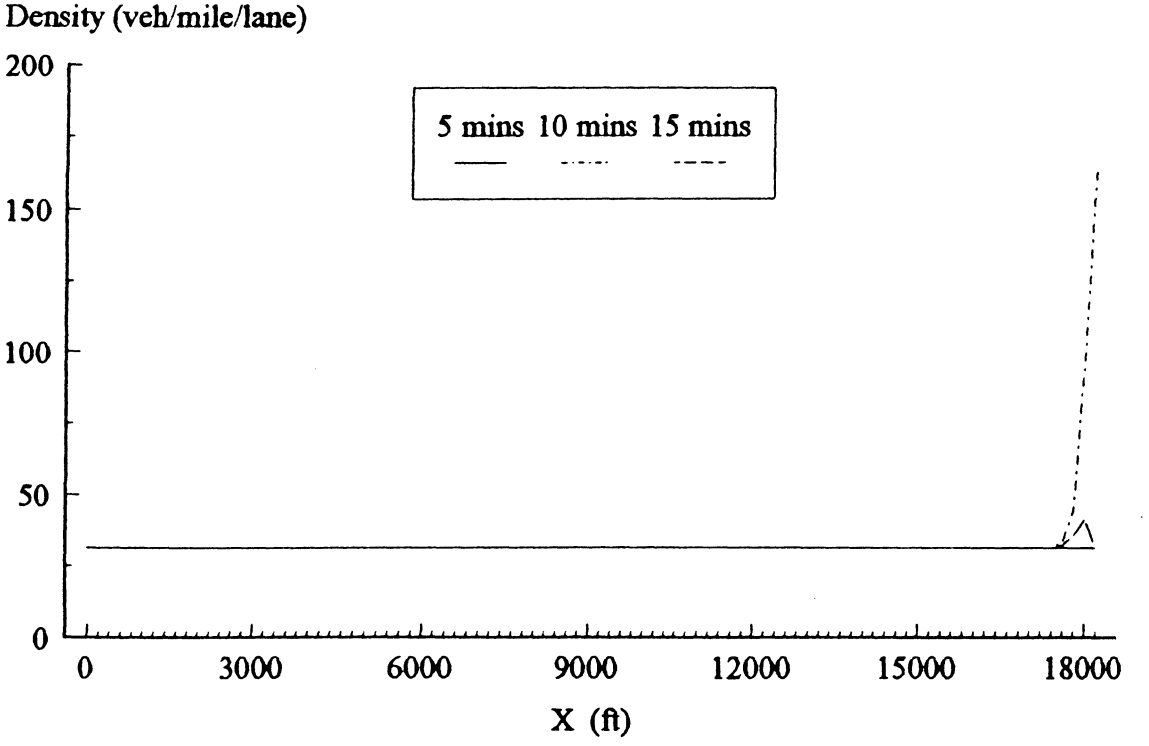

Figure 11.2 5-minute average density produced by the original high-order model (Euler method) for case 2 when $\nu = 3382.0$ (feet^2/sec) and $\tau = 2.0$ (sec).

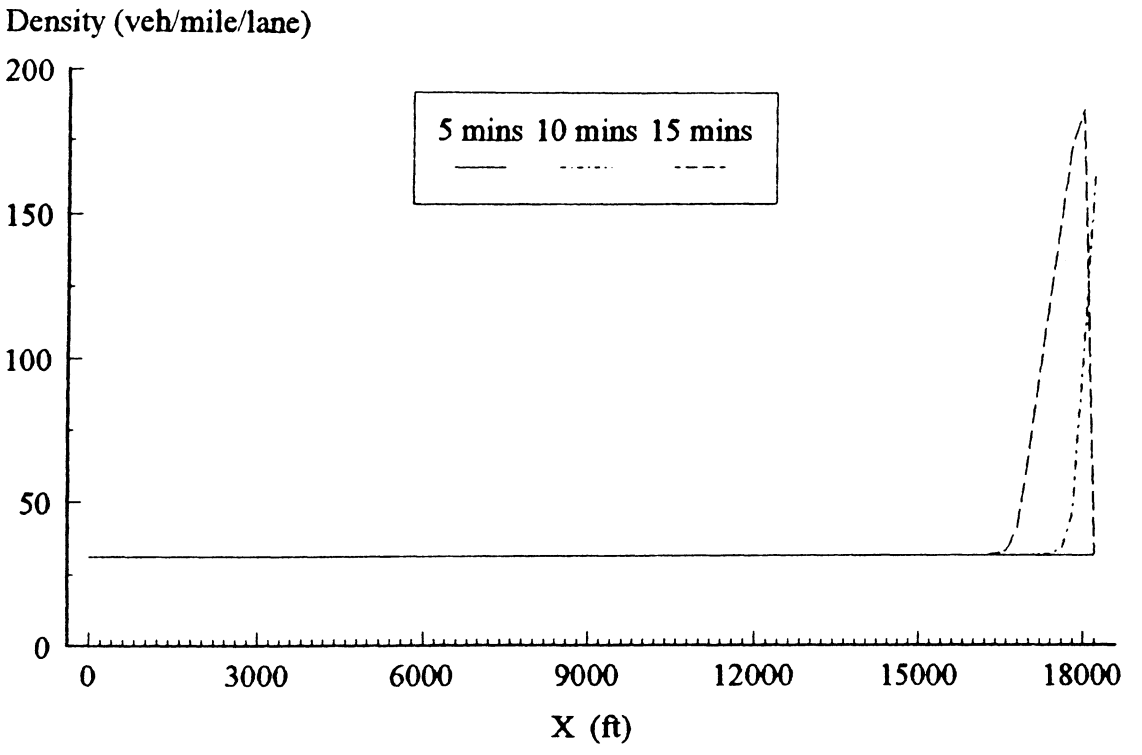

Figure 11.3 5-minute average density produced by the original high-order model (Euler method) for case 2 when $\nu = 3383.0$ (feet^2/sec) and $\tau = 2.0$ (sec).

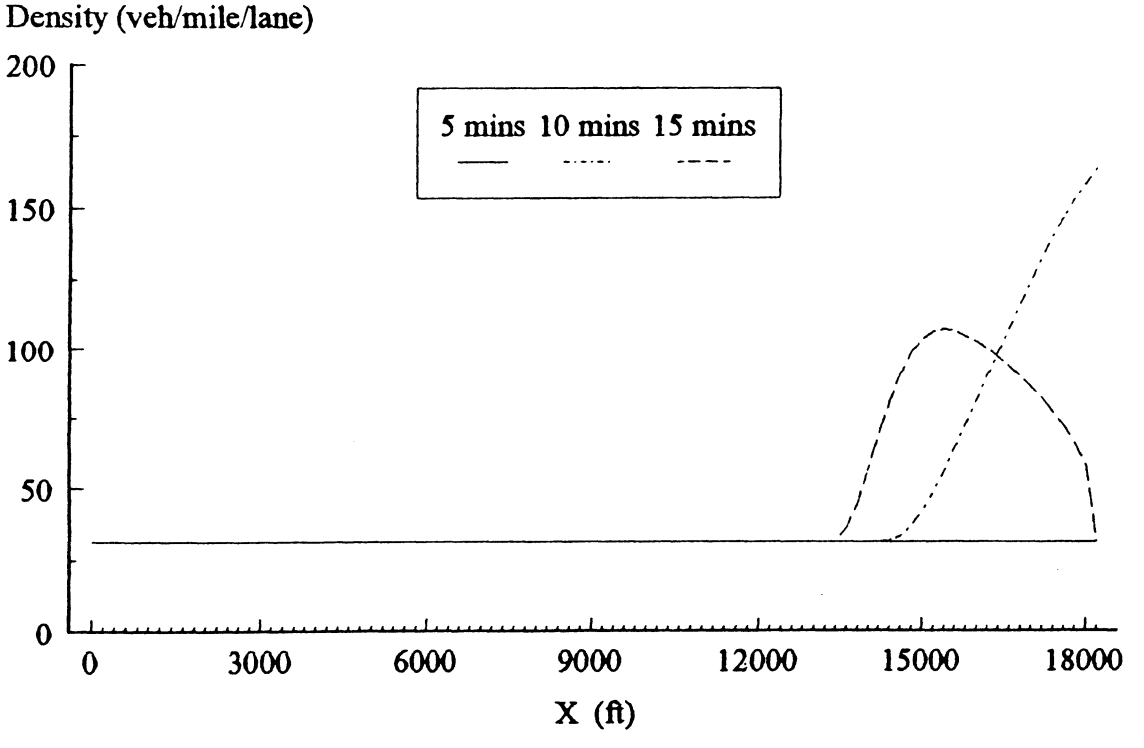

Figure 11.4 5-minute average density produced by the original high-order model (Upwind method) for case 2.

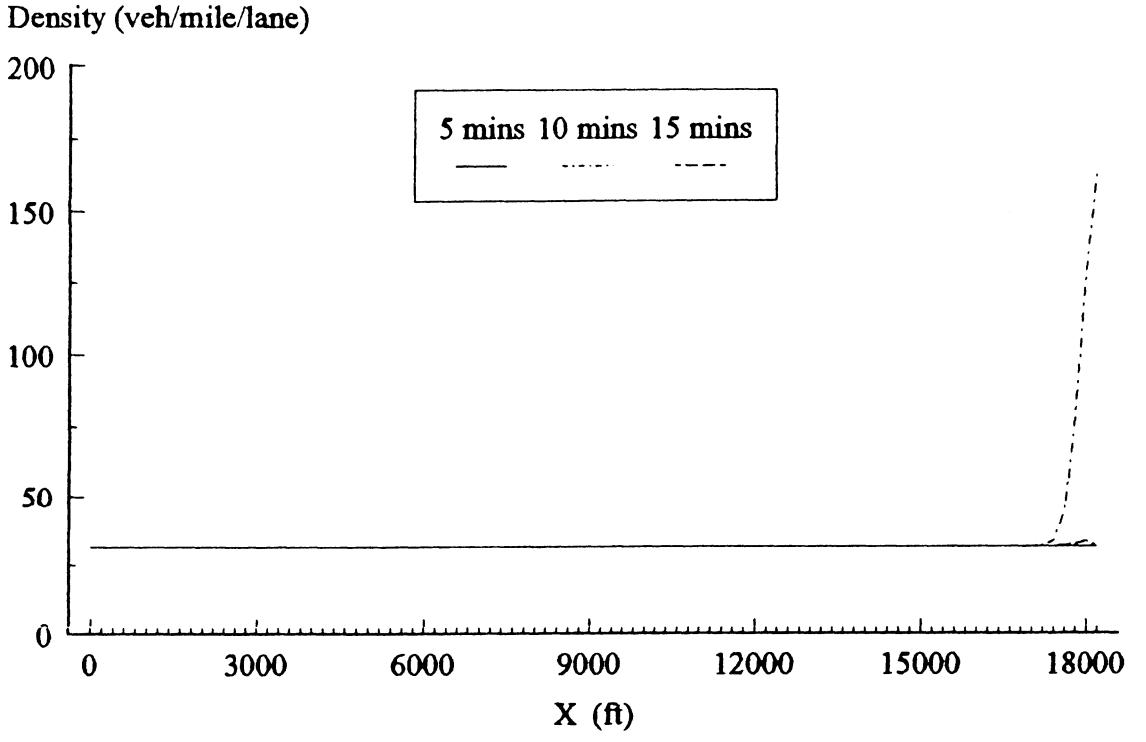

Figure 11.5 5-minute average density produced by the improved high-order model (Euler method) for case 2 when ν = 50229.0 (feet^2/sec) and τ = 36 (sec).

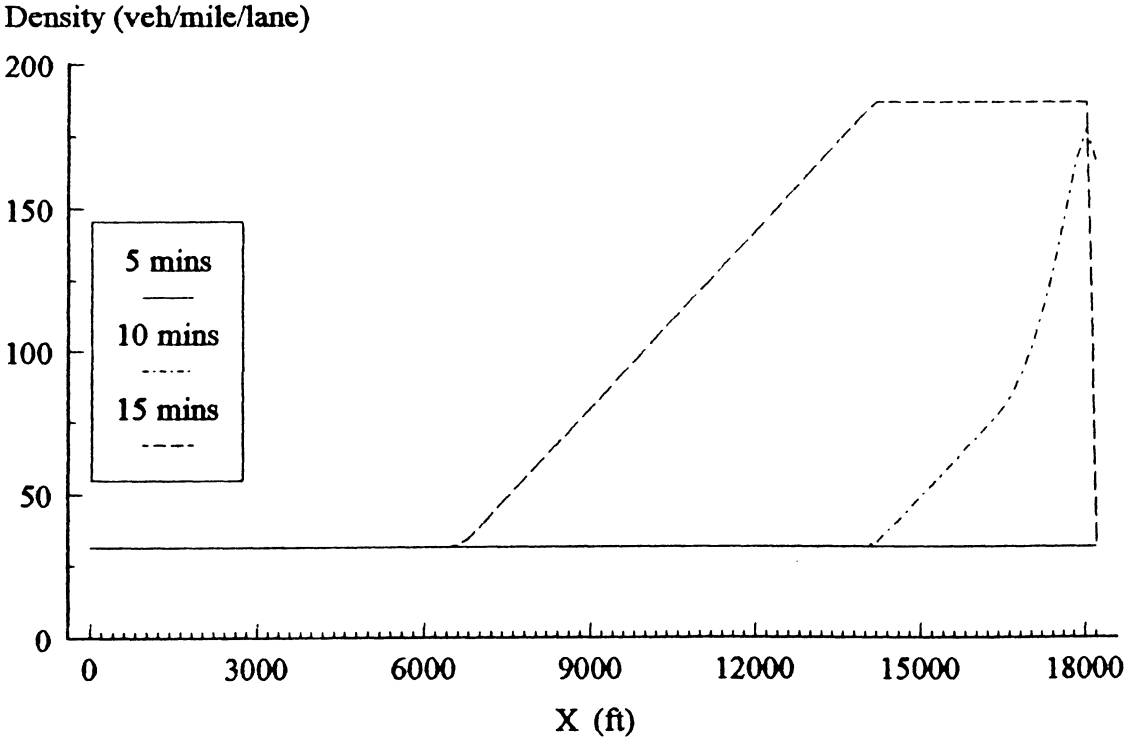

Figure 11.6 5-minute average density produced by the improved high-order model (Euler method) for case 2 when ν = 50230.0 (feet^2/hr) and τ = 36 (sec).

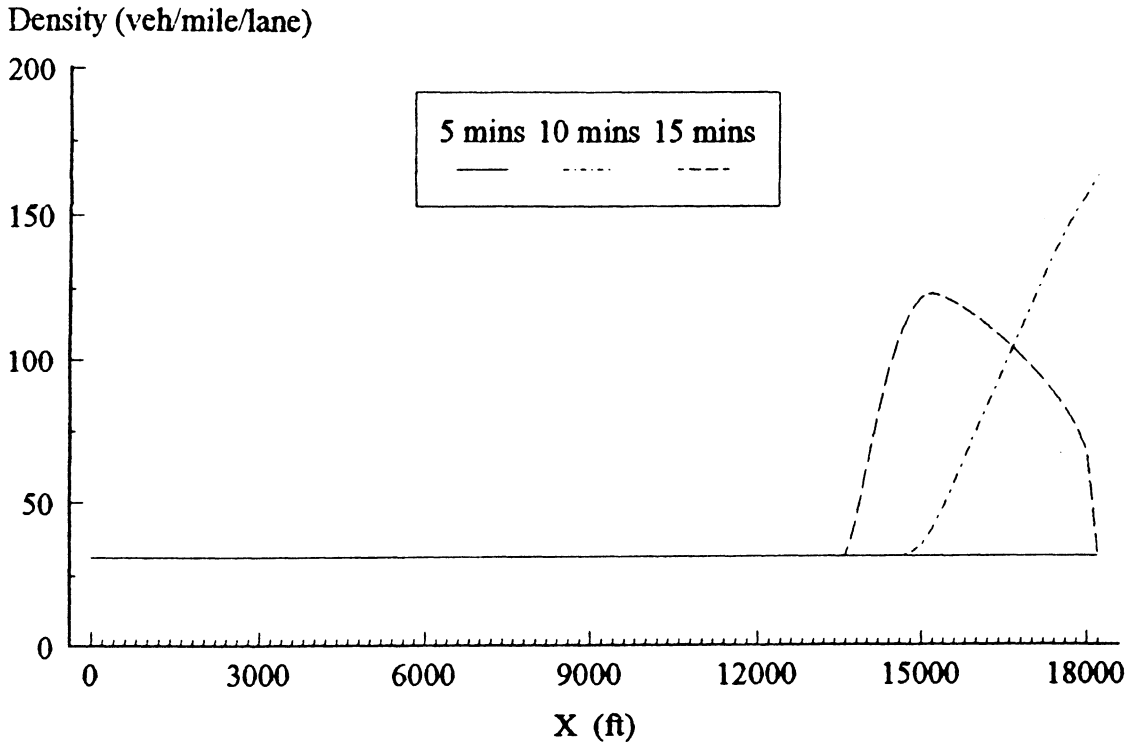

Figure 11.7 5-minute average density produced by the semi-viscous model (Upwind method) for case 2 .

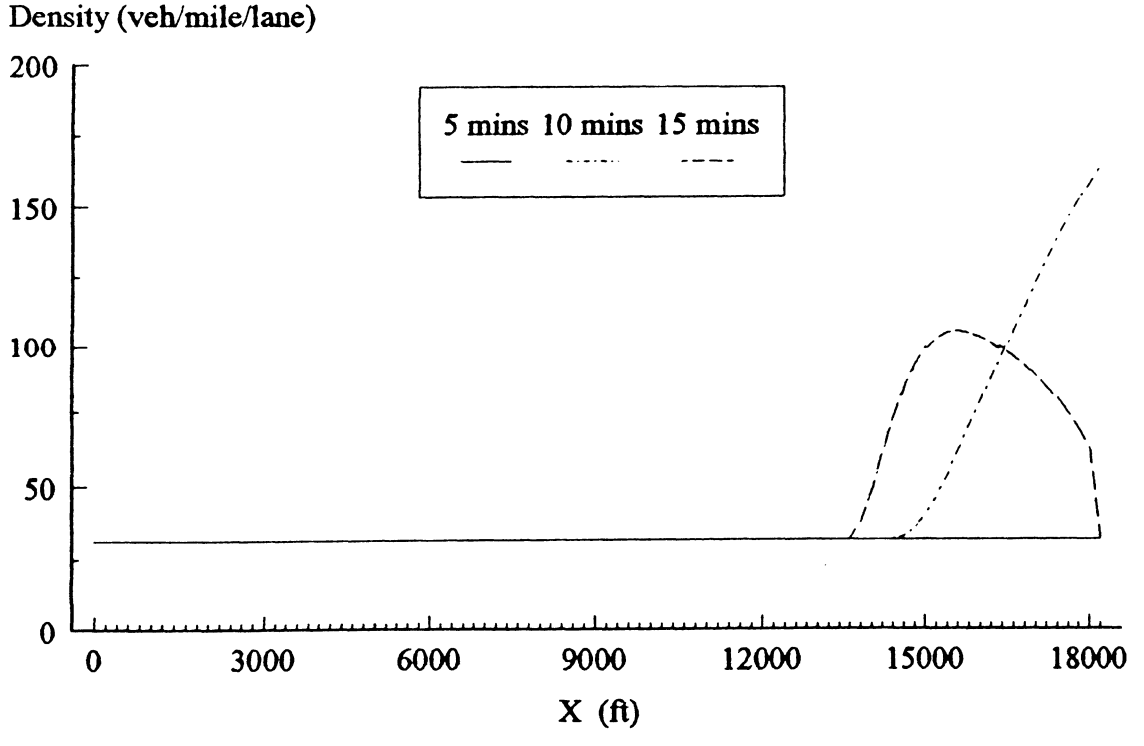

Figure 11.8 5-minute average density produced by the proposed high-order model (Upwind method) for case 2.

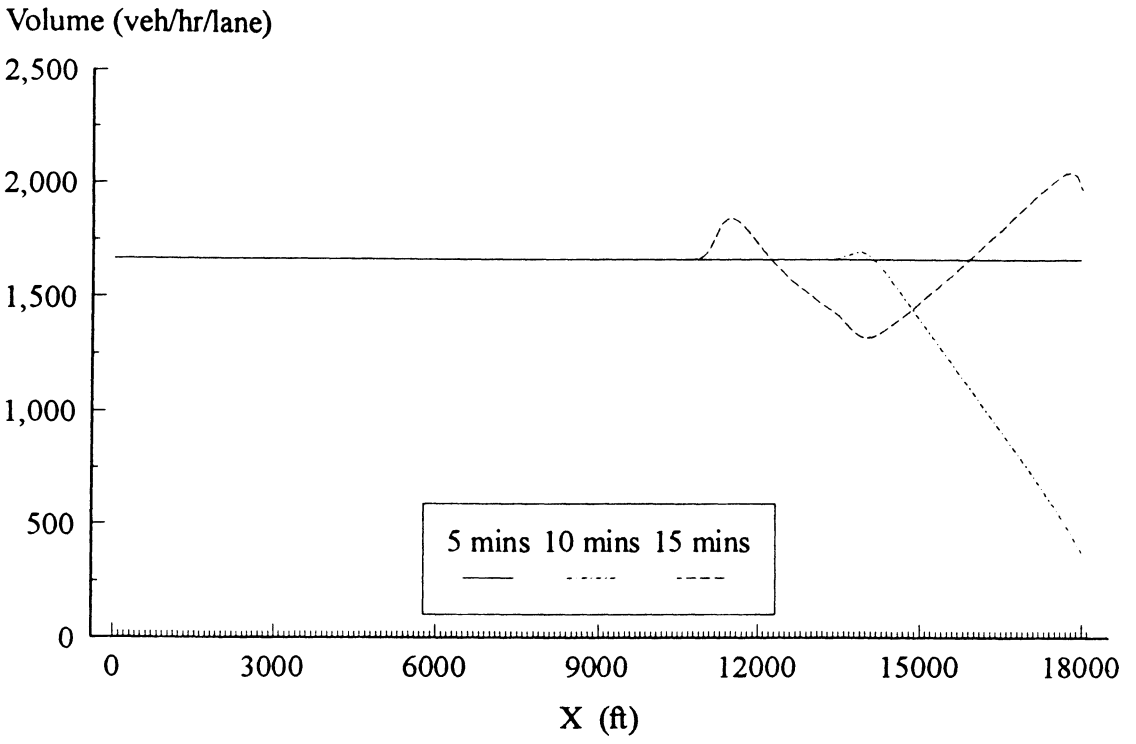

Figure 12.1 5-minute average volume produced by KRONOS for case 3.

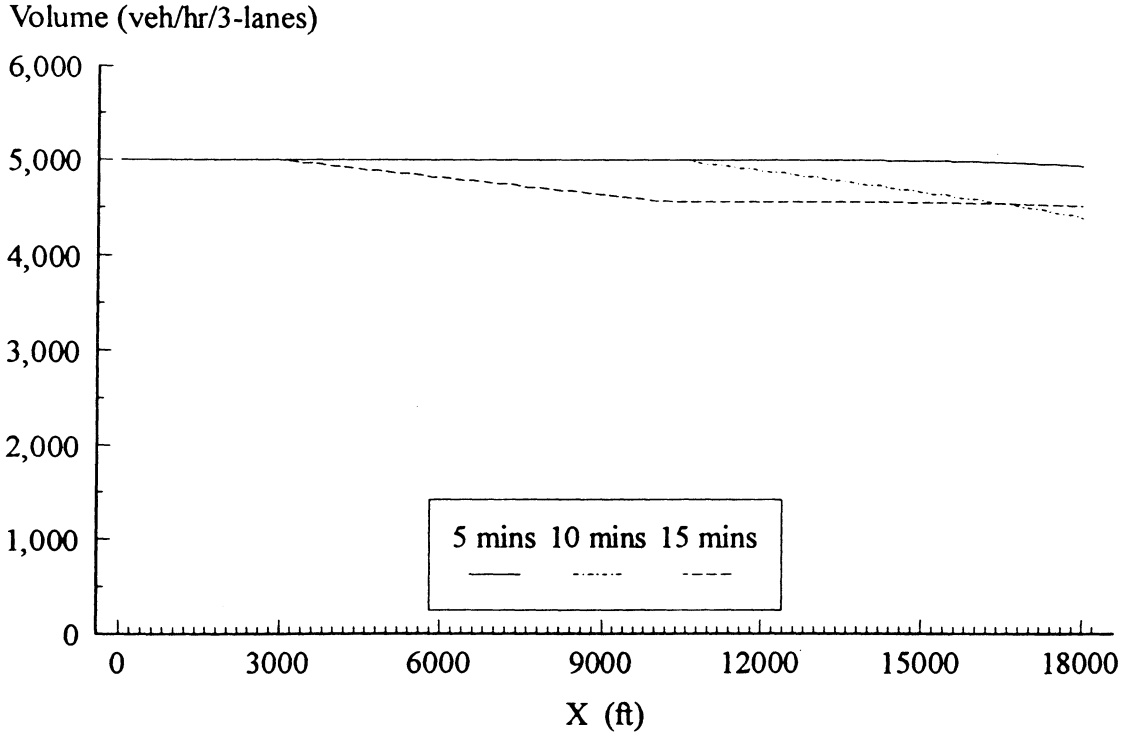

Figure 12.2 5-minute average volume produced by CORFLO (Euler method) for case 3.

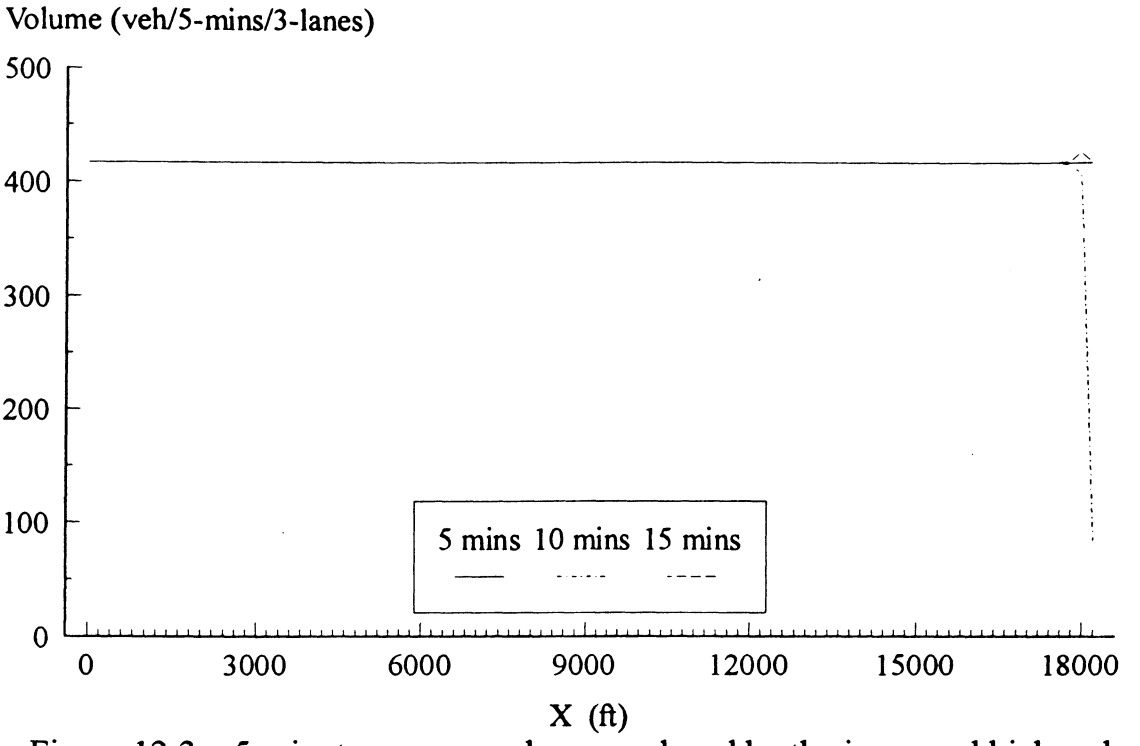

Figure 12.3 5-minute average volume produced by the improved high-order model (Euler method) for case 3 when $\nu = 45247.0$ (feet^2/sec) and $\tau = 36$ (sec).

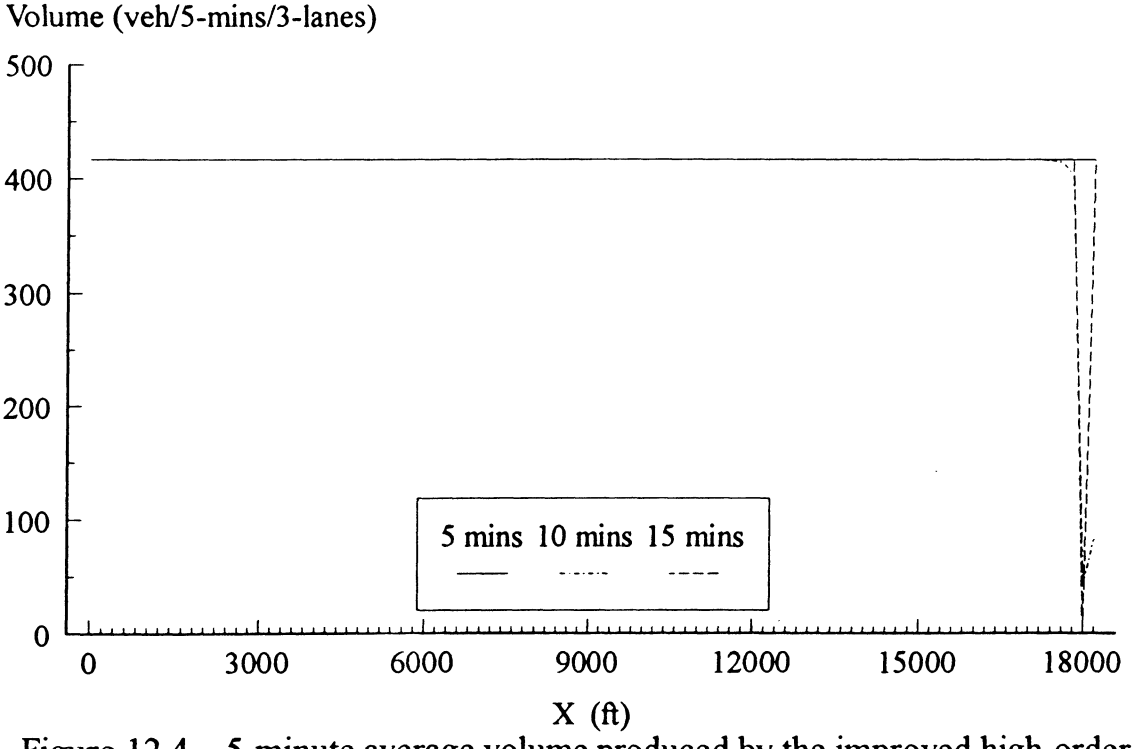

Figure 12.4 5-minute average volume produced by the improved high-order model (Euler method) for case 3 when $\nu = 45248.0$ (feet^2/sec) and $\tau = 36$ (sec).

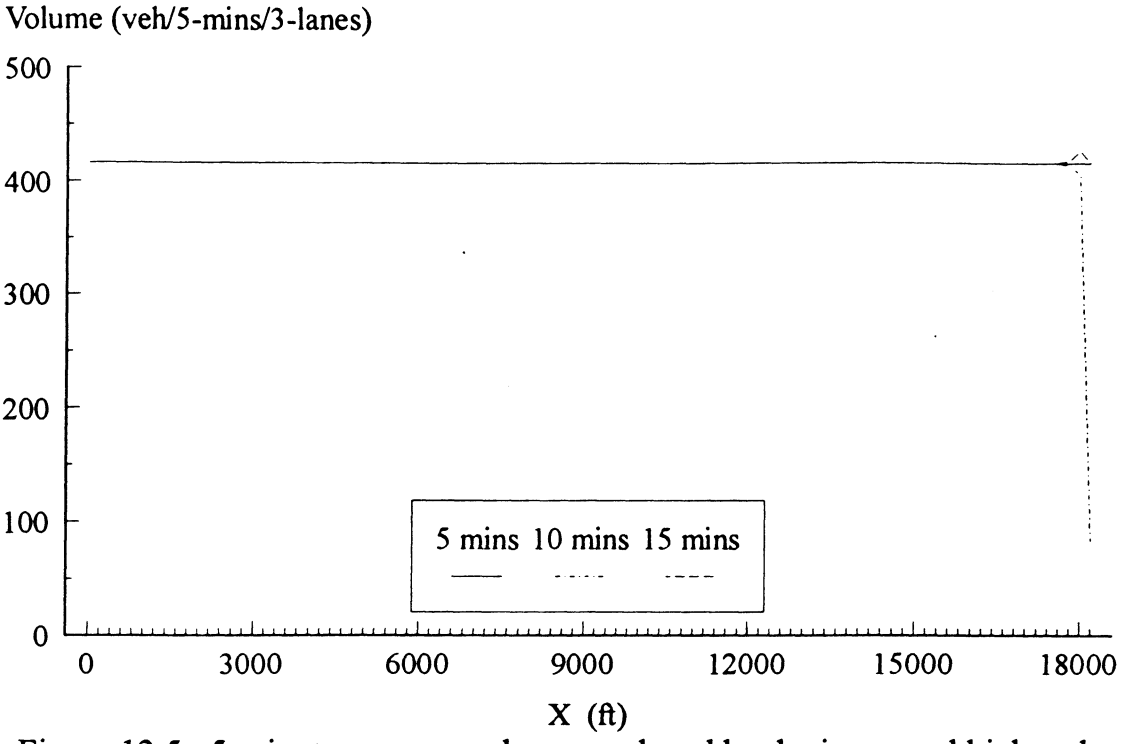

Figure 12.5 5-minute average volume produced by the improved high-order model (Euler method) for case 3 when $\nu = 33709.0$ (feet^2/sec) and $\tau = 26$ (sec).

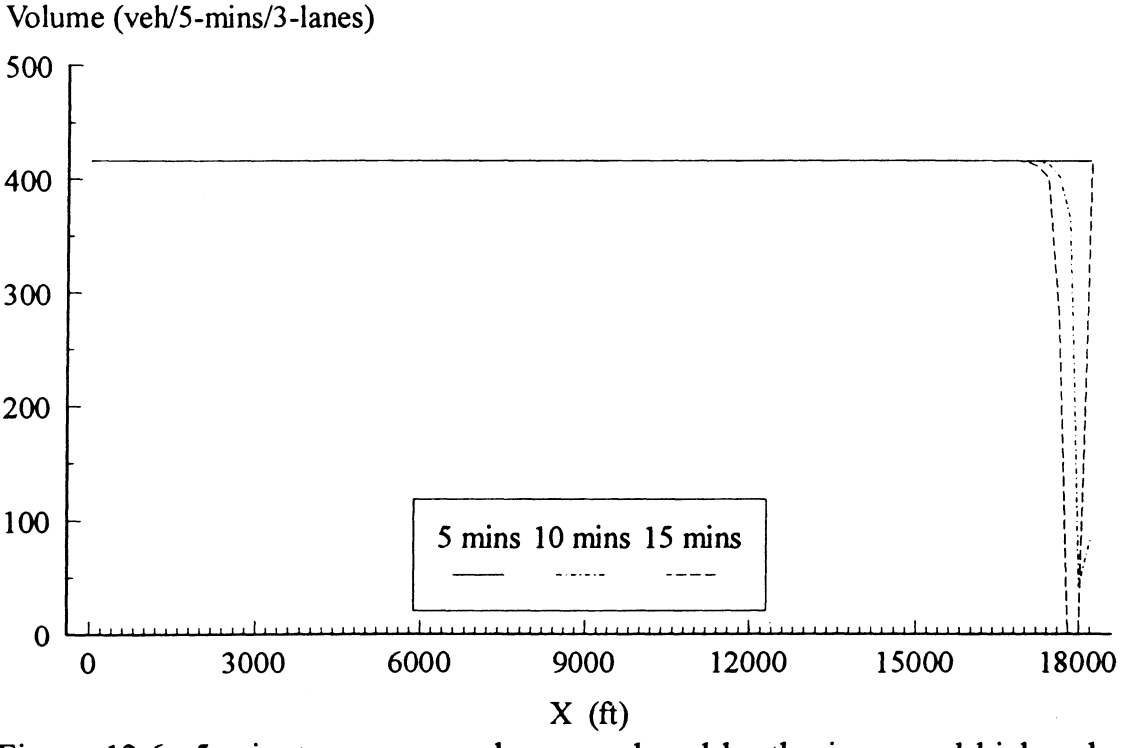

Figure 12.6 5-minute average volume produced by the improved high-order model (Euler method) for case 3 when $\nu = 33710.0$ (feet^2/sec) and $\tau = 26$ (sec).

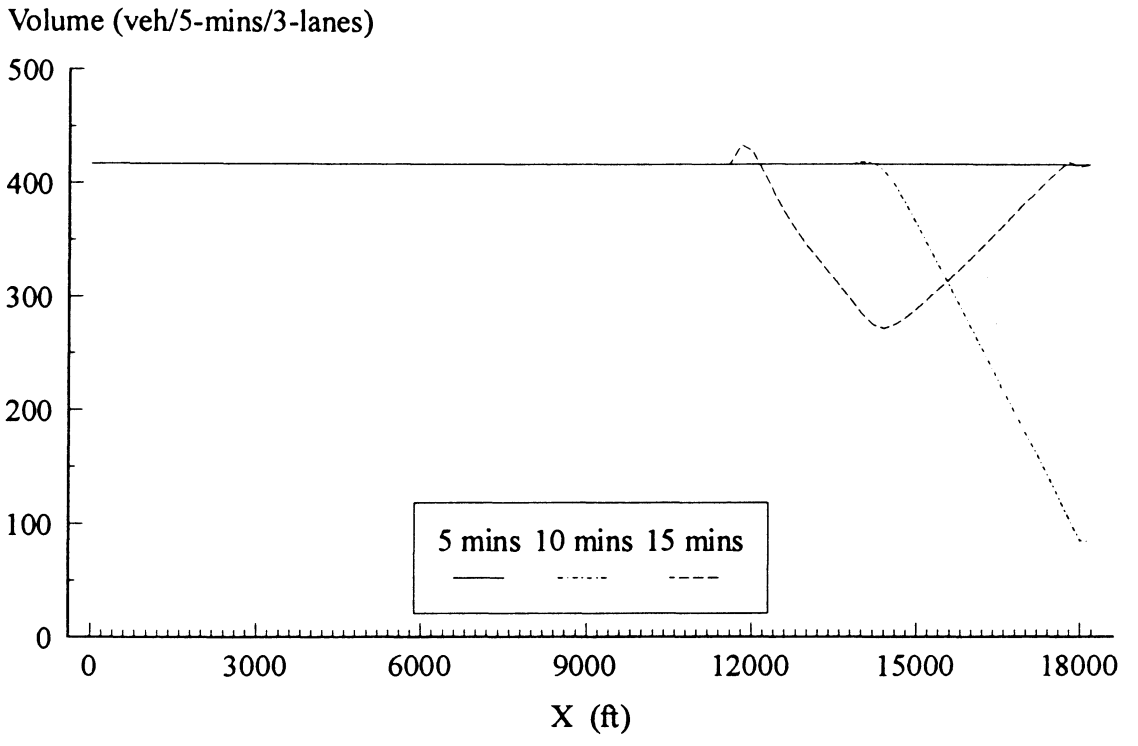

Figure 12.7 5-minute average volume produced by the semi-viscous model (Upwind method) for case 3.

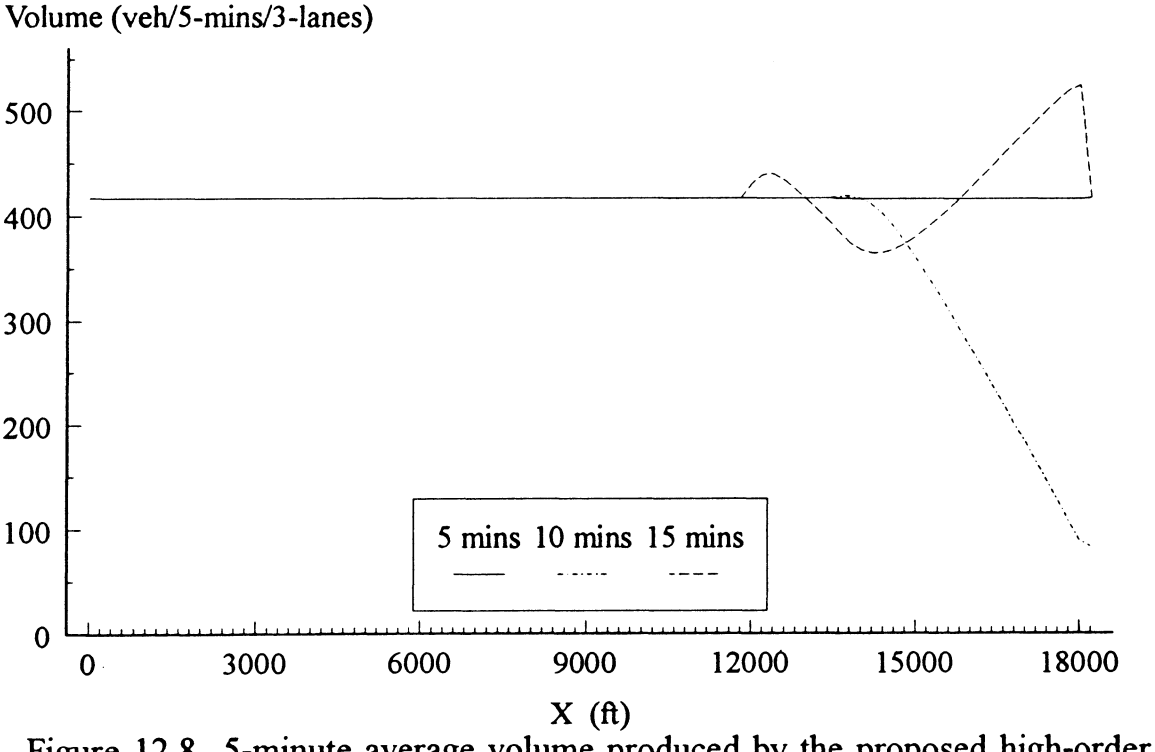

Figure 12.8 5-minute average volume produced by the proposed high-order model (Upwind method) for case 3.

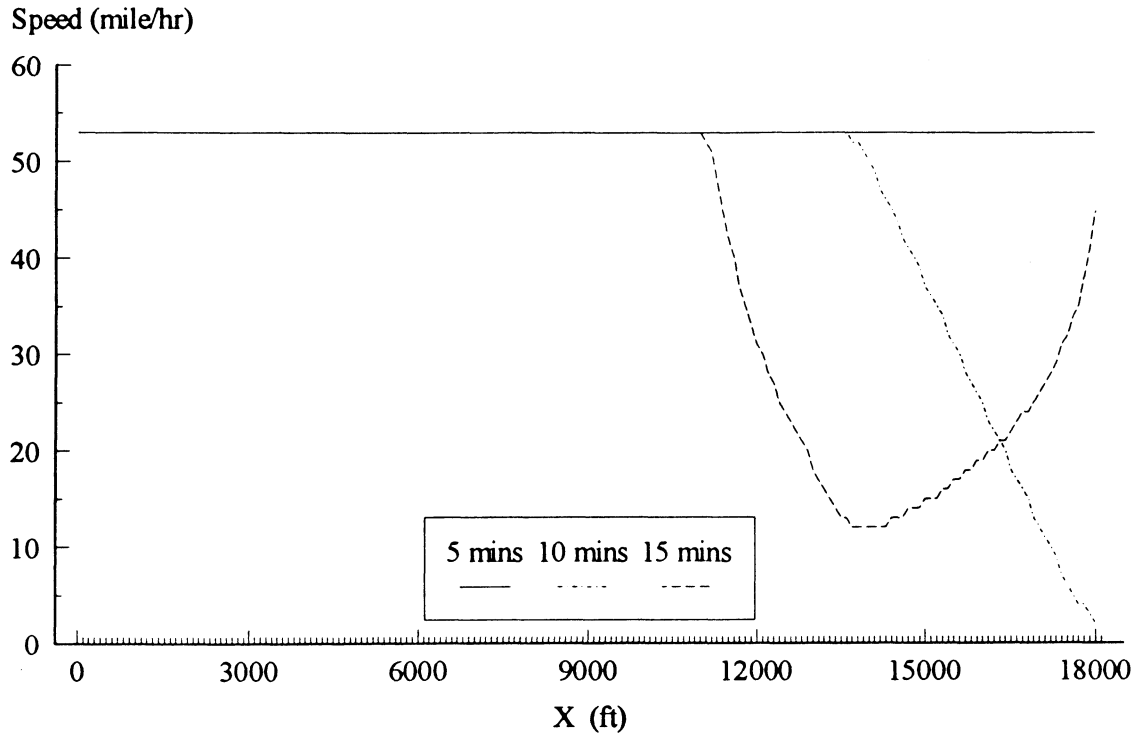

Figure 13.1 5-minute average speed produced by KRONOS for case 3.

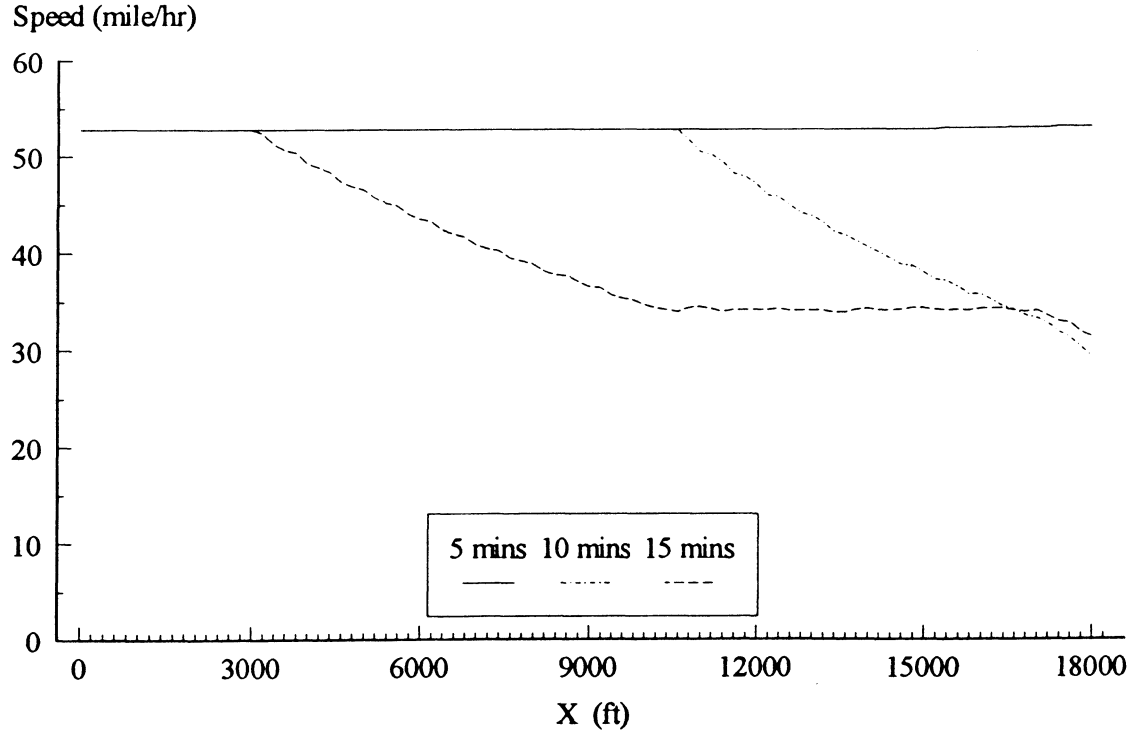

Figure 13.2 5-minute average speed produced by CORFLO (Euler method) for case 3.

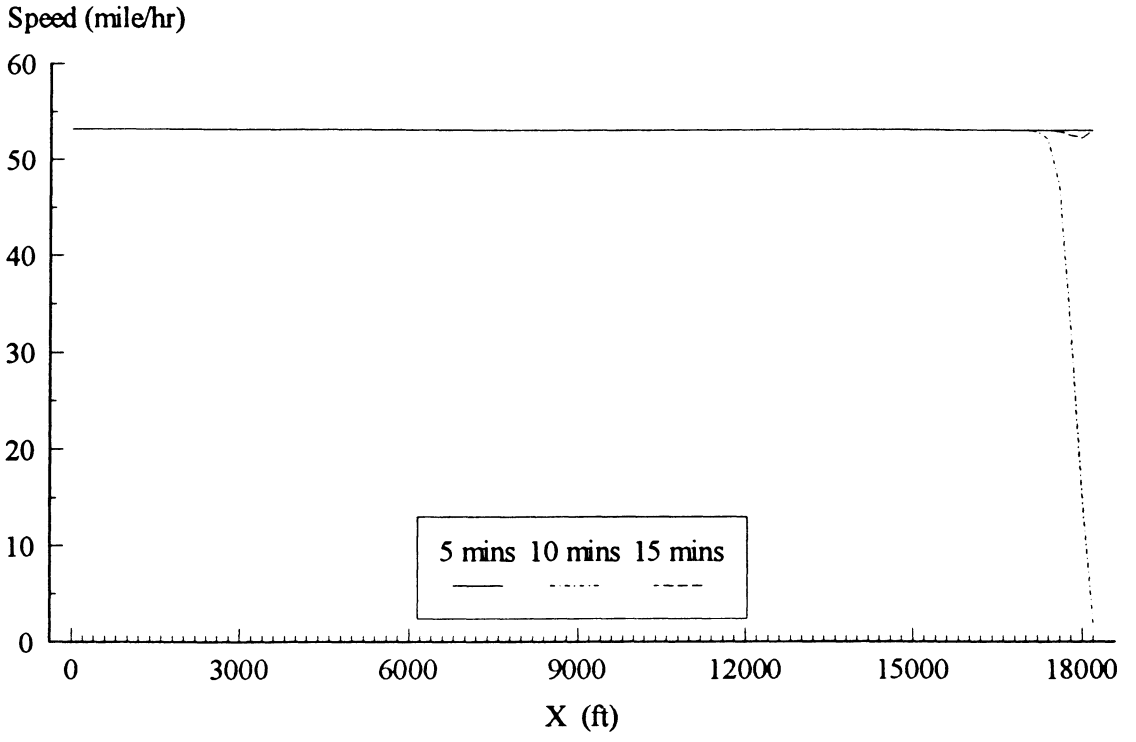

Figure 13.3 5-minute average speed produced by the improved high-order model (Euler method) for case 3 when n = 45247.0 (feet^2/sec) and t = 36 (sec).

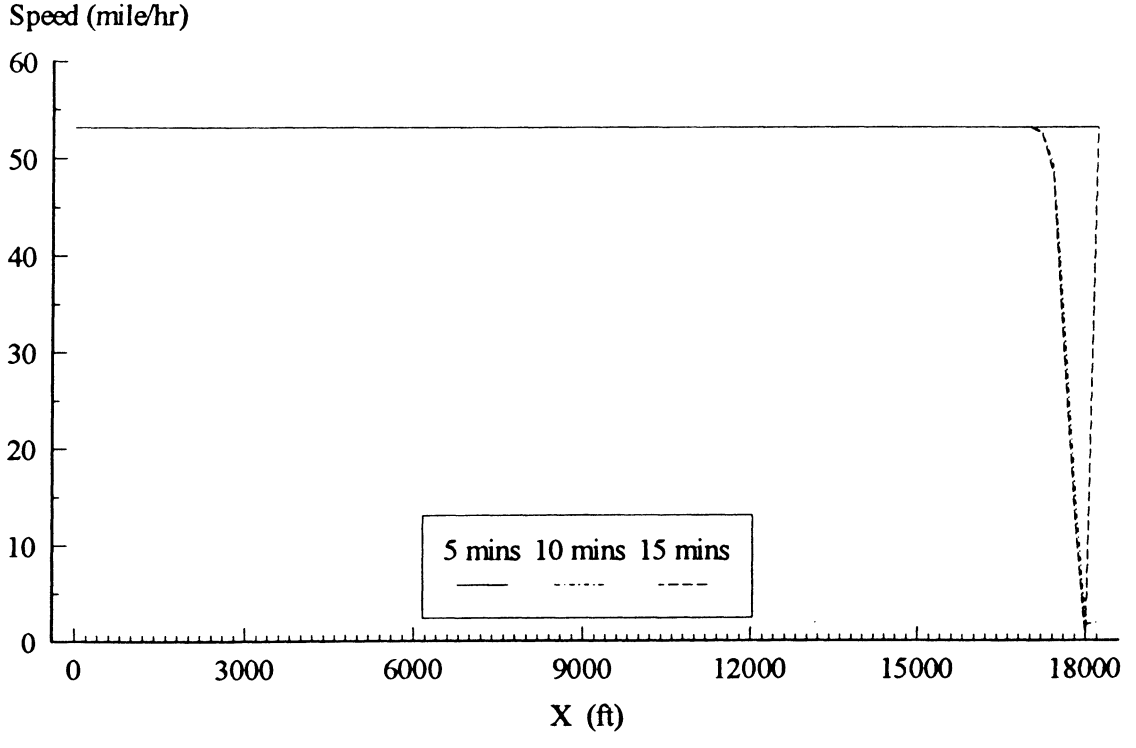

Figure 13.4 5-minute average speed produced by the improved high-order model (Euler method) for case 3 when $\nu = 45248.0$ (feet^2 /sec) and $\tau = 36$ (sec).

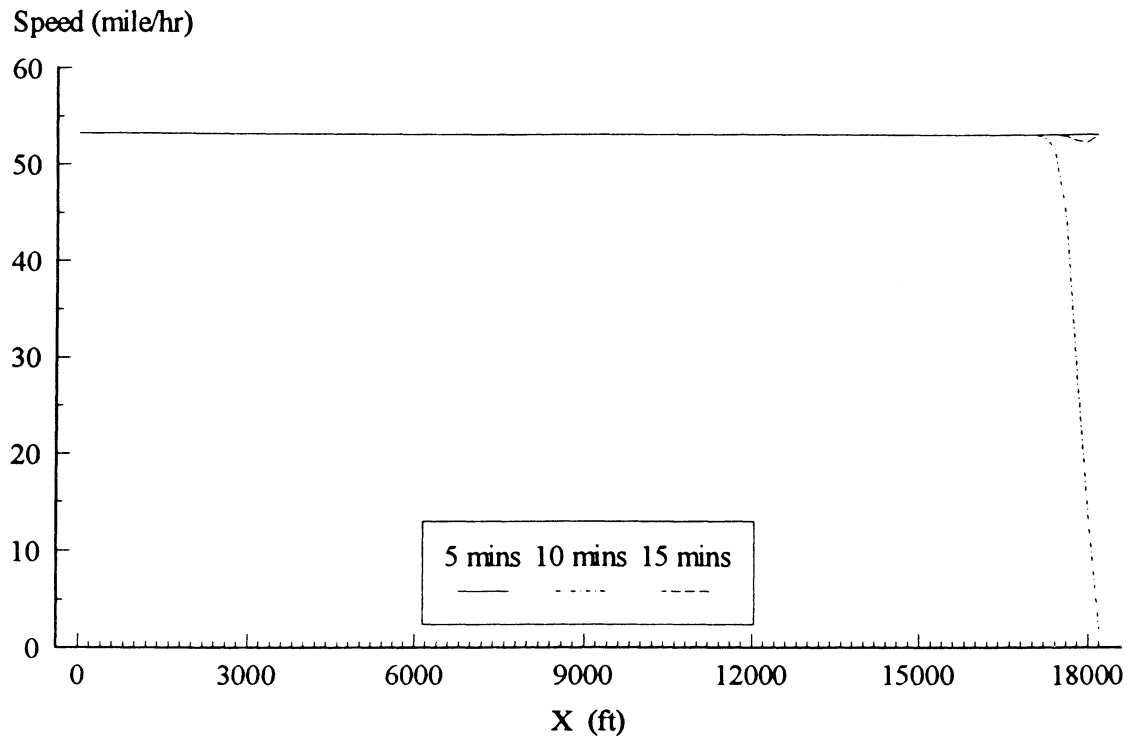

Figure 13.5 5-minute average speed produced by the improved high-order model (Euler method) for case 3 when $\nu = 33709.0$ (feet^2 /sec) and $\tau = 26$ (sec).

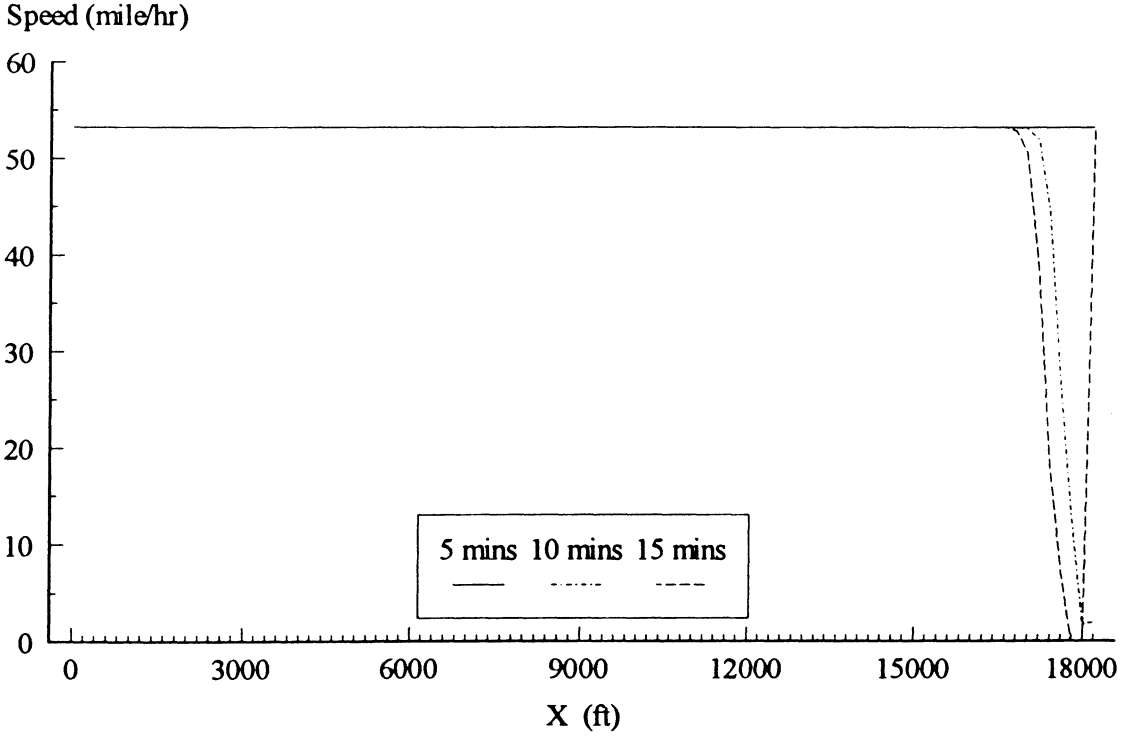

Figure 13.6 5-minute average speed produced by the improved high-order model (Euler method) for case 3 when $\nu = 33710.0$ (feet^2 /sec) and $\tau = 26$ (sec).

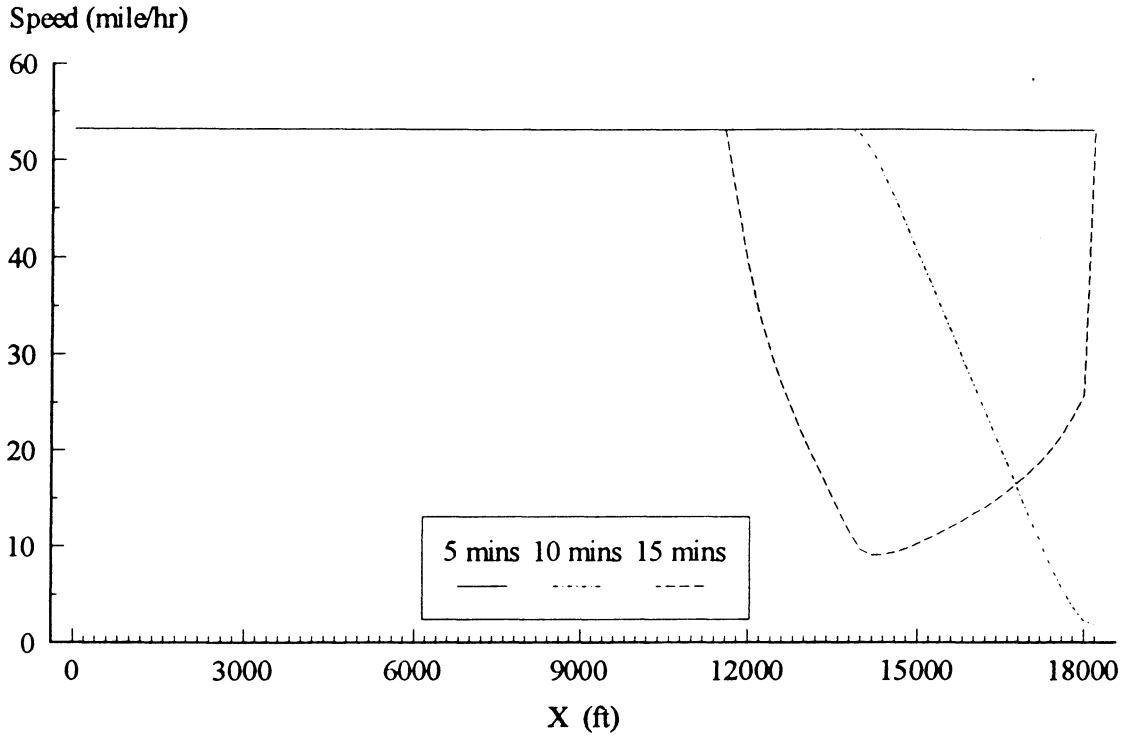

Figure 13.7 5-minute average speed produced by the semi-viscous model (Upwind method) for case 3.

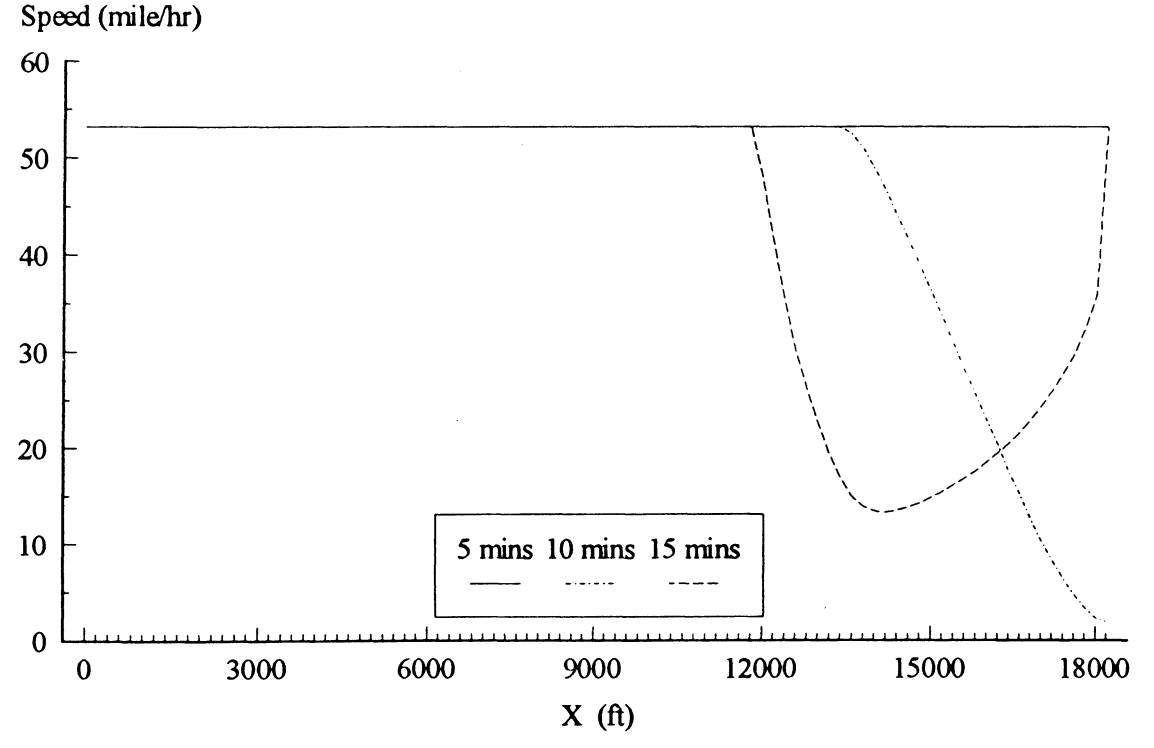

Figure 13.8 5-minute average speed produced by the proposed high-order model (Upwind method) for case 3.

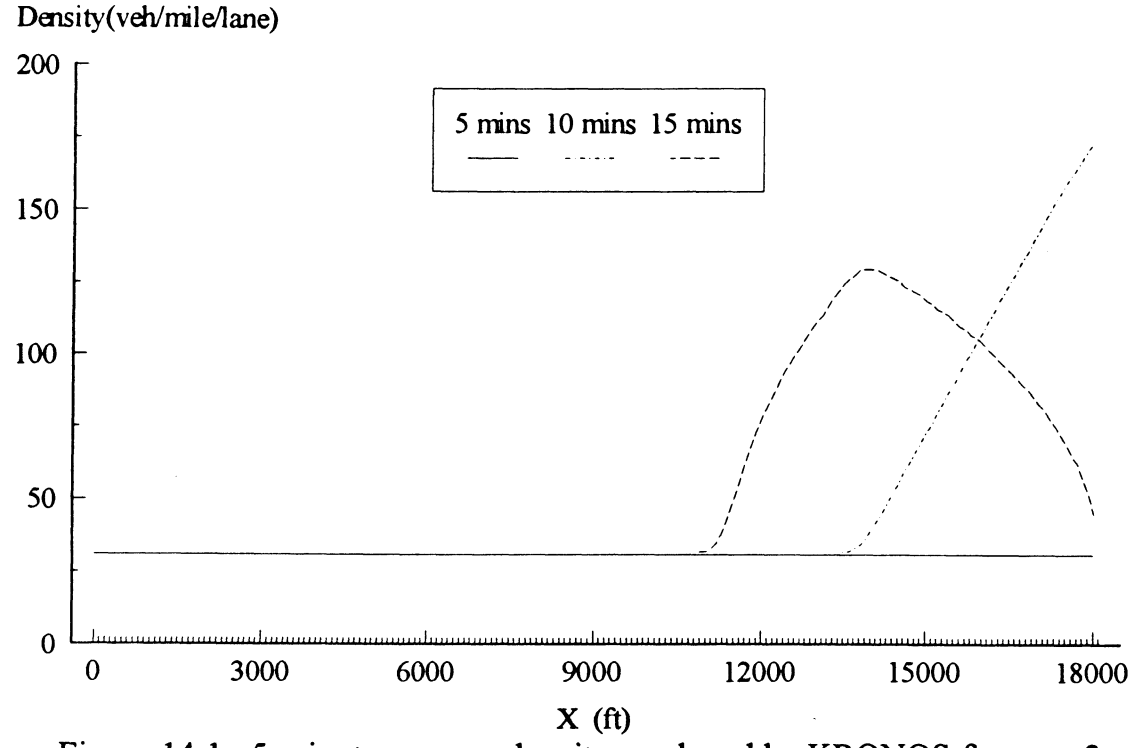

Figure 14.1 5-minute average density produced by KRONOS for case 3.

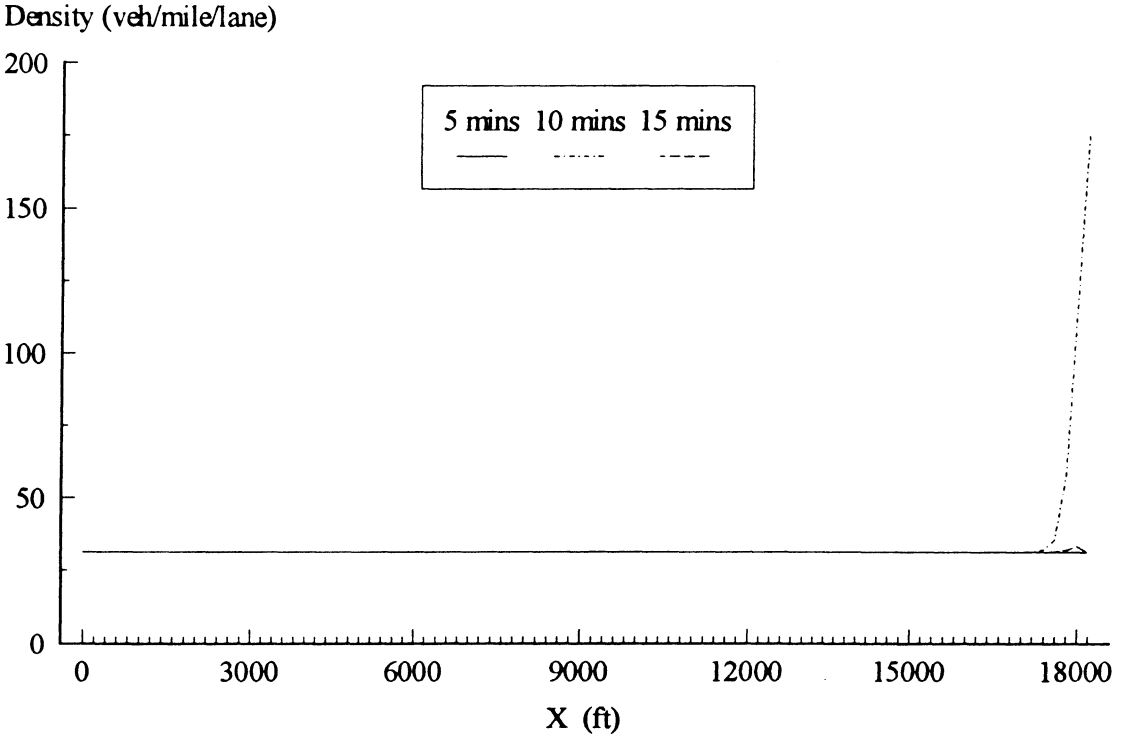

Figure 14.2 5-minute average density produced by the improved high-order model (Euler method) for case 3 when $\nu = 45247.0$ (feet^2/sec) and $\tau = 36$ (sec).

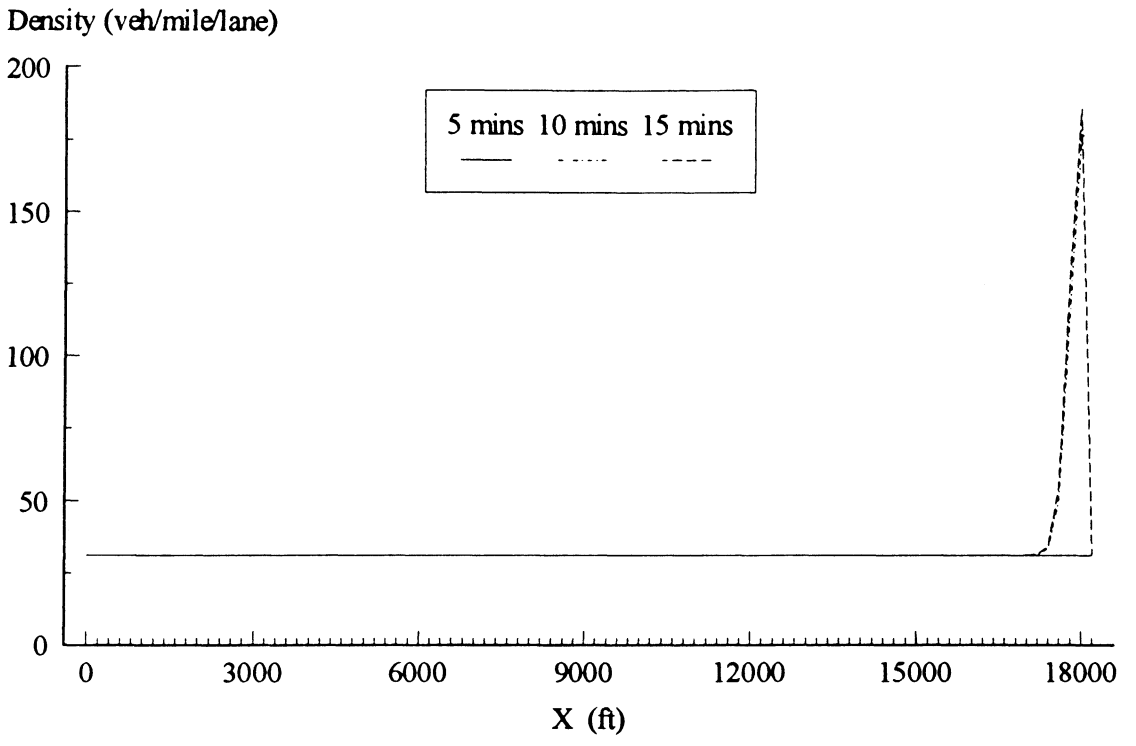

Figure 14.3 5-minute average density produced by the improved high-order model (Euler method) for case 3 when $\nu = 45248.0$ (feet^2/sec) and $\tau = 36$ (sec).

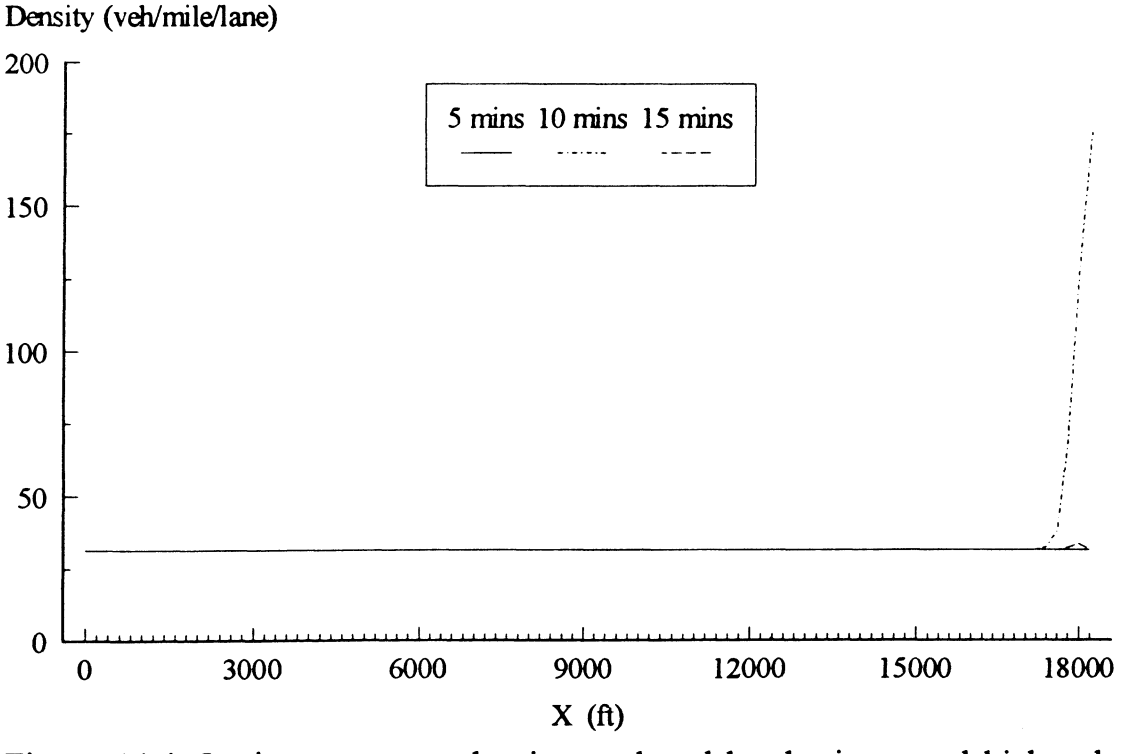

Figure 14.4 5-minute average density produced by the improved high-order model (Euler method) for case 3 when $\nu = 33709.0$ (feet^2/sec) and $\tau = 26$ (sec).

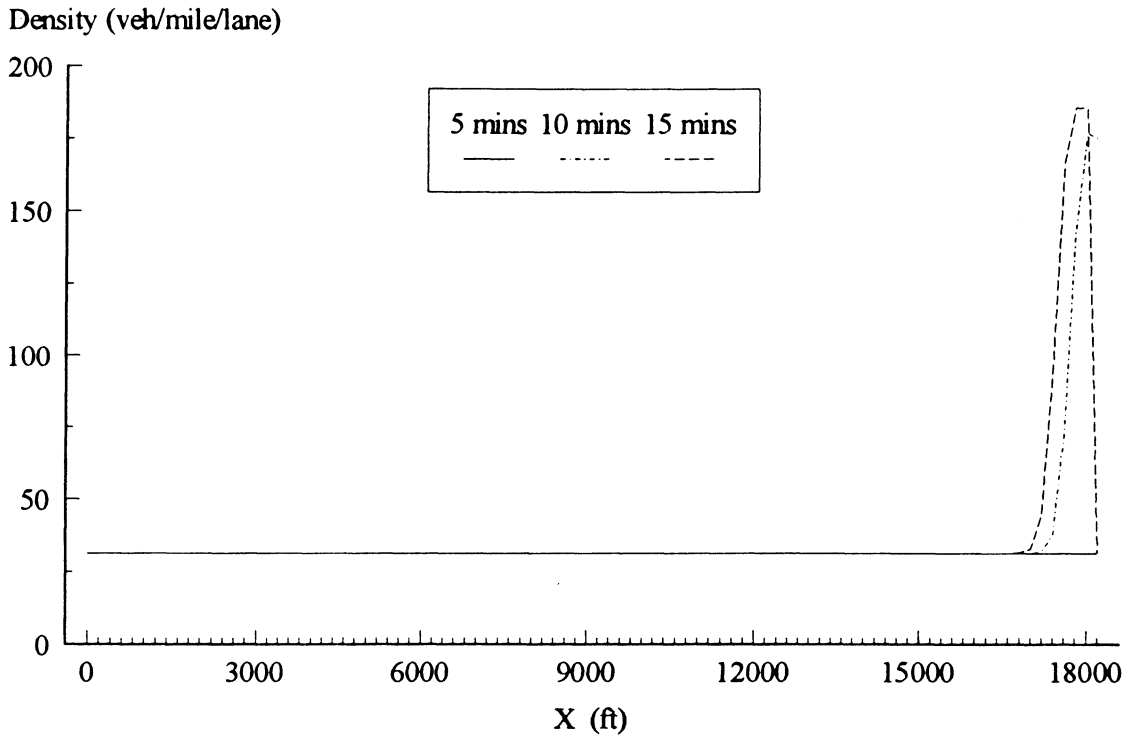

Figure 14.5 5-minute average density produced by the improved high-order model (Euler method) for case 3 when $\nu = 33710.0$ (feet^2/sec) and $\tau = 26$ (sec).

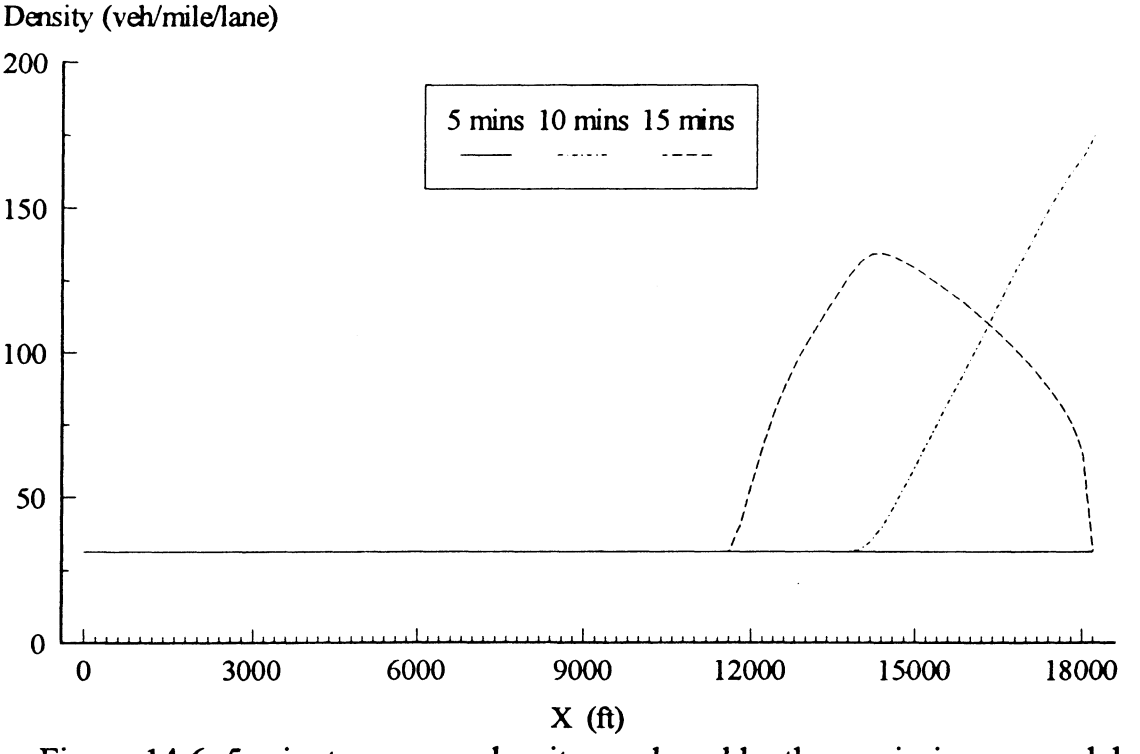

Figure 14.6 5-minute average density produced by the semi-viscous model for case 3.

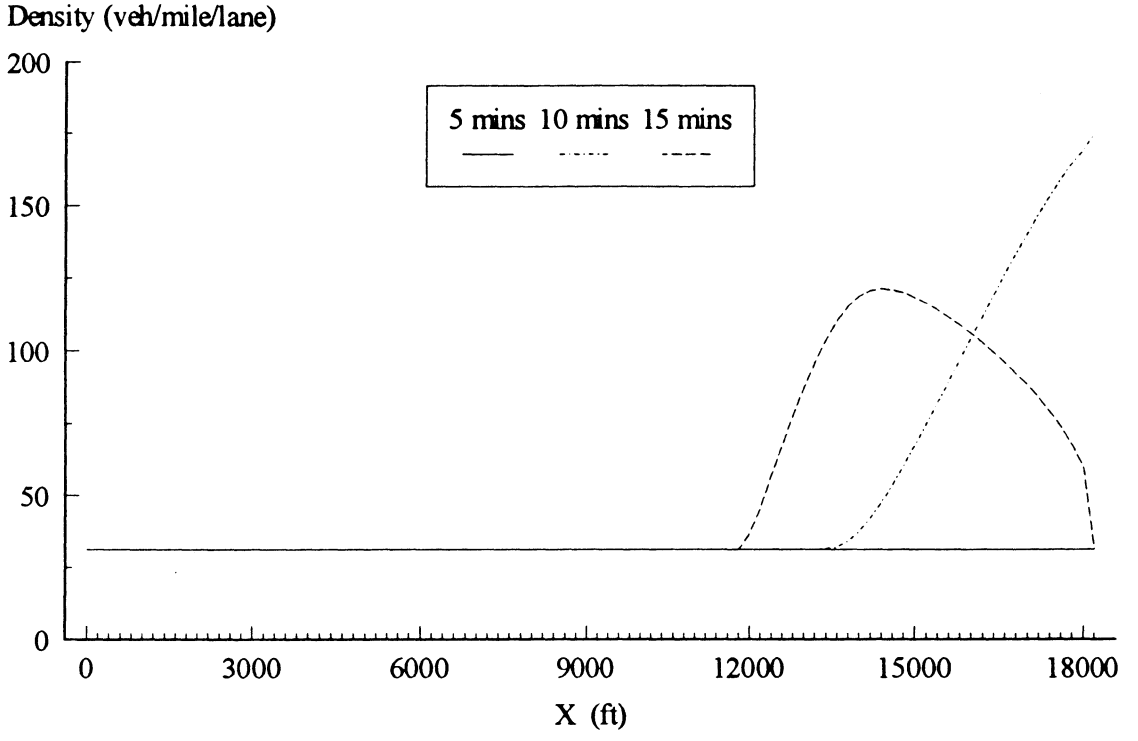

Figure 14.7 5-minute average density produced by the proposed high-order model for case 3.

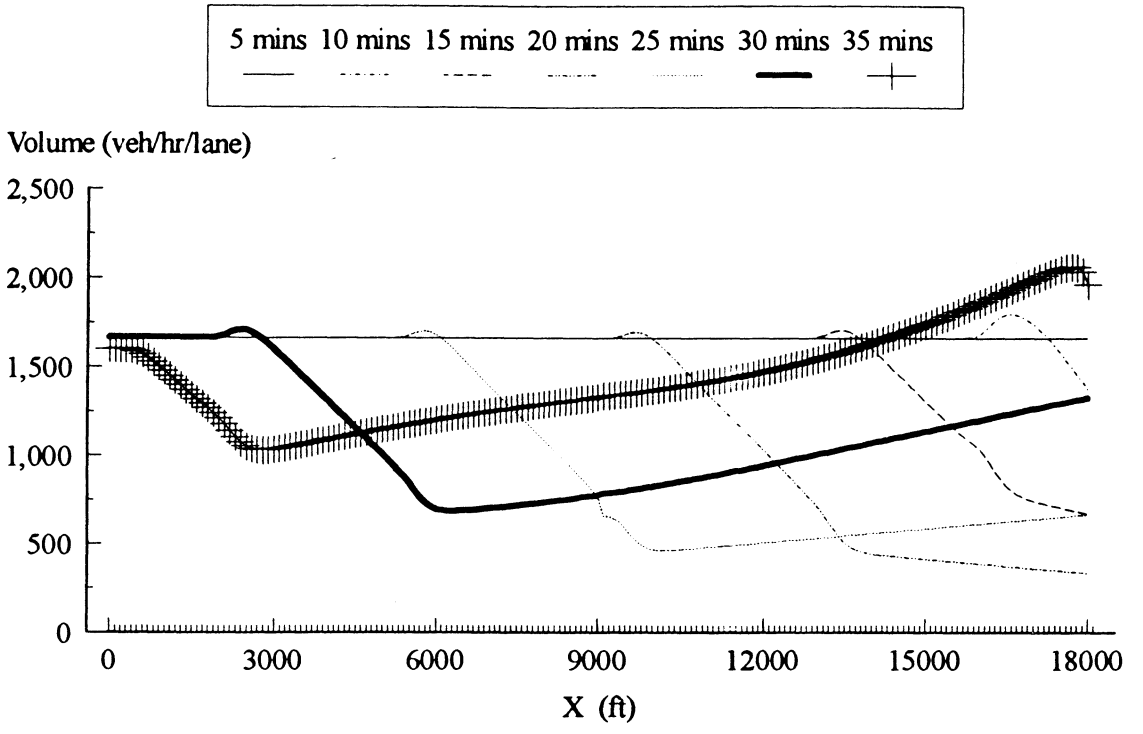

Figure 15.1 5-minute average volume produced by KRONOS for case 4.

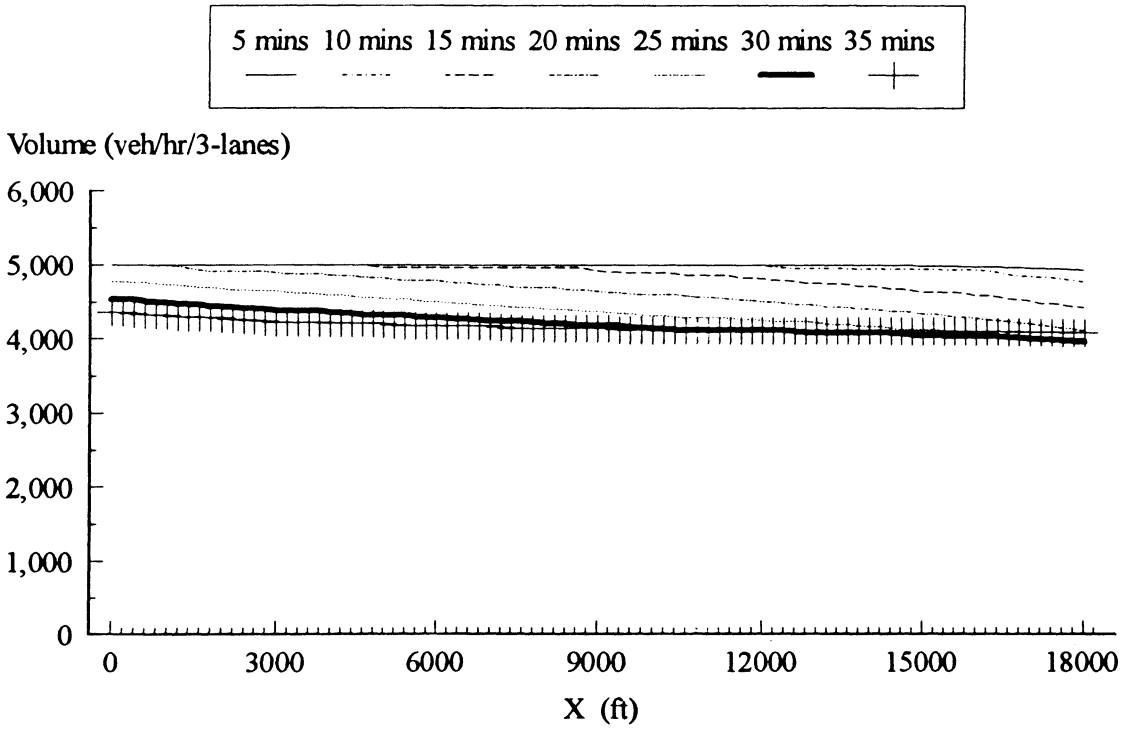

Figure 15.2 5-minute average volume produced by CORFLO (Euler method) for case 4.

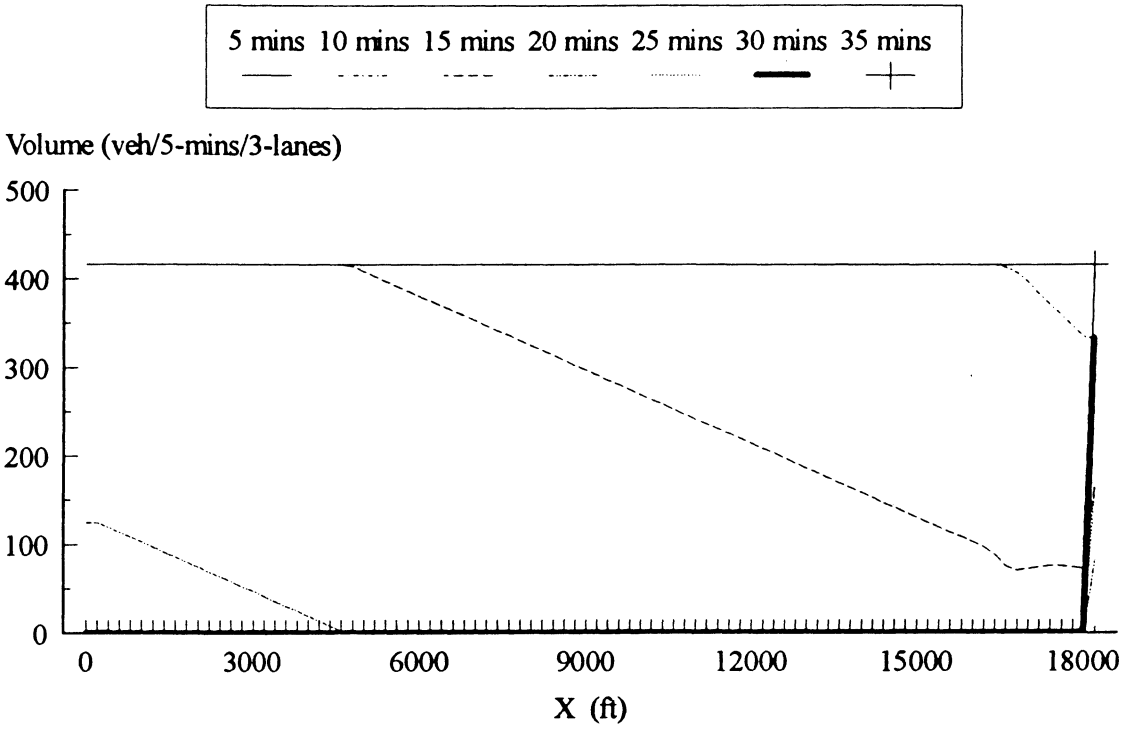

Figure 15.3 5-minute average volume produced by the improved high-order model (Euler method) for case 3 when $\nu = 68070.0$ (feet^2/sec) and $\tau = 36$ (sec).

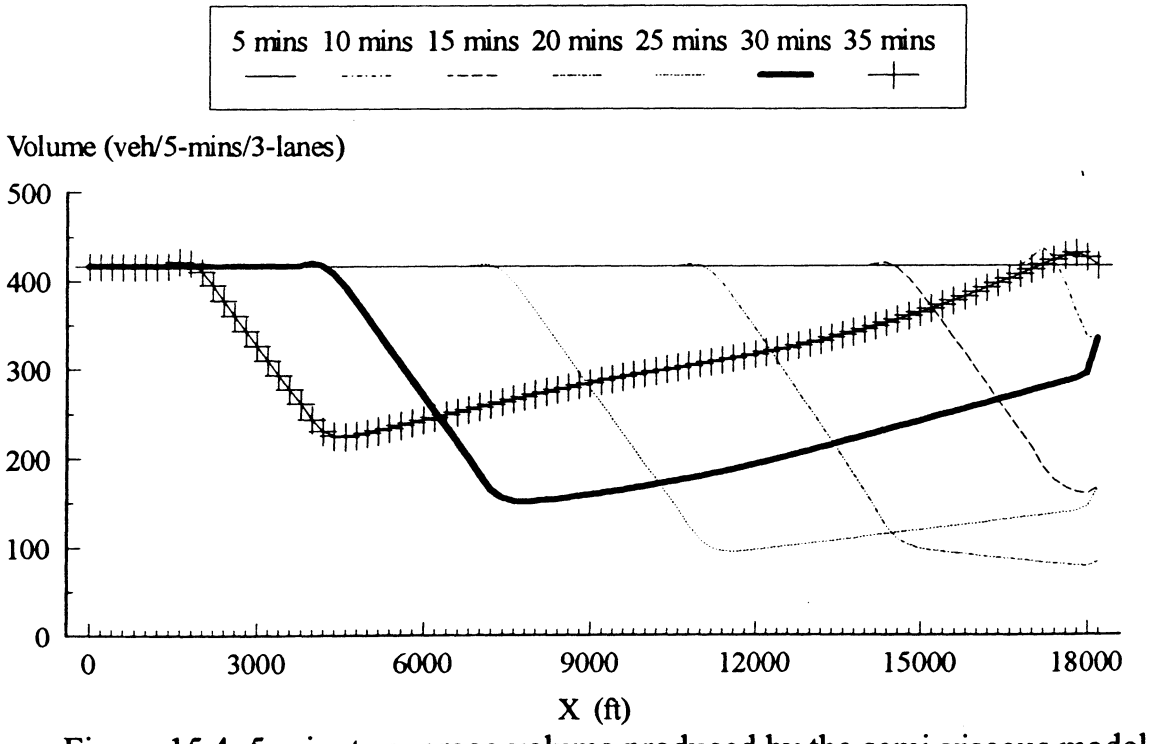

Figure 15.4 5-minute average volume produced by the semi-viscous model (Upwind method) for case 4.

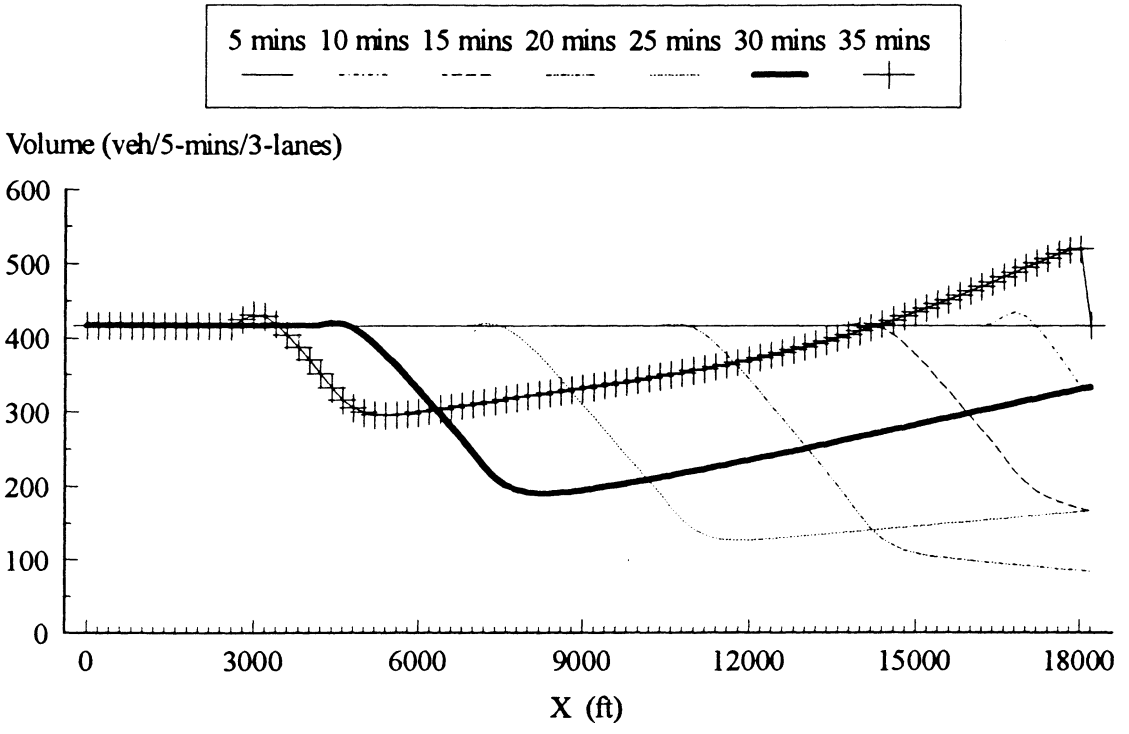

Figure 15.5 5-minute average volume produced by the proposed high-order model (Upwind method) for case 4.

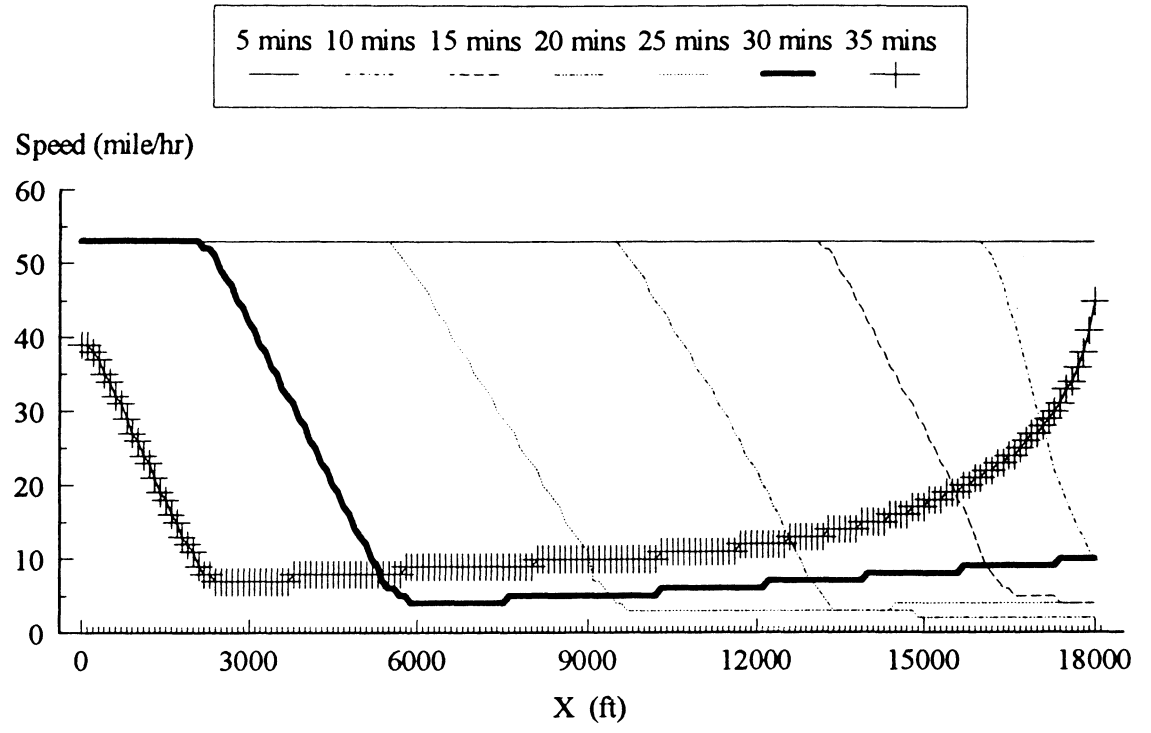

Figure 16.1 5-minute average speed produced by KRONOS for case 4.

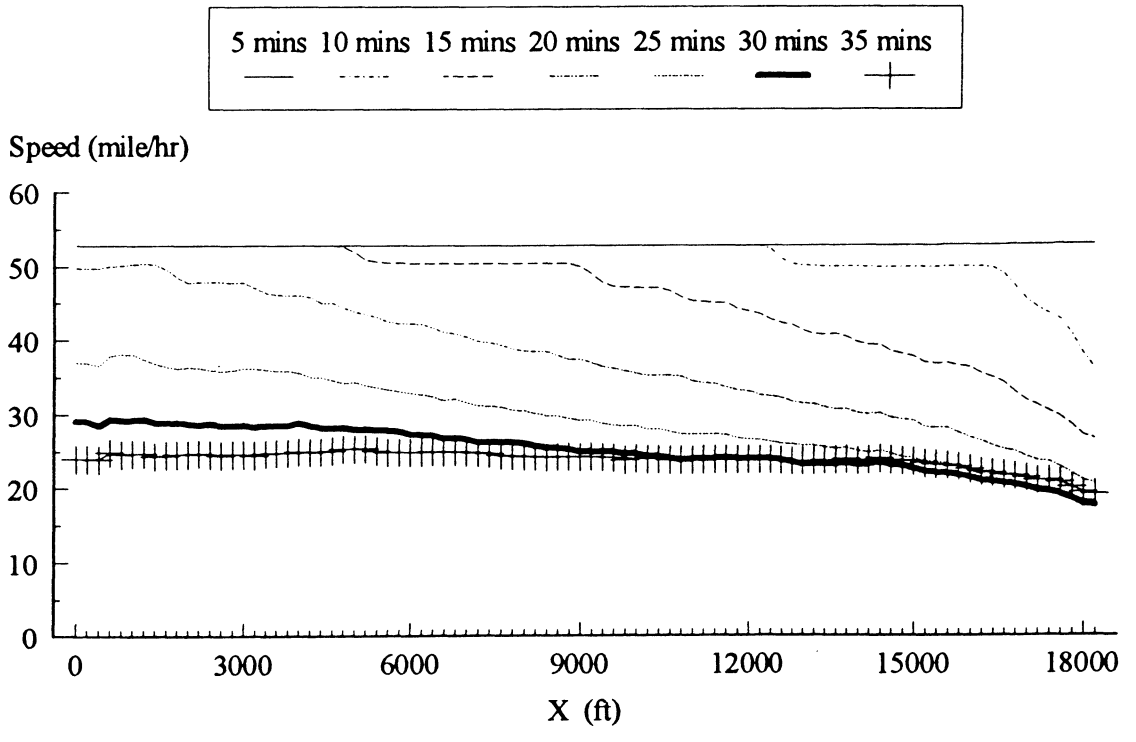

Figure 16.2 5-minute average speed produced by CORFLO (Euler method) for case 4.

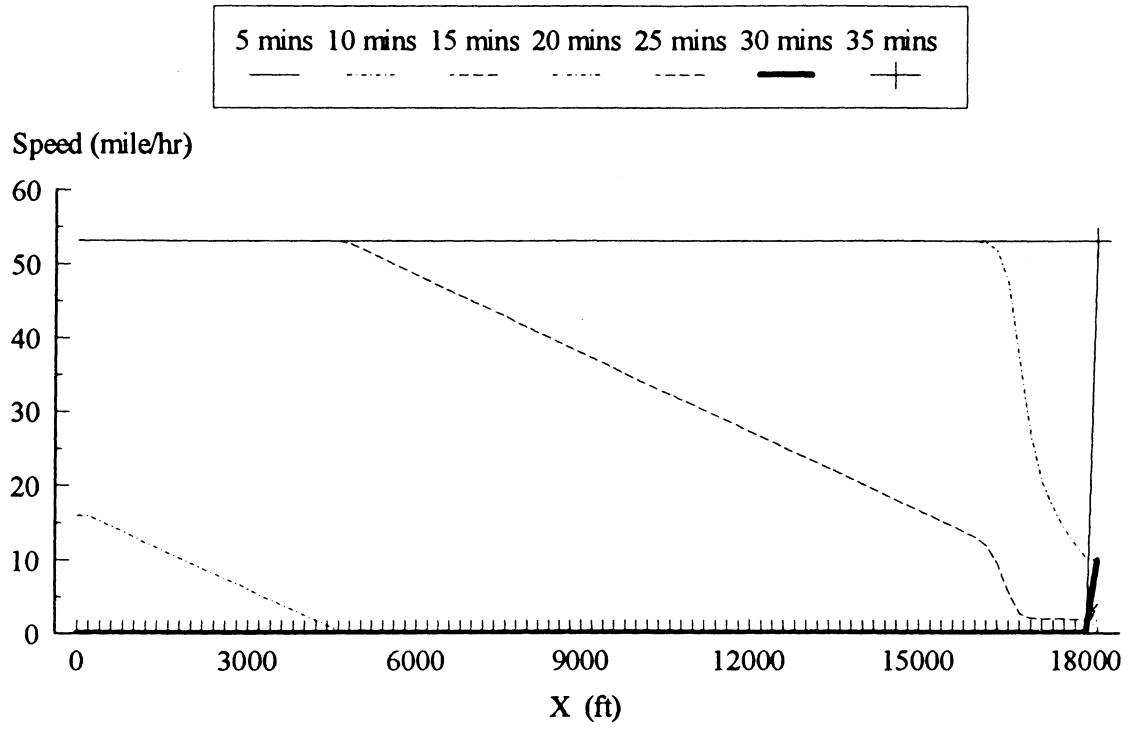

Figure 16.3 5-minute average speed produced by the improved high-order model (Euler method) for case 4 when $\nu = 68070.0$ (feet^2/sec) and $\tau = 36$ (sec).

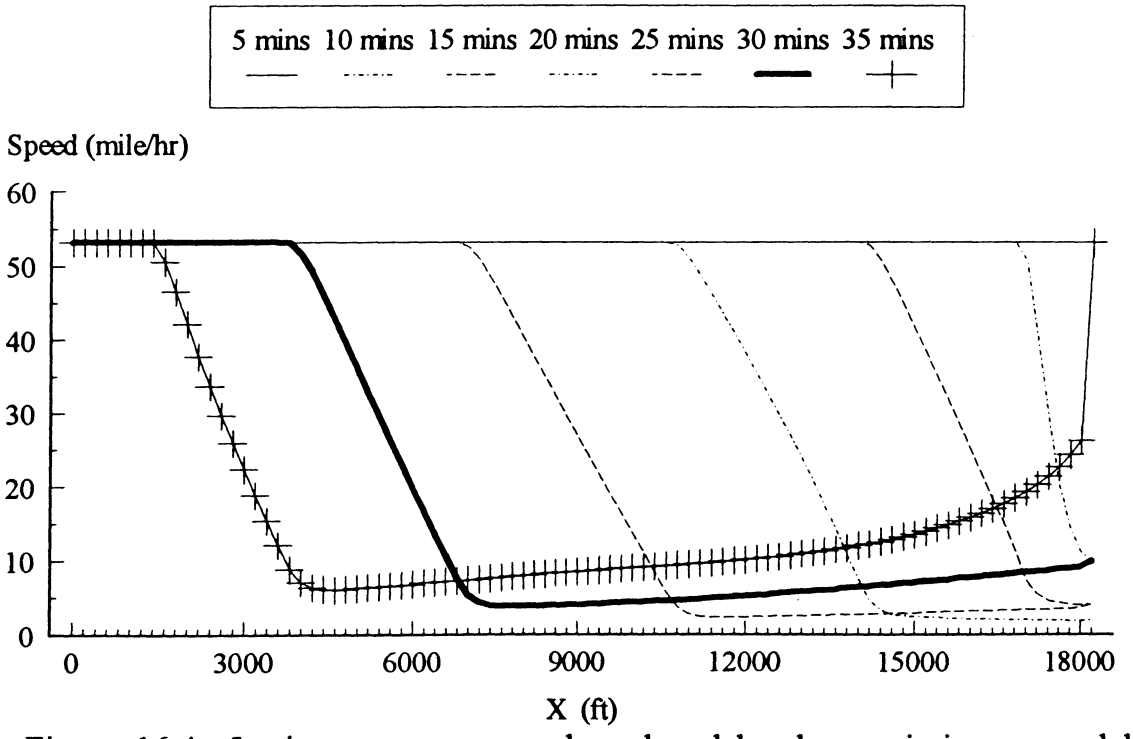

Figure 16.4 5-minute average speed produced by the semi-viscous model (Upwind method) for case 4.

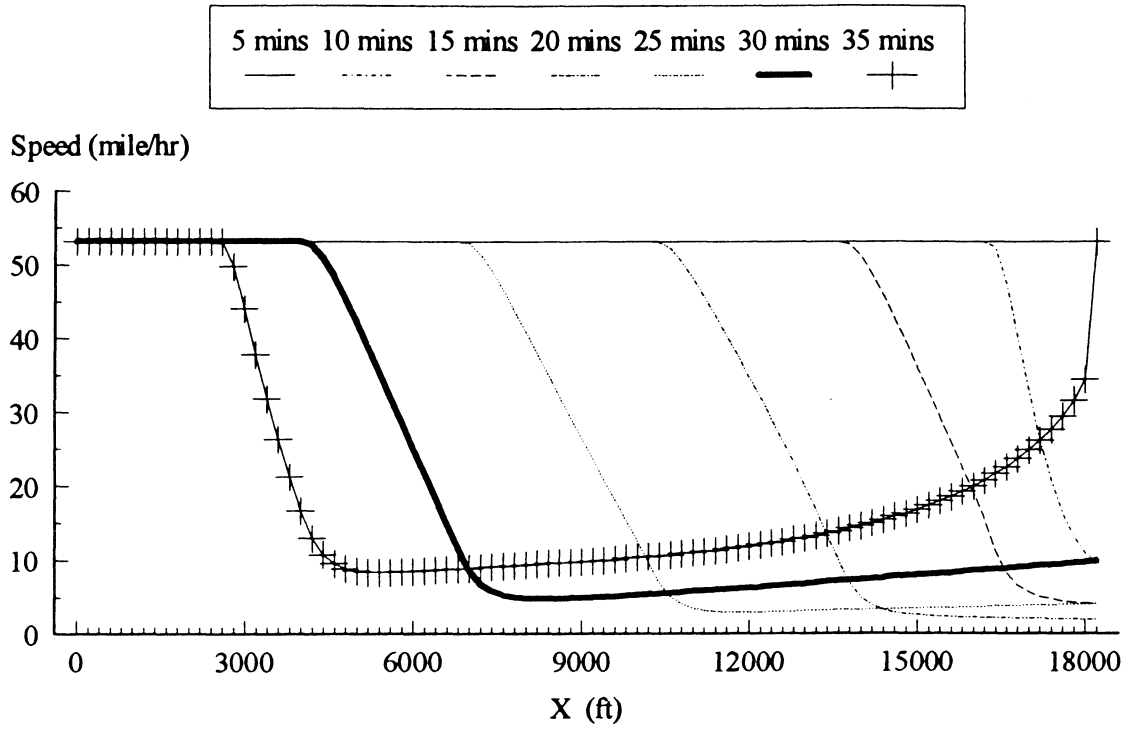

Figure 16.5 5-minute average speed produced by the proposed high-order model (Upwind method) for case 4.

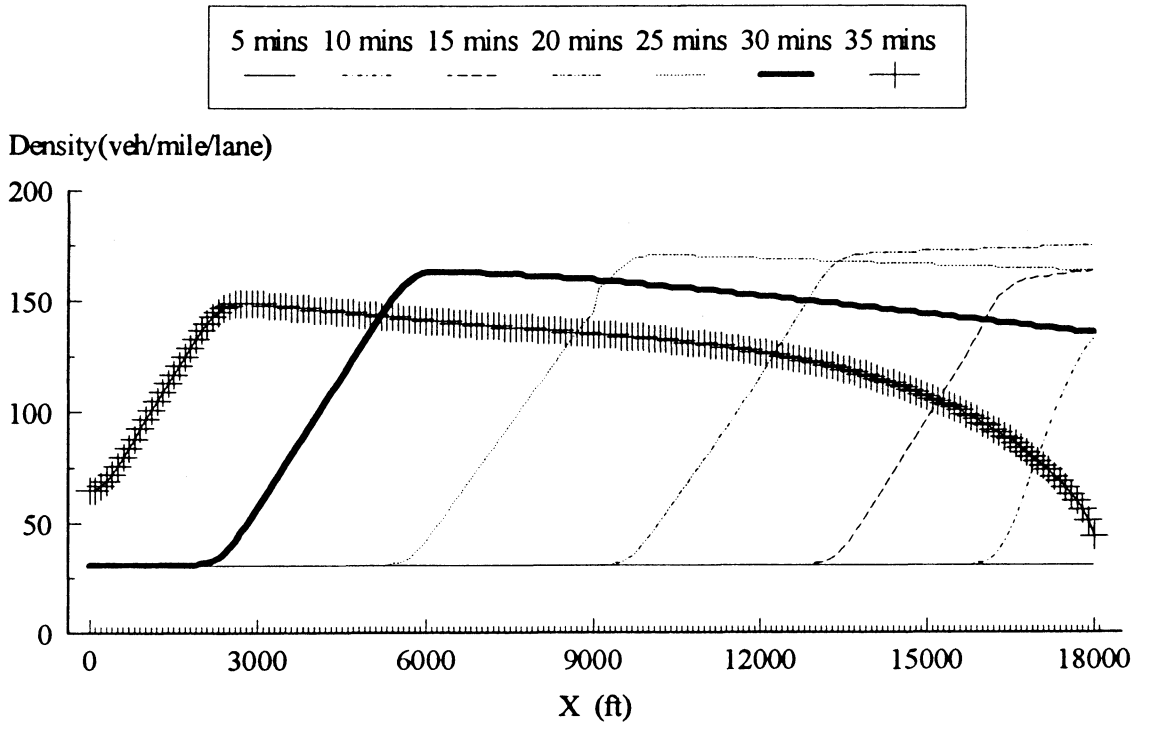

Figure 17.1 5-minute average density produced by KRONOS for case 4.

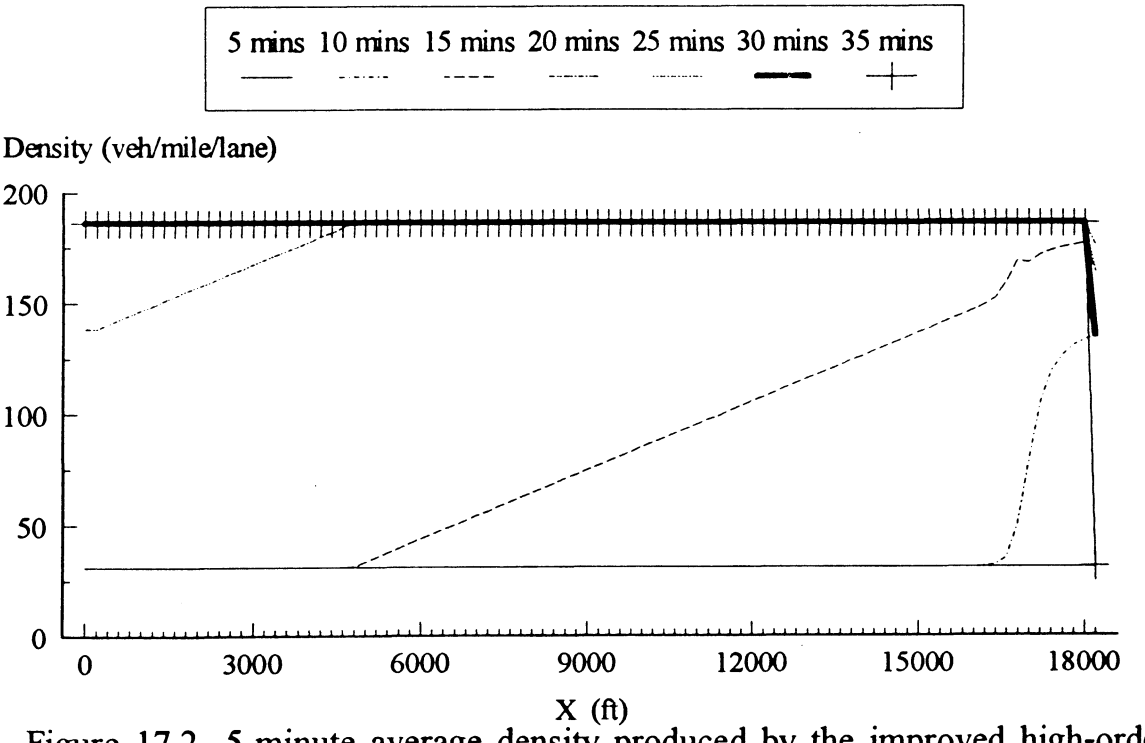

Figure 17.2 5-minute average density produced by the improved high-order model (Euler method) for case 4 when ν = 68070.0 (feet^2/sec) and τ = 36 (sec).

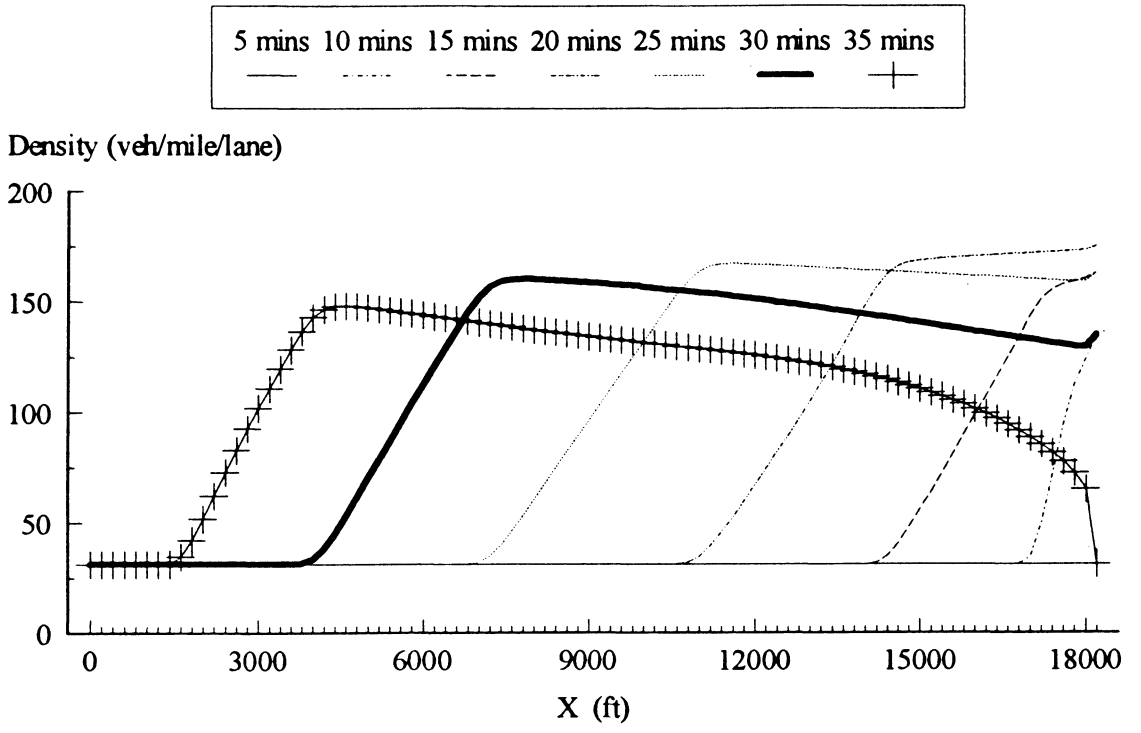

Figure 17.3 5-minute average density produced by the semi-viscous model (Upwind method) for case 4.

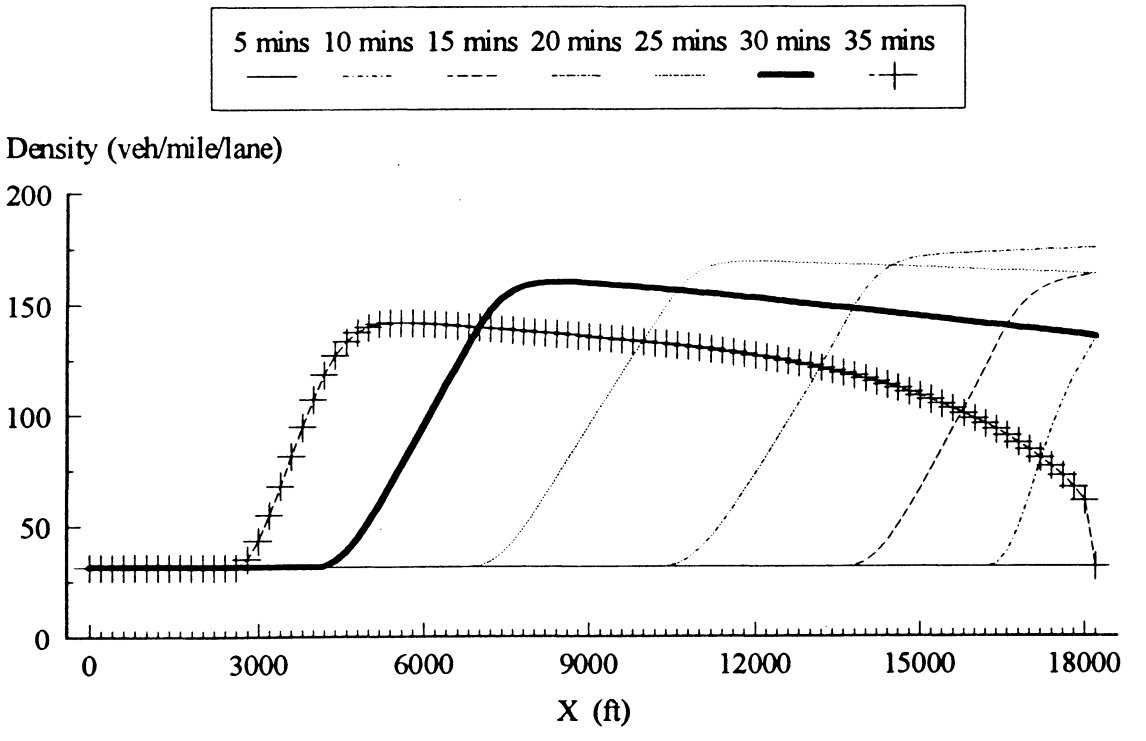

Figure 17.4 5-minute average density produced by the proposed high-order model (Upwind method) for case 4.

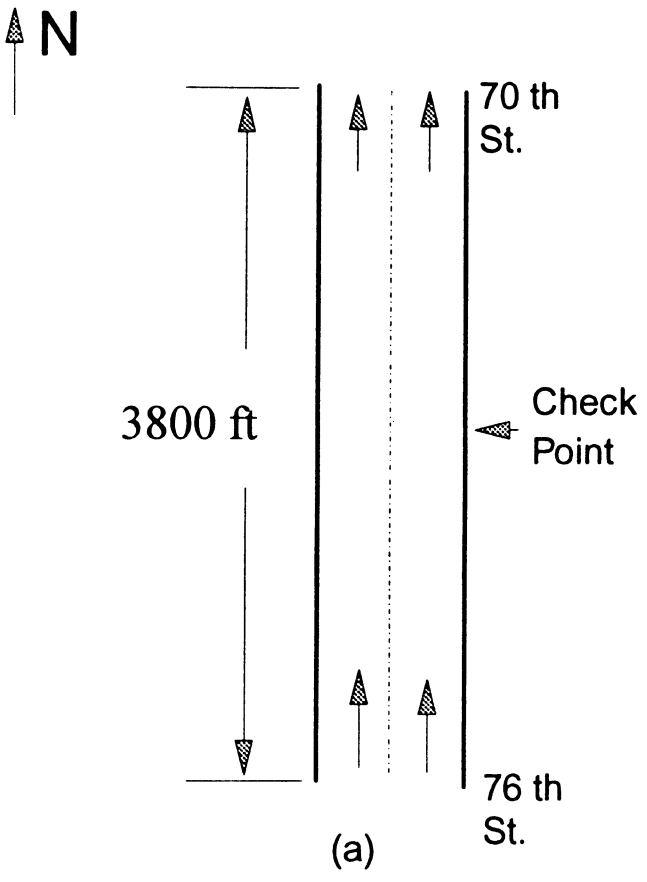

(a)

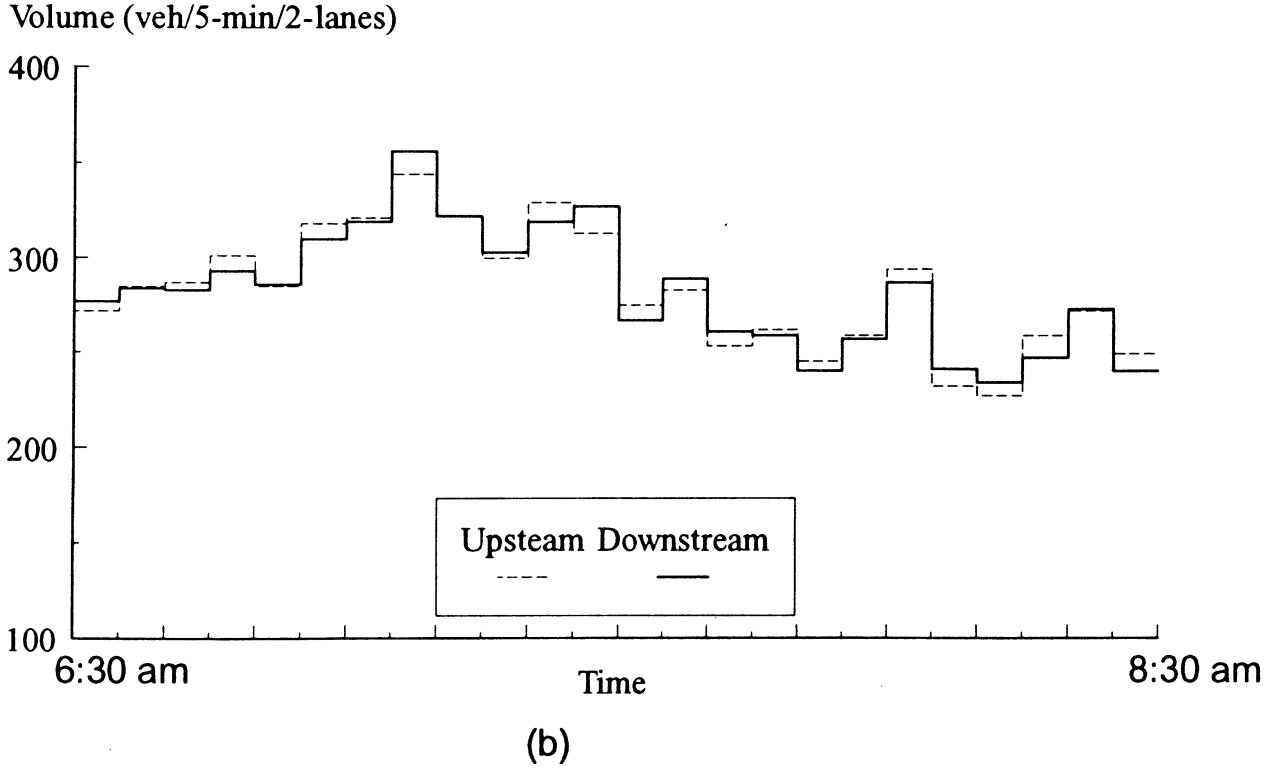

(b)

Figure 18. (a). Geometry; (b) Volume at the upstream and downstream boundaries for case 5

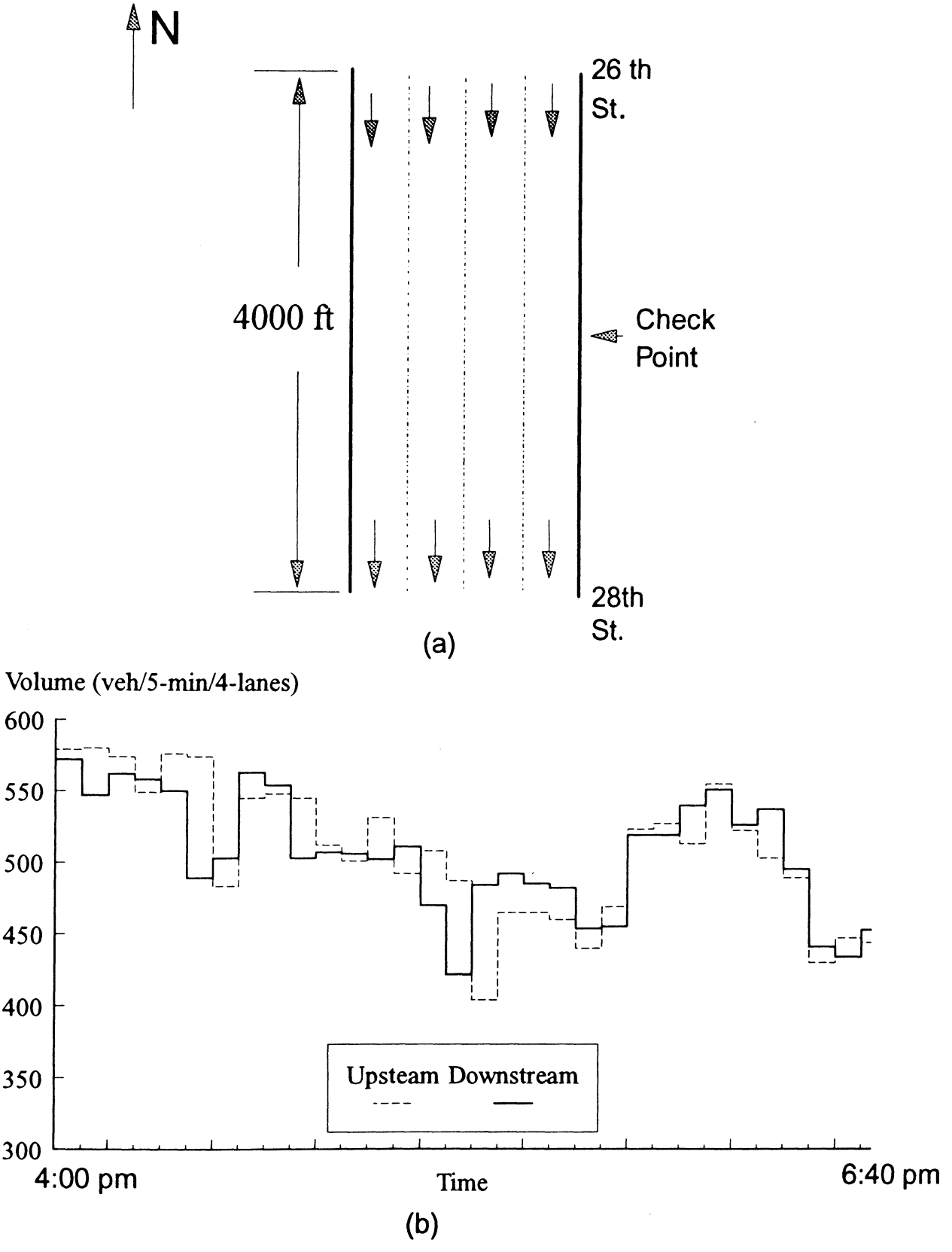

Figure 19. (a). Geometry; (b) Volume at the upstream and downstream boundaries for case 6

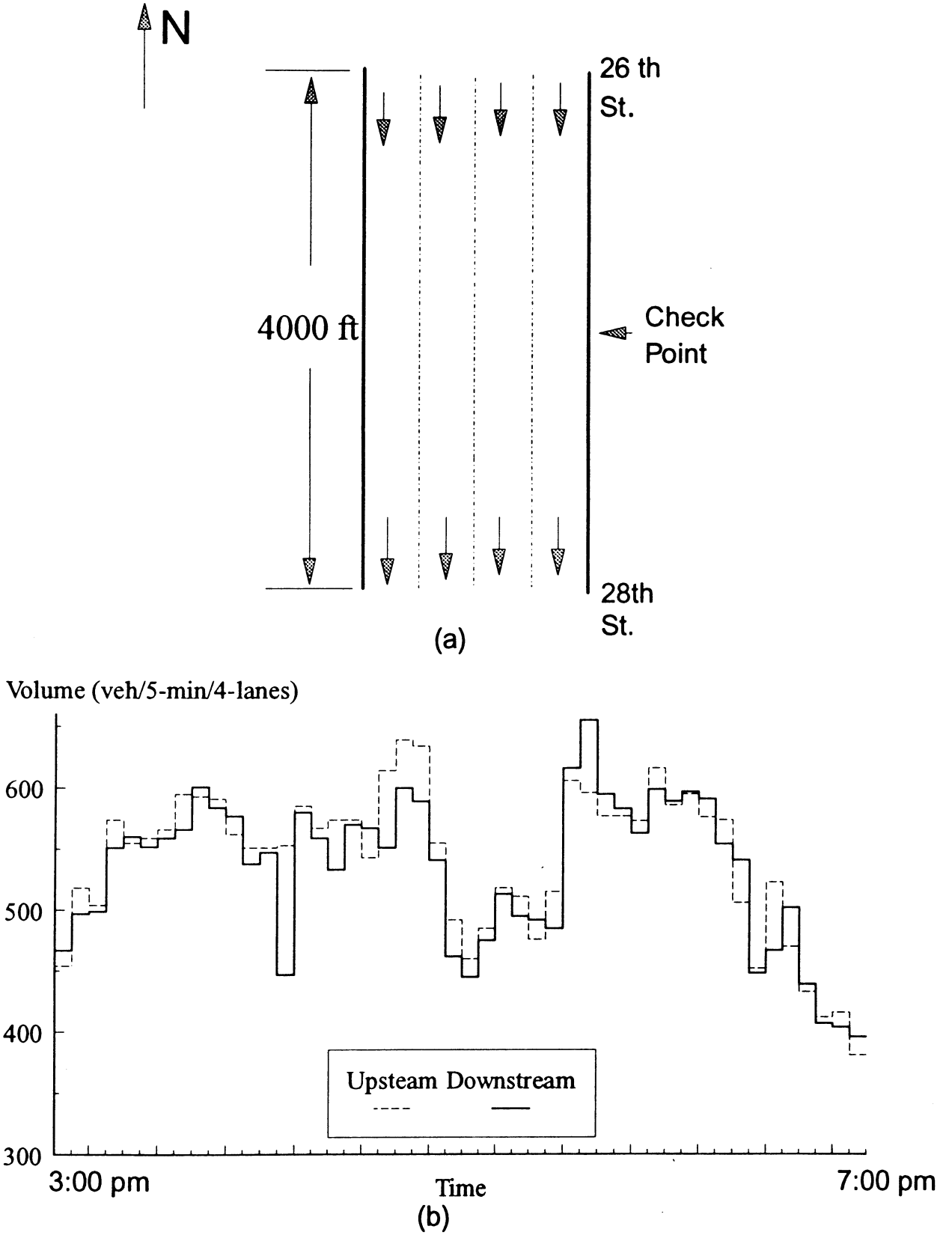

Figure 20. (a). Geometry; (b) Volume at the upstream and downstream boundaries for case 7.

Table 1 Error Indices for Case 5

Models (method)	Simple continuum model (Lax)	Improved High-order model (Euler)	CORFLO (Euler)	Original high-order model (Euler)	Original high-order model (Upwind)	Semi-Viscous model (Upwind)	Viscous model (Euler)	Proposed High-order model (Upwind)
MAE	4	4	8	4	4	4	4	4
MPE	2	2	2	2	2	2	2	2
MSE	27	27	52	27	27	22	27	22
Std.Dev	5	5	7	5	5	5	5	5

(1). MAE and Std.Dev: Veh/5-minutes;
(2). MSE: (Veh/5-minutes)^2.

Table 2.1 Error Indices for Case 6 (Capacity: 1825 (veh/hr/lane))

Models (method)	Simple continuum model (Lax)	Improved High-order model (Euler)	CORFLO (Euler)	Original high-order model (Euler)	Original high-order model (Upwind)	Semi-Viscous model (Upwind)	Viscous model (Euler)	Proposed High-order model (Upwind)
MAE	18	15	24	15	16	19	15	15
MPE	4	3	5	3	3	4	3	3
MSE	522	416	999	452	370	508	511	290
Std.Dev	23	21	32	22	20	23	23	17

(1). MAE and Std.Dev: Veh/5-minutes;
(2). MSE: (Veh/5-minutes)^2.

Table 2.2 Error Indices for Case 6 (Capacity: 1965 (veh/hr/lane))

Models (method)	Simple continuum model (Lax)	Proposed High-order model (Upwind)
MAE	19	16
MPE	4	3
MSE	670	325
Std.Dev	26	18

(1). MAE and Std.Dev: Veh/5-minutes;
(2). MSE: (Veh/5-minutes)^2.

Table 3.1 Error Indices for Case 7 (Capacity: 1965 (veh/hr/lane))

Models (method)	Simple continuum model (Lax)	Improved High-order model (Euler)	CORFLO (Euler)	Original high-order model (Euler)	Original high-order model (Upwind)	Semi-Viscous model (Upwind)	Viscous model (Euler)	Proposed High-order model (Upwind)
MAE	13	12	44	13	12	13	13	11
MPE	2	2	9	2	2	3	3	2
MSE	317	324	3328	336	265	360	428	216
Std.Dev	18	18	58	19	17	19	21	15

(1). MAE and Std.Dev: Veh/5-minutes;
(2). MSE: (Veh/5-minutes)^2.

Table 3.2 Error Indices for Case 6 (Capacity: 2100 (veh/hr/lane))

Models (method)	Simple continuum model (Lax)	Proposed High-order model (Upwind)
MAE	13	11
MPE	3	2
MSE	418	237
Std.Dev	21	16

(1). MAE and Std.Dev: Veh/5-minutes;
(2). MSE: (Veh/5-minutes)^2.

Development of advanced
traffic flow models and